Check for updates

International Journal of Energy Research

WILEY

REVIEW ARTICLE OPEN ACCESS

Biochar-Based Catalysts for Selective Biofuel Upgrading: Mechanisms, Functions, and Synthesis Rules

Seung Won Kim[1] | Eilhann E. Kwon[2] | Jechan Lee[1,3,4]

[1]Department of Global Smart City, Sungkyunkwan University, Suwon 16419, Republic of Korea | [2]Department of Earth Resources and Environmental Engineering, Hanyang University, Seoul 04763, Republic of Korea | [3]School of Civil, Architectural Engineering, and Landscape Architecture, Sungkyunkwan University, Suwon 16419, Republic of Korea | [4]SKKU National Lab for Intelligent Energy Solution Technology (SIEST), Sungkyunkwan University, Suwon 16419, Republic of Korea

Correspondence: Eilhann E. Kwon (ek2148@hanyang.ac.kr) | Jechan Lee (jechanlee@skku.edu)

Received: 22 July 2026 | **Revised:** 12 August 2026 | **Accepted:** 2 September 2026

Keywords: biochar | biofuel upgrading | biomass valorization | catalytic conversion

ABSTRACT

Biomass-derived fuels and bio-oils are characterized by substantial quantities of oxygenated species and unstable compounds, which diminish fuel quality and necessitate upgrading before practical application. In this regard, biochar has garnered increasing attention as a catalyst and support because it is derived from renewable biomass resources, and its physicochemical properties can be tailored through activation and chemical modification. This review explores the preparation of biochar-derived catalysts. It assesses the impacts of activation, metal incorporation, and heteroatom doping on the pore structure, surface functional groups, acidity/basicity, and redox characteristics pertinent to biofuel upgrading. The catalytic roles of these materials have been examined in processes including pyrolysis, microwave-assisted pyrolysis, hydrothermal liquefaction (HTL), catalytic transfer hydrogenation (CTH), steam reforming, and esterification/transesterification, with a focus on deoxygenation, denitrogenation, hydrogen transfer, and product stabilization. These studies indicate that the catalytic efficacy of biochar materials is contingent upon the synergistic effects of accessible pore networks and surface acid–base/redox properties, which vary with the upgrading route and feedstock. By integrating these structure-property relationships with process-specific catalytic performance and economic and environmental considerations, this review provides a comprehensive foundation for the rational design and evaluation of biochar-derived catalysts. It helps identify practical directions to advance sustainable biofuel upgrading technologies.

1 | Introduction

Biomass has emerged as a promising alternative energy source for sustainable carbon–neutral energy production. Derived from a wide range of sources, including plants, agricultural residues, seaweed, and organic waste from household and industrial activities, biomass is a viable and sustainable energy source for large-scale energy production, providing an effective alternative to fossil fuels [1–4]. Figure 1 shows the diverse end-use sectors that employ biofuels, including transportation (biojet fuel, marine fuel, and diesel/gasoline), electricity generation, industrial processes, heating, and chemical resource recovery (e.g., green chemicals and biogas).

Biofuel production technologies are key strategies for addressing climate change by promoting resource circulation and reducing waste. The International Energy Agency forecasts that ~27% of transportation fuels will be derived from biomass and waste resources by 2050 [5], underscoring the need to develop and enhance robust technological foundations to support this transition.

This is an open access article under the terms of the Creative Commons Attribution License, which permits use, distribution and reproduction in any medium, provided the original work is properly cited.

Copyright © 2026 Seung Won Kim et al. *International Journal of Energy Research* published by John Wiley & Sons Ltd.



FIGURE 1 | Schematic overview of representative utilization pathways for biomass-derived fuels and products, spanning transportation, stationary heat and power generation, industrial energy use, gaseous biofuels, and bio-based chemicals.

Various thermochemical conversion technologies have been developed to convert biomass into valuable resources. The primary products obtained from biomass include biochar, bio-oil, and gases, produced through processes such as pyrolysis, hydrothermal liquefaction (HTL), and gasification [6–10]. H_2 and CO are the primary gases generated, which can be converted into various fuels and chemical products [11, 12]. However, upgrading biofuels requires purification and quality enhancement processes due to feedstock heterogeneity and the presence of reaction byproducts [12]. Bio-oil is a mixture of oxygenated compounds, such as acids, phenols, and esters, that contain high levels of oxygen and acidity and exhibit a low heating value and high viscosity, resulting in instability that limits its direct use in industrial applications [13, 14]. Therefore, further refinement is essential to enhance its quality [15]. In this context, biofuel upgrading affords high-quality biofuels with high energy densities and improved stability from biomass thermochemical conversion products. Among the various biofuel upgrading technologies, the use of catalysts is particularly effective for improving fuel properties and controlling reaction selectivity [16]. Functionalized biochar has recently attracted attention as a potential catalyst for achieving both resource circularity and process efficiency [17–20]. The cost-effectiveness, exceptional catalytic activity, and energy recovery potential of biochar further demonstrate its potential as a biofuel-upgrading catalyst [21].

Figure 2 presents a scientometric keyword map based on the papers published between 2021 and 2026 on the topic of biochar catalysts. This indicates that research on biochar as a catalyst has recently received considerable attention, and a range of results are emerging. This map shows that research on biochar catalysis has expanded to encompass its use as a functional material for energy production and environmental remediation. Nevertheless, the reviews on biochar upgrading are often limited to individual process technologies, physicochemical properties, and environmental applications of biochar [22–25]. For instance, Ameen et al. [26] analyzed the efficiency of various pyrolysis techniques using corn-derived biomass and identified challenges

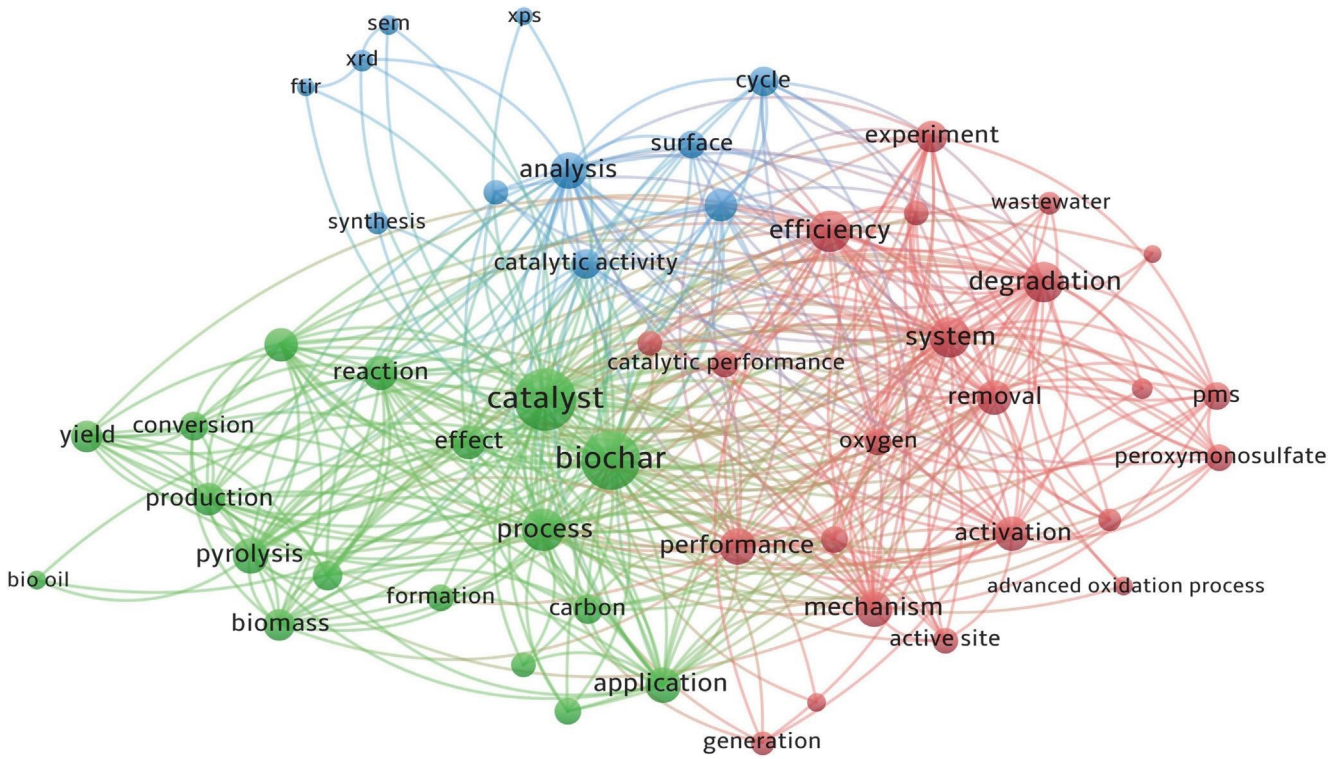


FIGURE 2 | Scientometric keyword map of 2814 publications (2021–2026) on "biochar catalyst."

ijer, 2026, 1, Downloaded from https://onlinelibrary.wiley.com/doi/10.1155/er/4175129 by Hanyang University Library, Wiley Online Library on [24/11/2026]. See the Terms and Conditions (https://onlinelibrary.wiley.com/terms-and-conditions) on Wiley Online Library for rules of use; OA articles are governed by the applicable Creative Commons License

to the commercialization of bio-oil and biochar production, as well as future research directions. Zhao et al. [27] examined the synthesis of element-doped biochar with enhanced functionality and sustainability, highlighting its potential for environmental remediation and energy conversion applications. Moreover, the discussions on biofuel upgrading processes are often fragmented. Lee et al. explored the catalytic potential of biochars. However, its application in specific domains, such as biodiesel production, has been discussed in only a single section of the review [28]. Comprehensive analyses of the improved reaction characteristics, catalytic performance, and reaction mechanisms of biochar-based catalysts are scarce.

This review advances the understanding that biochar-based catalyst used for biofuel upgrading (BCBU) should be conceptualized and assessed as a route-specific catalytic platform, rather than as isolated catalyst applications within individual upgrading pathways. Table 1 shows a comparison of the differences between this paper and review papers on similar topics published over the past 5 years. In contrast to previous reviews, which often focus on selected biochar applications, specific upgrading processes, or general catalyst preparation, this review offers a comparative analysis of how preparation-derived descriptors are transformed into catalytic functions and product outcomes across various processes, including pyrolysis, microwave-assisted pyrolysis, catalytic transfer hydrogenation (CTH), HTL, steam reforming, and esterification/transesterification. By integrating aspects such as catalyst synthesis, physicochemical properties, mechanisms, process-specific performance, stability, scalability, and economic/environmental trade-offs, this review provides a comprehensive framework for the selective upgrading of biofuel.

2 | Methodology

This section elucidates the methodology for the collection and analysis of research data (available in earlier literature) regarding biochar-based catalysts for biofuel upgrading reactions, including catalytic pyrolysis, CTH, HTL, steam reforming, and esterification/transesterification. The research articles cited in this review were drawn from reputable peer-reviewed journals from SCIE, ESCI, and other sources (e.g., book chapters, patents, and reports). For the literature search, keywords searches were performed using well-known research databases such as Web of Science, Scopus, and various publishers including American Chemical Society, Multidisciplinary Digital Publishing Institute, Royal Society of Chemistry, ScienceDirect, Springer, Taylor & Francis, and Wiley. The following search string was used: TITLE (biochar catalysts OR biofuel upgrading OR biooil upgrading OR hydrodeoxygenation OR esterification OR biodiesel OR steam reforming) AND TITLE, ABSTRACT, AND KEYWORDS (biomass OR biomass conversion OR biochar OR catalytic transfer hydrogenation OR hydrothermal liquefaction OR heterogeneous catalysis OR supported metal). This string ensured a broad consideration of biochar-based catalysts used for a range of biofuel upgrading reactions.

All the papers, book chapters, patents, and reports were initially screened for relevance to this review so as to efficiently screen any irrelevant publications. To focus on recent advances, relevant but relatively outdated studies were excluded, and only studies published between 2021 and 2026 were included in this review. In total, 214 research articles, including scientific papers and book chapters, were selected through the search. The selected data were first categorized according to the preparation and modification methods for biochar catalysts (Section 3) and then according to the biofuel-upgrading routes (Section 4). For each category, catalyst properties, reaction conditions, product yields and selectivities, and catalyst stability were summarized. Catalytic performance was compared among studies conducted under similar conditions, while scale-up and economic and environmental aspects were also reviewed (Sections 5–7).

3 | Synthesis and Characteristics of Biochar Catalysts

Biochar-based catalysts utilized for biofuel upgrading do not constitute a singular material class. The feedstock, synthesis methodology, and posttreatment processes influence the catalytic characteristics of this group of carbon-based solids. As outlined in Tables 2 and 3, the preparation method dictates the degree of carbonization, the retention or removal of inorganic minerals, pore formation, heteroatom incorporation, and the ease with which metals can be dispersed or anchored. Considering that the preparation method considerably affects the final catalytic properties, it is more effective to discuss BCBU in relation to the three primary methods documented in the literature: conventional pyrolysis, microwave-assisted pyrolysis, and hydrothermal carbonization (HTC). This discussion also includes the specific strategies employed in each method to tailor the physicochemical properties relevant to biofuel upgrading. Figure 3 outlines the preparation and posttreatment options.

3.1 | Pyrolysis-Derived Biochar Catalysts

Pyrolysis is the most widely used method for preparing BCBU because it directly converts relatively dry biomass into a carbon-rich framework under oxygen-limited conditions [28]. As summarized in Table 2, pyrolytic preparation was typically performed at 400–850°C under N_2, Ar, CO_2, or vacuum, with heating rates of 5–30°C/min and holding times of 10 min to 4 h. This route has been applied to lignocellulosic residues, macro- and microalgae, sewage sludge (SS), manure, and other wastes, demonstrating its versatility in converting chemically diverse feedstocks into catalytic char materials. Compared with lower-temperature wet routes, pyrolysis generally produces a more carbonized matrix with better thermal stability while retaining sufficient mineral matter and surface functionality to participate in upgrading reactions [93].

During pyrolysis, biomass undergoes distinct yet overlapping decomposition pathways. Hemicellulose and cellulose devolatilize earlier at 220–400°C, whereas lignin decomposes over a broader temperature window (160–900°C) and contributes disproportionately to aromatic char formation [94]. Consequently, feedstocks with different biochemical compositions produced biochars with varying aromaticity, ash content, and functional group distributions. Increasing the carbonization temperature typically reduces the hydrogen-to-carbon (H/C) and oxygen-to-carbon (O/C) ratios, thereby enhancing thermal stability. However, the range in which these improvements are effective

ijer, 2026, 1, Downloaded from https://onlinelibrary.wiley.com/doi/10.1155/er/4175129 by Hanyang University Library, Wiley Online Library on [24/11/2026]. See the Terms and Conditions (https://onlinelibrary.wiley.com/terms-and-conditions) on Wiley Online Library for rules of use; OA articles are governed by the applicable Creative Commons License

TABLE 1 | Comparison of this review with recent reviews related to biochar-based catalysts and biofuel upgrading.

Entry	Main focus	Biochar-catalyst/biofuel upgrading route coverage	Comparative advantage of this paper	Ref.
1	Biochar production techniques and biochar-based catalysts for biofuel production from algae	• Algae-derived biochar production • Mainly algal biofuel production and related thermochemical/catalytic routes	Feedstock-specific	[29]
2	Experimental parameters for upgrading pyrolysis bio-oil to biofuel by catalytic HDO	• Biochar is not treated as the central catalyst platform • HDO of pyrolysis bio-oil	HDO-centered parameter review	[22]
3	Emerging applications of biochar-based catalysts, including synthesis, properties, catalytic uses, and sustainability	• Broad biochar-catalyst platform across multiple applications • Biorefinery applications are included together with air/soil/water pollutant degradation	Biofuel upgrading is one subtopic	[17]
4	Progress and challenges of mesoporous catalysts for upgraded biomass pyrolysis to biofuels	• Mesoporous catalyst classes are emphasized • Upgraded pyrolysis of biomass	Focusing on the application of various mesoporous catalysts in pyrolysis processes	[24]
5	Role of biochar as a greener catalyst in biofuel production, including production, activation, and utilization	• Biochar production and activation are reviewed broadly • Biofuel production applications are discussed broadly	Less emphasis on route-specific descriptor-mechanism maps and focusing on broader biochar and biofuel production	[21]
6	Biochar catalysts for pyrolytic conversion of biomass into valuable biofuels	• Biochar synthesis, properties, and catalytic roles in pyrolysis are highlighted • Primarily pyrolysis-centered production of bio-oil, syngas, and char-related products	Strong pyrolysis focus	[30]
7	Biochar-driven green separation and catalytic upgrading of bio-oil	• Biochar adsorptive and catalytic functions for bio-oil are emphasized • Bio-oil separation and catalytic upgrading	Focusing on bio-oil separation and upgrading	[31]
8	Biochar-based catalysts for selective biofuel upgrading	• BCBU preparation, activation, heteroatom doping, and metal loading are integrated • Pyrolysis, microwave-assisted pyrolysis, CTH/HDO, HTL, steam reforming, and esterification/transesterification	Builds a synthesis-descriptor-mechanism-performance framework and evaluates reusability, regeneration, scale-up, and economic/environmental impacts	This study

remains unclear. In practical applications, BCBUs are typically carbonized at temperatures between 200 and 1000°C; excessively severe treatment can eliminate oxygen-containing anchoring sites, overgraphitize the surface, and, in certain systems, cause pore collapse or fusion despite continued increases in conductivity [21].

Postsynthesis and in situ modifications have been extensively employed to customize pyrolysis-derived catalysts. Physical activation with CO_2 or steam increases the pore volume because the oxidizing gas selectively gasifies reactive carbon domains and etches the block pore mouths at elevated temperatures [95]. Chemical activation using KOH, NaOH, H_3PO_4, or $ZnCl_2$ produces even larger changes through etching, dehydration/cross-linking, or mineral-assisted pore formation. For KOH activation, representative pore-forming reactions include $2KOH + CO_2 \rightarrow K_2CO_3 + H_2O$, $2C + 2KOH \rightarrow 2CO + 2K + H_2$, $2KOH + C + H_2O \rightarrow K_2CO_3 + 2H_2$, and $4KOH + C \rightarrow K_2CO_3 + H_2O + 2H_2$ [96]. The chemical composition of the feedstock is also important. Biomass derived from mineral-rich saline environments may exhibit

ijer, 2026, 1, Downloaded from https://onlinelibrary.wiley.com/doi/10.1155/er/4175129 by Hanyang University Library, Wiley Online Library on [24/11/2026]. See the Terms and Conditions (https://onlinelibrary.wiley.com/terms-and-conditions) on Wiley Online Library for rules of use; OA articles are governed by the applicable Creative Commons License

TABLE 2 | Biochar production and the catalyst preparation method.

Entry	Feedstock	Method	Biochar production method condition	Activation method	Ref.
1	*Eucalyptus nicholii* (EUC)	Pyrolysis	• Temperature: 800°C • Heating rate: 5°C/min • Retention time: 1 h • Atmosphere: N_2	Activation with H_3PO_4	[32]
2	Horticultural waste (HW)	Pyrolysis	• Temperature: 600°C • Retention time: 1 h • Atmosphere: N_2	Ni and Ce loading, followed by simultaneous steam activation and calcination	[33]
3	Cigarette butts	Pyrolysis	• Temperature: 700°C • Heating rate: 5°C/min • Retention time: 2 h • Atmosphere: N_2	Ni loading	[34]
4	Straw and woodchip	Pyrolysis	• Temperature: 800°C • Heating rate: 10°C/min • Retention time: 2 h • Atmosphere: N_2	Fe loading	[35]
5	RS	Pyrolysis	• Temperature: 750°C • Heating rate: 15°C/min • Retention time: 40 min • Atmosphere: N_2	Ni loading	[36]
6	SCB	Pyrolysis	• Temperature: 600°C • Heating rate: 15°C/min • Retention time: 1 h • Atmosphere: N_2	Heteroatom (N, P, O, and B) doping	[37]
7	Bamboo	Pyrolysis	• Temperature: 600°C • Heating rate: 5°C/min • Retention time: 2 h • Atmosphere: N_2	Zn and Zr loading	[38]
8	PW sawdust	Pyrolysis	• Temperature: 600°C • Heating rate: 15°C/min • Retention time: 1.5 h • Atmosphere: N_2	Cu and Fe loading and activation with CO_2 and H_2O	[39]
9	*Enteromorpha clathrate* (EN)	Pyrolysis	• Temperature: 500°C • Heating rate: 5°C/min • Retention time: 1 h • Atmosphere: N_2	Activation with KOH, NaOH, and CO_2	[40]
10	Seaweed	Pyrolysis	• Temperature: 800°C • Heating rate: 10°C/min • Retention time: 1.5 h • Atmosphere: N_2	Cu and Fe loading	[41]
11	RH	Pyrolysis	• Temperature: 800°C • Heating rate: 10°C/min		[42]

(Continues)

ijer, 2026, 1, Downloaded from https://onlinelibrary.wiley.com/doi/10.1155/er/4175129 by Hanyang University Library, Wiley Online Library on [24/11/2026]. See the Terms and Conditions (https://onlinelibrary.wiley.com/terms-and-conditions) on Wiley Online Library for rules of use; OA articles are governed by the applicable Creative Commons License

TABLE 2 | (Continued)

Entry	Feedstock	Method	Biochar production method condition	Activation method	Ref.
			• Atmosphere: CO_2	Activation with $ZnCl_2$ before pyrolysis and Ni, Fe, Co, and Cu loading	
12	FR	Pyrolysis	• Temperature: 450–650°C • Heating rate: 20°C/min • Retention time: 100 min • Atmosphere: N_2	Mn and Fe loading	[43]
13	PW sawdust	Pyrolysis	• Temperature: 800°C • Heating rate: 10°C/min • Retention time: 1 h • Atmosphere: N_2	Ni and Fe loading	[44]
14	Bagasse	Pyrolysis	• Temperature: 600°C • Retention time: 1 h • Atmosphere: N_2	AAEM loading	[45]
15	Lignin	Pyrolysis	• Temperature: 700°C • Retention time: 3 h • Atmosphere: vacuum	Ni loading	[46]
16	SCB and *Chlorella vulgaris* (CV)	Microwave pyrolysis	—	Co, Mg, and Fe loading	[47]
17	Cellulose nanocrystals (CNCs)	Microwave pyrolysis	• Power: 700 W • Reaction time: 40 min	—	[48]
18	CP	Pyrolysis	• Temperature: 800°C • Heating rate: 10°C/min • Retention time: 10 min • Atmosphere: N_2	Steam activation	[49]
19	Rape straw	Pyrolysis	• Temperature: 450°C • Retention time: 30 min • Atmosphere: N_2	CuO loading	[50]
20	PW sawdust	Pyrolysis	• Temperature: 800°C • Retention time: 1 h • Atmosphere: CO_2	Fe loading	[51]
21	PW needle	Pyrolysis	• Temperature: 700°C • Heating rate: 10°C/min • Retention time: 1 h	Activation with $ZnCl_2$, H_3PO_4, and NaOH before pyrolysis and Ni loading	[52]
22	Corn stover	Microwave pyrolysis	• Power: 700 W • Reaction time: 40 min • Atmosphere: N_2	—	[53]
23	Peanut shell (PS)	Microwave pyrolysis	• Power: 750 W • Reaction time: 15 min • Temperature: 550°C	Fe, Zn, and Co loading	[54]

(Continues)

ijer, 2026, 1, Downloaded from https://onlinelibrary.wiley.com/doi/10.1155/er/4175129 by Hanyang University Library, Wiley Online Library on [24/11/2026]. See the Terms and Conditions (https://onlinelibrary.wiley.com/terms-and-conditions) on Wiley Online Library for rules of use; OA articles are governed by the applicable Creative Commons License

TABLE 2 | (Continued)

Entry	Feedstock	Method	Biochar production method condition	Activation method	Ref.
24	PW sawdust	Pyrolysis	• Temperature: 800°C • Retention time: 1 h • Atmosphere: N_2	Activation with CO_2 and H_2O and Fe loading	[55]
25	Bamboo	Pyrolysis	• Temperature: 600°C • Heating rate: 5°C/min • Retention time: 2 h • Atmosphere: N_2	Zn and Zr loading	[56]
26	Soybean straw	Microwave pyrolysis	• Temperature: 700°C • Heating rate: 80–100°C/min • Retention time: 30 min • Atmosphere: vacuum	Phosphorus doping	[57]
27	Olive pomace	Pyrolysis	• Temperature: 700°C • Retention time: 2 h • Atmosphere: N_2	NiO, Co_3O_4, MgO, and CaO loading	[58]
28	Paper mill sludge	Pyrolysis	• Temperature: 600–800°C • Heating rate: 10°C/min • Retention time: 30 min • Atmosphere: Ar	—	[59]
29	EN	Pyrolysis	• Temperature: 500°C • Heating rate: 5°C/min • Retention time: 1 h • Atmosphere: N_2	Activation with KOH	[60]
30	Bamboo powder	Microwave pyrolysis	• 1st temperature: 350°C • Retention time: 1 h • 2nd temperature: 800–900°C • Heating rate: 5°C/min • Retention time: 20 to 30 min • Atmosphere: N_2	Nitrogen doping and Fe loading	[61]
31	SS	Pyrolysis	• Temperature: 600°C • Heating rate: 10°C/min • Retention time: 4 h • Atmosphere: N_2	—	[62]
32	CHR	Pyrolysis	• Temperature: 800°C • Heating rate: 10°C/min • Retention time: 1 h • Atmosphere: N_2	Activation with $ZnCl_2$ before pyrolysis and Ni, Fe, Co, and Cu loading	[63]
33	Palm fibers	Pyrolysis	• Temperature: 400°C • Retention time: 2 h • Atmosphere: N_2	Ni phosphide and Fe phosphide loading	[64]

(Continues)

ijer, 2026, 1, Downloaded from https://onlinelibrary.wiley.com/doi/10.1155/er/4175129 by Hanyang University Library, Wiley Online Library on [24/11/2026]. See the Terms and Conditions (https://onlinelibrary.wiley.com/terms-and-conditions) on Wiley Online Library for rules of use; OA articles are governed by the applicable Creative Commons License

TABLE 2 | (Continued)

Entry	Feedstock	Method	Biochar production method condition	Activation method	Ref.
34	Poplar sawdust	Pyrolysis	• Temperature: 700°C • Heating rate: 10°C/min • Retention time: 2 h • Atmosphere: N_2	Ni loading	[65]
35	CM	Pyrolysis	• Temperature: 500°C • Retention time: 4 h • Atmosphere: Ar	Cu, Pb, and Zn loading	[66]
36	SS	Pyrolysis	• Temperature: 650°C • Heating rate: 10°C/min • Retention time: 1 h • Atmosphere: Ar	Washed with HCl for demineralization	[67]
37	PW sawdust	Pyrolysis	• Temperature: 800°C • Heating rate: 10°C/min • Retention time: 1 h • Atmosphere: N_2	Activation in CO_2	[15]
38	Pine nut shell	Pyrolysis	• Temperature: 650°C • Retention time: 10 min	Ni loading	[68]
39	*Choerospondias axillaris*	Microwave pyrolysis	• Temperature: 600°C	Fe loading	[69]
40	EN	Pyrolysis	• Temperature: 800°C • Retention time: 1 h • Atmosphere: N_2	Cu, Ce, and Fe loading	[70]
41	*Spirulina platensis* (SP)	Hydrothermal	• Temperature: 280°C • Retention time: 35 min	Ni, Co, NiO, and CoO loading	[71]
42	Chicken manure	Pyrolysis	• Temperature: 550°C • Retention time: 1 h • Atmosphere: N_2	Ni_2P loading	[72]
43	SP	Pyrolysis of hydrothermal solid residue	• Temperature: 700°C • Retention time: 2 h • Atmosphere: N_2	CeO_2 loading	[73]
44	CNC	Microwave pyrolysis	• Power: 700 W • Reaction time: 40 min • Atmosphere: N_2	—	[74]
45	Waste palm kernel cake (WPKC)	Microwave pyrolysis	• Power: 150 W • Reaction time: 30 to 240 min	Cu, Ni, and Fe loading	[75]
46	RH	Pyrolysis	• Temperature: 800°C • Retention time: 1 h • Atmosphere: N_2	Fe loading	[76]
47	Bamboo waste	Pyrolysis	• Temperature: 600°C • Retention time: 30 min • Atmosphere: Ar	Activation with KOH K_2CO_3, $KHCO_3$, or CH_3COOK	[77]

(Continues)

ijer, 2026, 1, Downloaded from https://onlinelibrary.wiley.com/doi/10.1155/er/4175129 by Hanyang University Library, Wiley Online Library on [24/11/2026]. See the Terms and Conditions (https://onlinelibrary.wiley.com/terms-and-conditions) on Wiley Online Library for rules of use; OA articles are governed by the applicable Creative Commons License

TABLE 2 | (Continued)

Entry	Feedstock	Method	Biochar production method condition	Activation method	Ref.
48	SS and RH	Pyrolysis	• Temperature: 850°C • Retention time: 30 min • Atmosphere: N_2	—	[78]
49	CV	Pyrolysis	• Temperature: 450–850°C • Heating rate: 100°C/min • Retention time: 30 min • Atmosphere: Ar	Fe loading	[79]
50	Freshwater reed straw (FRS)	Pyrolysis	• Temperature: 700°C • Heating rate: 20°C/min • Retention time: 1 h • Atmosphere: N_2	Sulfonation	[80]
51	Acid-washed *Cladophora glomerata* (CG)	Pyrolysis	• Temperature: 600–800°C • Heating rate: 30°C/min • Retention time: 60, 120, and 180 min • Atmosphere: Ar	Zn loading	[81]
52	Defatted cottonseed	Pyrolysis	• Temperature: 600°C • Heating rate: 10°C/min • Atmosphere: N_2 or 80 vol.% CO_2 and 20 vol.% N_2	—	[82]
53	PS, wheat straw, sesame straw, and kraft lignin	Pyrolysis	• Temperature: 700°C • Heating rate: 10°C/min • Retention time: 2 h • Atmosphere: N_2	—	[83]
54	*Gracilaria corticata* (GC)	Pyrolysis and hydrothermal	• Pyrolysis temperature: 700°C • Pyrolysis retention time: 1 h • Hydrothermal temperature: 180°C • Hydrothermal reaction time: 12 h	NiFe-LDO (layered double oxide) and Ga loading	[84]
55	Methylene blue (MB) adsorbed EN-derived biochar	Pyrolysis	• Temperature: 800°C • Heating rate: 10°C/min • Retention time: 90 min • Atmosphere: N_2	—	[85]
56	PW sawdust	Microwave pyrolysis	• Temperature: 800°C • Retention time: 1 h	Activation with KOH and $ZnCl_2$ FeCo and FeNi alloy loading	[86]
57		Hydrothermal and pyrolysis	• Hydrothermal temperature: 200°C	Nitrogen doping	[87]

(Continues)

ijer, 2026, 1, Downloaded from https://onlinelibrary.wiley.com/doi/10.1155/er/4175129 by Hanyang University Library, Wiley Online Library on [24/11/2026]. See the Terms and Conditions (https://onlinelibrary.wiley.com/terms-and-conditions) on Wiley Online Library for rules of use; OA articles are governed by the applicable Creative Commons License

TABLE 2 | (Continued)

Entry	Feedstock	Method	Biochar production method condition	Activation method	Ref.
	Hydrothermal liquid from cow dung (CD) and corn straw (CS)		• Hydrothermal reaction time: 1 h • Pyrolysis temperature: 600°C • Pyrolysis heating rate: 10°C/min • Pyrolysis retention time: 3 h		
58	PW sawdust	Pyrolysis	• Temperature: 500°C • Heating rate: 10°C/min • Retention time: 90 min • Atmosphere: N_2	Activating with KOH, $ZnCl_2$, and H_3PO_4	[88]
59	Distillers dried grains with solubles (DDGSs)	Pyrolysis	• Temperature: 500°C • Heating rate: 10°C/min • Retention time: 2 h	Fe and Co loading	[89]
60	SP	Microwave pyrolysis	• Power: 1200 W • Reaction time: 30 min • Atmosphere: N_2	Activation with $ZnCl_2$	[90]
61	PW	Hydrothermal and microwave pyrolysis	• Hydrothermal temperature: 200°C • Hydrothermal reaction time: 6 h • Microwave power: 800 W • Microwave temperature: 800°C • Microwave reaction time: 1 h	Fe, Ni, and Co loading	[91]
62	Corncob	Pyrolysis	• Temperature: 550°C • Retention time: 2 h	—	[92]

properties that are different from those sourced from freshwater environments. Yue et al. [80] showed that seawater-reed–derived chars experienced stronger matrix erosion and lower sulfonic acid loading above 500°C because chloride/alkali salts and higher lignin/mineral contents intensified pore coalescence. Heteroatom doping with N, P, B, or O modifies the electron density, acidity/basicity, and surface polarity through the formation of N-containing defects, P–O groups, or boron–oxygen moieties [37]. Metal loading (with Fe, Ni, Co, Cu, Zn, and related species) introduces redox sites for bond scission, deoxygenation, and reforming [33, 39, 70]. Depending on the loading sequence and metal content, these treatments can either increase surface area via catalytic gasification or decrease it via pore blocking [17]. For the pyrolysis-derived catalysts listed in Table 3, these combined strategies yielded average pore diameters of 0.45–30.41 nm and surface areas spanning more than two orders of magnitude, highlighting the exceptional tunability of the pyrolysis route.

3.2 | Microwave-Assisted Pyrolysis-Derived Biochar Catalysts

Microwave-assisted pyrolysis provides an alternative route for directly converting electromagnetic energy into heat within a biomass/catalyst bed. As shown in Table 2, microwave-based preparation was conducted at 150–1200 W for 15–240 min, often under N_2 or vacuum and, in some cases, coupled with a preliminary carbonization step or HTC-derived precursors. Because heating is volumetric rather than surface-driven, microwave pyrolysis rapidly generates catalytic char and often shortens the preparation time compared to conventional furnace heating [97].

A unique characteristic of this approach is the dielectric heating mechanism. Polar species, defects, and metal-containing phases absorb microwave energy via dipole polarization, interfacial polarization, conduction loss, and, in some cases, magnetic

ijer, 2026, 1, Downloaded from https://onlinelibrary.wiley.com/doi/10.1155/er/4175129 by Hanyang University Library, Wiley Online Library on [24/11/2026]. See the Terms and Conditions (https://onlinelibrary.wiley.com/terms-and-conditions) on Wiley Online Library for rules of use; OA articles are governed by the applicable Creative Commons License

TABLE 3 | Biochar catalyst characteristics.

Entry	Catalyst type	Functional groups	Porosity	Ref.
1	P-doped EUC biochar	Hydroxyl, carboxyl, carbonyl, C–O, and P-containing groups	• Average pore diameter: 5.9 nm • Surface area: 616 m^2/g	[32]
2	Ni and Ce-loaded and steam-activated HW biochar	C = O and C–O groups	• Average pore diameter: 23.1 nm • Surface area: 351 m^2/g	[33]
3	Ni-loaded cigarette butts biochar	C = O, C–O, and OH groups	• Average pore diameter: 4.7 nm • Surface area: 156 m^2/g	[34]
4	Fe-loaded straw and woodchip biochar	C = O and C–O groups	• Surface area: 586 m^2/g	[35]
5	Ni-loaded RS biochar	—	—	[36]
6	B-doped SCB biochar	Hydroxyl, carboxyl, and boron–oxygen groups	• Average pore diameter: 4.0 nm • Surface area: 432 m^2/g	[37]
7	Zr-loaded bamboo biochar	C = O, C–O, and OH groups	• Average pore diameter: 2.3 nm • Surface area: 214 m^2/g	[38]
8	CO_2-activated and Fe-loaded PW biochar	C = O and C–O groups	• Average pore diameter: 30.4 nm • Surface area: 773 m^2/g	[39]
9	NaOH and CO_2-activated EN biochar	Oxygen and nitrogen-containing functional groups	• Average pore diameter: 4.0 nm • Surface area: 988 m^2/g	[40]
10	Cu-loaded seaweed biochar	—	• Surface area: 1067 m^2/g	[41]
11	Fe-loaded RH biochar	—	• Average pore diameter: 1.4 nm • Surface area: 868 m^2/g	[42]
12	Mn-loaded FR biochar	C–O and OH groups	• Average pore diameter: 4.3 nm • Surface area: 165 m^2/g	[43]
13	Fe and Ni coloaded PW biochar	C–O, C = O, and OH groups	• Average pore diameter: 2.1 nm • Surface area: 466 m^2/g	[44]
14	AAEM removed bagasse biochar	—	• Average pore diameter: 4.2 nm • Surface area: 412 m^2/g	[45]
15	Ni-loaded lignin biochar	C–O and OH groups	—	[46]
16	Fe-loaded CV and bagasse biochar	—	• Average pore diameter: 4.4 nm • Surface area: 126 m^2/g	[47]
17	Nanocellulose biochar	C–O and C = O groups	• Surface area: 155 m^2/g	[48]
18	CP biochar	Oxygen and nitrogen-containing groups	• Surface area: 682 m^2/g	[49]
19	CuO-loaded rape straw biochar	C–O and C = O groups	• Average pore diameter: 2.8 nm • Surface area: 754 m^2/g	[50]
20	Fe-loaded PW biochar	C = O and C–O groups	• Surface area: 779 m^2/g	[51]
21	Ni and P coloaded PW biochar	O–H, C–O, C = O, and P-containing groups	• Average pore diameter: 4.4 nm • Surface area: 489 m^2/g	[52]
22	Corn stover biochar	C–O, C = O, and N-containing groups	• Surface area: 54 m^2/g	[53]
23	Fe-loaded PS biochar	—	• Average pore diameter: 3.5 nm • Surface area: 258 m^2/g	[54]
24	Fe-loaded PW biochar	C = O and C–O groups	• Average pore diameter: 2.5 nm • Surface area: 518 m^2/g	[55]

(Continues)

ijer, 2026, 1, Downloaded from https://onlinelibrary.wiley.com/doi/10.1155/er/4175129 by Hanyang University Library, Wiley Online Library on [24/11/2026]. See the Terms and Conditions (https://onlinelibrary.wiley.com/terms-and-conditions) on Wiley Online Library for rules of use; OA articles are governed by the applicable Creative Commons License

TABLE 3 | (Continued)

Entry	Catalyst type	Functional groups	Porosity	Ref.
25	Zr-loaded bamboo biochar	C = O, C–O, and OH groups	• Average pore diameter: 2.3 nm • Surface area: 214 m^2/g	[56]
26	P-doped soybean straw biochar	C = O, C = C, OH, and P-containing groups	• Average pore diameter: 27.4 nm • Surface area: 1086 m^2/g	[57]
27	NiO-loaded olive pomace biochar	—	• Average pore diameter: 7.1 nm • Surface area: 73 m^2/g	[58]
28	Paper mill sludge biochar	—	• Surface area: 52 m^2/g	[59]
29	EN biochar	C = O, C–O, and N-containing groups	• Average pore diameter: 3.1 nm • Surface area: 1067 m^2/g	[60]
30	N and Fe coloaded bamboo biochar	C–O, C = O, and N-containing groups	• Surface area: 265 m^2/g	[61]
31	SS biochar	—	• Average pore diameter: 12.9 nm • Surface area: 189 m^2/g	[62]
32	Co-loaded CHR biochar	—	• Average pore diameter: 1.7 nm • Surface area: 24 m^2/g	[63]
33	Fe-P–loaded palm fiber biochar	C = O, C–O, and OH groups	• Surface area: 851 m^2/g	[64]
34	Ni-loaded poplar biochar	—	• Average pore diameter: 1.1 nm • Surface area: 348 m^2/g	[65]
35	Pb-loaded CM biochar	C = O, C–O, and OH groups	• Average pore diameter: 6.7 nm • Surface area: 15 m^2/g	[66]
36	SS biochar	—	—	[67]
37	CO_2-activated PW biochar	C = O, C–O, and OH groups	• Average pore diameter: 2.7 nm • Surface area: 906 m^2/g	[15]
38	Ni-loaded and pine nut shell biochar modified Hβ zeolite	—	• Average pore diameter: 8.9 nm • Surface area: 277 m^2/g	[68]
39	Fe and P codoped *Choerospondias axillaris* biochar	—	• Surface area: 733 m^2/g	[69]
40	Cu-loaded EN biochar	C = O and OH groups	• Average pore diameter: 5.4 nm • Surface area: 65 m^2/g	[70]
41	Ni-loaded SP biochar	—	• Average pore diameter: 3.2 nm • Surface area: 197 m^2/g	[71]
42	Ni_2P-loaded chicken manure biochar	—	• Average pore diameter: 15.0 nm • Surface area: 321 m^2/g	[72]
43	CeO_2-loaded SP biochar	OH groups	• Surface area: 136 m^2/g	[73]
44	Nanocellulose biochar	C = O and C–O groups	• Surface area: 155 m^2/g	[74]
45	Ni-loaded WPKC biochar	—	• Average pore diameter: 2.3 nm • Surface area: 305 m^2/g	[75]
46	Fe-loaded RH	—	—	[76]
47	CH_3COOK-activated bamboo biochar	C = O, C–O, and OH groups	• Average pore diameter: 1.7 nm • Surface area: 803 m^2/g	[77]
48	RH biochar	C = O, C–O, and OH groups	• Average pore diameter: 5.1 nm	[78]

(Continues)

ijer, 2026, 1, Downloaded from https://onlinelibrary.wiley.com/doi/10.1155/er/4175129 by Hanyang University Library, Wiley Online Library on [24/11/2026]. See the Terms and Conditions (https://onlinelibrary.wiley.com/terms-and-conditions) on Wiley Online Library for rules of use; OA articles are governed by the applicable Creative Commons License

TABLE 3 | (Continued)

Entry	Catalyst type	Functional groups	Porosity	Ref.
49	Fe-loaded CV biochar	C = O, C–O, and OH groups	• Surface area: 128 m^2/g • Average pore diameter: 2.1 nm • Surface area: 365 m^2/g	[79]
50	Sulfonated FRS biochar	C–O, C = O, OH, and S-containing groups	• Average pore diameter: 0.5 nm • Surface area: 14 m^2/g	[80]
51	Zn-loaded CG biochar	C–O and OH groups	• Surface area: 769 m^2/g	[81]
52	Defatted cottonseed biochar	—	—	[82]
53	Wheat straw biochar	C–O and OH groups	• Average pore diameter: 3.8 nm • Surface area: 9 m^2/g	[83]
54	Ga and NiFe-LDO–loaded GC biochar	—	• Surface area: 513 m^2/g	[84]
55	MB adsorbed EN-derived biochar	C = O and N-containing groups	• Average pore diameter: 4.4 nm • Surface area: 453 m^2/g	[85]
56	FeCo-loaded PW biochar	—	—	[86]
57	CS and CD-derived biochar	C–O and N-containing groups	• Average pore diameter: 9.9 nm • Surface area: 52 m^2/g	[87]
58	P-doped PW sawdust biochar	O and P-containing groups	• Average pore diameter: 2.2 nm • Surface area: 1476 m^2/g	[88]
59	Fe–Co–loaded DDGS biochar	C = O and OH groups	• Average pore diameter: 3.3 nm • Surface area: 355 m^2/g	[89]
60	Zn-loaded SP biochar	C = O, C–O, and N-containing groups	• Average pore diameter: 2.9 nm • Surface area: 1416 m^2/g	[90]
61	Co–Ni–loaded PW biochar	—	• Surface area: 352 m^2/g	[91]
62	Corncob biochar	—	—	[92]

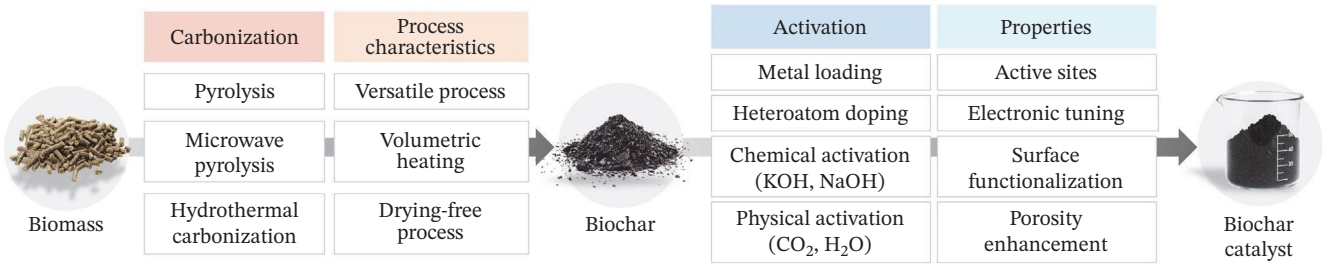


FIGURE 3 | Process flow diagram of BCBU synthesis from various biomass.

loss, thereby creating localized hotspots and steep internal temperature gradients [61]. These features accelerate devolatilization and suppress secondary carbon deposition on the external surface, yielding cleaner and more open structures than those produced by conventional external heating. Microwave loss should be understood as a cause of faster heating rather than merely a consequence of higher temperatures. For example, Luo et al. [61] showed that increasing catalyst loading increased the average heating rate from 63.78 to 107.84°C/min under microwave irradiation because the catalyst converted electromagnetic energy into heat more efficiently. Property control in microwave-derived BCBU relies on activation, and the microwave-specific heating behavior amplifies the effects. $ZnCl_2$ or KOH pretreatment can create highly porous scaffolds, and N-doping creates defect sites and polar functionalities that strengthen microwave absorption and facilitate rapid internal heating, as demonstrated for N–Fe coloaded biochar [61]. Overall, microwave pyrolysis–derived biochars combine catalytically active sites with energy-coupling functionalities, making this route particularly suitable when the catalyst must mediate both heating and chemistry.

3.3 | HTC-Derived Biochar Catalysts

HTC is preferred when the feedstock has a high moisture content or when drying imposes a large energy penalty [98]. In the studies compiled in Table 2, HTC or hydrochar-mediated routes were

ijer, 2026, 1, Downloaded from https://onlinelibrary.wiley.com/doi/10.1155/er/4175129 by Hanyang University Library, Wiley Online Library on [24/11/2026]. See the Terms and Conditions (https://onlinelibrary.wiley.com/terms-and-conditions) on Wiley Online Library for rules of use; OA articles are governed by the applicable Creative Commons License

typically conducted at 180–280°C for 35 min to 12 h in water, after which the resulting hydrochar was used directly, loaded with metal, or subjected to secondary pyrolysis or microwave treatment. Unlike dry pyrolysis, HTC proceeds in subcritical water, which simultaneously acts as a solvent, a reactant, and a transport medium [98]; this makes this route particularly attractive for wet algae, SS, and other aqueous residues.

The mechanism of hydrochar formation differs fundamentally from that of pyrochar. Under hydrothermal conditions, biomass components are hydrolyzed into smaller oxygenated intermediates, which then undergo dehydration, decarboxylation, polymerization, condensation, and progressive aromatization, ultimately forming carbonaceous solids [99, 100]. Because these reactions occur in aqueous environments at relatively low temperatures, hydrothermally carbonized chars typically retain higher concentrations of oxygen-containing functional groups and exhibit less-developed pore structures than high-temperature pyrochars. However, they offer oxygenated anchoring sites that facilitate metal deposition and interfacial catalysis [101–103]. HTC-derived solids are frequently upgraded via postloading or secondary thermal conversion. Hybrid HTC-pyrolysis or HTC-microwave strategies further broaden the tunability by combining oxygen-rich precursor surfaces with later pore development or enhanced microwave responses [87, 91].

The three preparation routes produced catalysts with distinct structure–function profiles. Conventional pyrolysis offers the broadest control over carbonization and pore development, microwave-assisted pyrolysis provides rapid volumetric heating and strong energy coupling, and HTC is best suited to wet feedstocks and oxygen-rich precursor surfaces. Across all routes, the catalyst performance is ultimately tuned by the coupled effects of process severity, reactive atmosphere, activation chemistry, heteroatom doping, and metal–support interactions, which together determine the pore architecture, surface functionality, and acid–base/redox properties, as summarized in Table 3.

4 | Bio-Oil Upgrading Reaction

Biochar-based catalysts improve bio-oil quality by intercepting primary vapors or liquid intermediates and shifting the competition between dehydration, decarboxylation, decarbonylation, hydrogen transfer, cyclization, denitrogenation, esterification, and reforming [33, 52, 62, 71]. The optimal outcome is contingent on the upgrading pathway and feed composition, with the preferred product potentially being a phenol-rich liquid, a hydrocarbon-rich liquid, a stabilized ester-containing oil, biodiesel, or an H_2-rich gas stream, rather than a single product. Figures 4 and 5 illustrate the pathways for producing biofuels from lignocellulosic and algal biomasses, respectively. Figure 6 summarizes the comprehensive decomposition of biomass products and the catalytic reactions during the process.

The key design question in bio-oil upgrading is not which catalyst is universally the most active but which catalyst properties best relieve the dominant bottleneck of a given route, feedstock, and target product. Therefore, direct ranking across studies should be made cautiously because the feedstock class, reactor configuration, catalyst-to-feed ratio, residence time, and product reporting metrics vary substantially. The trends discussed below are best interpreted as route-specific design tendencies, rather than universal performance rankings. Quantitative data regarding the changes in products facilitated by BCBU are presented in Table 4.

4.1 | Upgrading Routes

Catalytic pyrolysis is a dry thermochemical route in which dried biomass, such as cellulose, hemicellulose, lignin, lipids, or protein fragments, is heated under oxygen-lean conditions into vapors, radicals, and light gases [104]. These primary products come in contact with the catalyst either in situ in the reactor bed or ex situ in the secondary catalytic bed before condensation [105]. In practice, the process is selected when the objective is to rapidly upgrade vapor-phase intermediates without adding a solvent or external hydrogen by converting oxygen-rich condensables into phenols, monoaromatics, hydrocarbons, and/or lighter gases via secondary cracking (Figure 7).

Microwave-assisted catalytic pyrolysis uses the same broad decomposition chemistry as conventional catalytic pyrolysis, but the heating principles are different. The feed and catalyst are exposed to microwave irradiation, and the polar groups, defects, graphitized domains, and metal-containing phases directly convert the electromagnetic energy into localized heat [61, 86]. Therefore, the catalyst serves as both a chemically active phase and an energy-coupling material. This route is applied when rapid internal heating, short thermal lag, and localized hot spots are advantageous for accelerating depolymerization, cracking, and aromatization while limiting long residence times in the bulk reactor [61]. Therefore, in microwave systems, the catalytic performance depends not only on acidity or redox chemistry but also on the catalyst's efficiency in converting microwave energy into heat at the particle scale.

CTH is a liquid-phase upgrading route in which hydrogen is supplied from hydrogen-donor solvents (e.g., methanol, alcohols, or formic acid) rather than from externally supplied H_2 [107], as described in Figure 8. In the process of biofuel upgrading, CTH primarily serves to stabilize carbonyl- and C–O–rich compounds. This stabilization is achieved through mechanisms such as hydrogen transfer, hydrogenation, and hydrogenolysis, resulting in the production of alcohols, furfuryl alcohol, 2-methylfuran, or other partially deoxygenated intermediate. Due to the catalyst's operation in a liquid phase, its critical properties differ from those required for vapor-phase pyrolysis. Specifically, mesoporosity, accessibility in the liquid phase, metal dispersion, and the balance of acid and redox sites are more important than vapor-contact efficiency alone [107, 109].

Platform molecule hydrodeoxygenation (HDO) is closely related to CTH but is typically conducted using representative biomass-derived intermediates, such as furfural, hydroxymethylfurfural (HMF), levulinic acid, or vanillin, rather than whole bio-oil [107, 110, 111]. Figure 9 shows HDO routes of oxygenated compounds. This route is useful for understanding how biochar catalysts control liquid-phase hydrogenation, hydrogenolysis, and C–O bond transformation in oxygenated intermediates. Therefore, platform molecule upgrading provides mechanistic insight into liquid-phase BCBU behavior, even though its performance

ijer, 2026, 1, Downloaded from https://onlinelibrary.wiley.com/doi/10.1155/er/4175129 by Hanyang University Library, Wiley Online Library on [24/11/2026]. See the Terms and Conditions (https://onlinelibrary.wiley.com/terms-and-conditions) on Wiley Online Library for rules of use; OA articles are governed by the applicable Creative Commons License

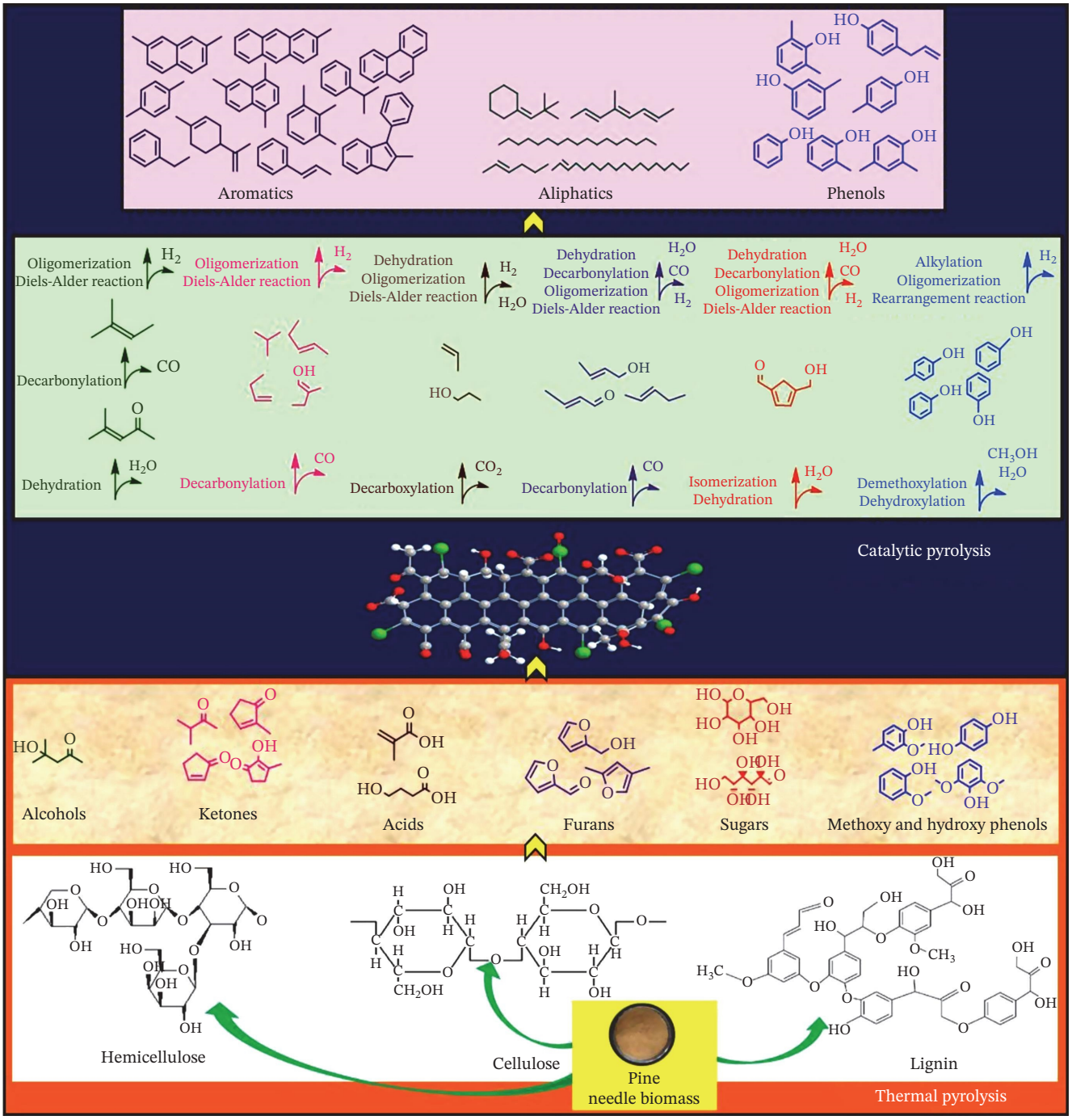


FIGURE 4 | Mechanism for lignocellulosic biomass–derived biofuel upgrading. Reprinted with permission from Gupta et al. [52]. Copyright (2022) American Chemical Society.

metrics should be distinguished from those of direct whole-bio-oil upgrading.

Catalytic HTL is a wet-upgrading route used for biomass slurries such as algae, SS, and other high-moisture feeds, for which drying is energetically unfavorable [113]. Biomass is processed with water in a sealed reactor under hot-compressed conditions; therefore, hydrolysis occurs first, and the catalyst acts mainly in the liquid phase rather than in a dry vapor stream [114]. The key process sequence is the hydrolysis of biopolymers into smaller soluble intermediates, followed by catalytic hydrogen transfer, decarboxylation, denitrogenation, rearrangement, and suppression of liquid-phase repolymerization [114, 115], as depicted in Figure 10. Because the catalyst operates in hot compressed water, HTL places strong emphasis on liquid-phase accessibility, mesopore accessibility for liquid intermediates, and metal functions that facilitate denitrogenation and hydrogen transfer [117, 118].

Steam reforming is a downstream upgrading step that occurs after bio-oil, tar, or oxygenated vapors have formed. Figure 11 shows general reaction pathways for steam reforming of bio-oil. In this process, oxygenated liquids or vapors are mixed with steam and passed over a catalyst bed at elevated temperatures, where steam activation, C–C/C–H cleavage, water-gas shift

ijer, 2026, 1, Downloaded from https://onlinelibrary.wiley.com/doi/10.1155/er/4175129 by Hanyang University Library, Wiley Online Library on [24/11/2026]. See the Terms and Conditions (https://onlinelibrary.wiley.com/terms-and-conditions) on Wiley Online Library for rules of use; OA articles are governed by the applicable Creative Commons License

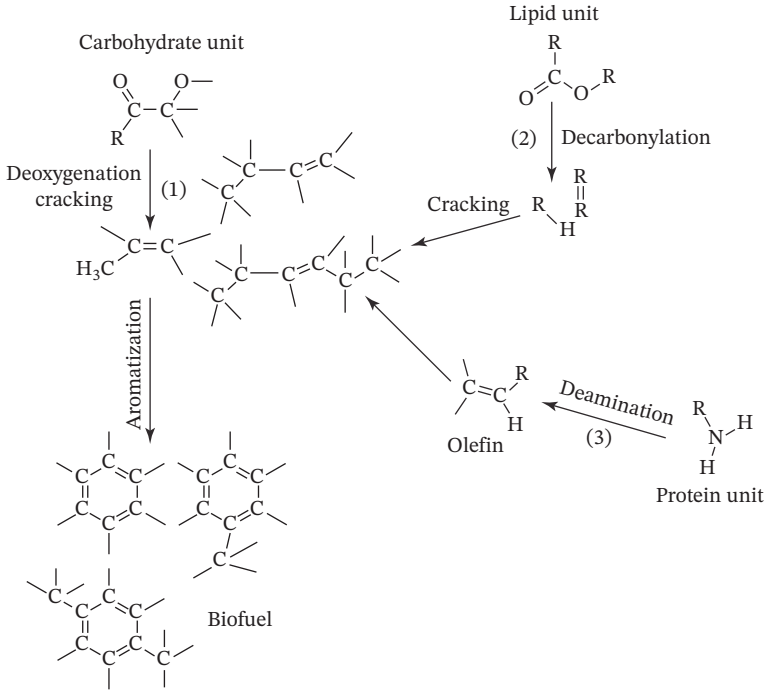


FIGURE 5 | Mechanism for algal biomass–derived biofuel upgrading. Reprinted from Nawaz et al. [90], Copyright (2024), with permission from Elsevier.

Feedstock components	Primary intermediates	BCBU-promoted reactions	Main product pools
Cellulose	Primary vapors: Levoglucosan, furans, aldehydes, ketones	Catalytic pathway: Dehydration ketonization cyclization / Diels-Alder aromatization	Upgraded products: Mono-aromatics/BTX, hydrocarbon-rich vapors
Hemicellulose	Primary vapors: Acetic acid, carbonyls, light volatiles	Catalytic pathway: Decarboxylation decarbonylation hydrogen assisted decarboxylation	Upgraded products: Reduced-acidity vapors, aromatics/hydrocarbons
Lignin	Primary vapors: Guaiacols, syringols, catechols, phenols	Catalytic pathway: Demethoxylation dehydroxylation C–O bond cleavage hydrogen transfer reactions	Upgraded products: Phenol-rich oil after deeper O-removal: BTX/ hydrocarbons
Carbohydrates	Primary vapors: Sugars, furans, small oxygenates	Catalytic pathway: Dehydration decarboxylation cyclization /aromatization cracking	Upgraded products: Mono-aromatics/BTX, hydrocarbon-rich vapors
Lipids	Primary vapors: FFAs, long-chain hydrocarbons, olefin precursors	Catalytic pathway: Decarboxylation/decarbonylation hydrodeoxygenation β-scission/cracking hydrogen transfer	Upgraded products: Long-chain hydrocarbons, diesel-range/hydrocarbon-rich oil aromatics after deeper upgrading
Proteins	Primary vapors: Amides, nitriles, pyrroles, N-containing intermediates	Catalytic pathway: Deamination/denitrogenation C–N cleavage hydrogen transfer	Upgraded products: Lower-N bio-oil, aromatics/hydrocarbons, suppressed N-species

FIGURE 6 | Comprehensive decomposition of biomass products and the catalytic reactions facilitated during the process.

ijer, 2026, 1, Downloaded from https://onlinelibrary.wiley.com/doi/10.1155/er/4175129 by Hanyang University Library, Wiley Online Library on [24/11/2026]. See the Terms and Conditions (https://onlinelibrary.wiley.com/terms-and-conditions) on Wiley Online Library for rules of use; OA articles are governed by the applicable Creative Commons License

TABLE 4 | Biofuel upgrading performance with biochar catalyst.

Entry	Biofuel upgrading process and feedstock	Biochar catalyst	Gas selectivity change	Bio-oil selectivity change (area%)	Ref.
1	Catalytic pyrolysis of EUC	P-doped EUC biochar	—	• Carbonyls: 25→12.09 • Phenolics: 49.61→69.7	[32]
2	Steam reforming of HW derived bio-oil	Ni and Ce-loaded and steam-activated HW biochar	• H_2: 46.8	• Monoaromatic hydrocarbons (MAH): 57.1	[33]
3	Steam reforming of cigarette butt–derived bio-oil	Ni-loaded cigarette butts biochar	—	• Phenols: ≈2.1 • Acids: ≈30	[34]
4	Heavy bio-oil catalytic pyrolysis	Fe-loaded straw and woodchip biochar	—	• Phenols: 60.07→76.49 • Ketones: 26.77→12.69	[35]
5	Catalytic pyrolysis of RS	Ni-loaded RS biochar	• H_2: 3.85→ ≈23 • CO_2: 48.5→33.4	• Phenols: 44→52 • Aromatics: 4→12	[36]
6	Catalytic copyrolysis of walnut shells and palm oil fatty acid distillate	B-doped SCB biochar	—	• Hydrocarbons: 71.5→86.8 • Aromatics: 24.4→36.7 • Aliphatics: 75.5→63.2	[37]
7	Microwave catalytic copyrolysis of bamboo and PE	Zr-loaded bamboo biochar	—	• Aromatics: 31.38→74.13 • Phenols: 0.75→9.39	[38]
8	Catalytic pyrolysis of PW sawdust	CO_2-activated and Fe-loaded PW biochar	—	• Aromatics: ≈4→ ≈20 • Phenols: ≈6→ ≈48	[39]
9	Catalytic pyrolysis of wood dust	NaOH and CO_2-activated EN biochar	• H_2: 0.77→ 2.46 • CO: 5.69→8.6	• Monophenols: 11.61→ 59.46	[40]
10	Catalytic pyrolysis of seaweed	Cu-loaded seaweed biochar	—	• Toluene: 84.24	[41]
11	Catalytic pyrolysis of tobacco stem	Fe-loaded RH biochar	• H_2: ≈38→ 49.91 • CO_2: ≈20→12.87	• Phenols: 22.18→ 57.99	[42]
12	Microwave catalytic pyrolysis of FR	Mn-loaded FR biochar	—	• Phenols: 61→63.66	[43]
13	Catalytic pyrolysis of lignin	Fe and Ni coloaded PW biochar	—	• Phenolics: ≈70→ 90.46 • Phenol: 14.52→ 49.02	[44]
14	Catalytic pyrolysis of bagasse	AAEM removed bagasse biochar	—	• Phenols: 25.8→ 47.7	[45]
15	Catalytic copyrolysis of CV and LDPE	Ni-loaded lignin biochar mixed with HZSM-5	—	• Benzene, toluene, and xylene: 0→ ≈49	[46]
16	Microwave catalytic copyrolysis of CV and bagasse	Fe-loaded CV and bagasse biochar	—	• Hydrocarbons: ≈15→ 26.01 • Aromatics: ≈4→19.53	[47]
17	Catalytic copyrolysis of DF and LDPE	Nanocellulose biochar	• H_2: ≈13→ ≈57 • CO_2: ≈30→≈10	• MAH: ≈17→ 57	[48]
18	Catalytic copyrolysis of CP and polystyrene	CP biochar	—	• Mono-aromatics: ≈60→≈96	[49]
19	CTH of rape straw bio-oil	CuO-loaded rape straw biochar	—	• Alcohols: ≈40→ 70	[50]

(Continues)

ijer, 2026, 1, Downloaded from https://onlinelibrary.wiley.com/doi/10.1155/er/4175129 by Hanyang University Library, Wiley Online Library on [24/11/2026]. See the Terms and Conditions (https://onlinelibrary.wiley.com/terms-and-conditions) on Wiley Online Library for rules of use; OA articles are governed by the applicable Creative Commons License

TABLE 4 | (Continued)

Entry	Biofuel upgrading process and feedstock	Biochar catalyst	Gas selectivity change	Bio-oil selectivity change (area%)	Ref.
20	Catalytic pyrolysis of PW	Fe-loaded PW biochar	—	• Phenols: 15.42→ 91.67	[51]
21	Catalytic pyrolysis of PW	Ni and P coloaded PW biochar	—	• Aliphatics: 5→ 10.12 • Aromatics: 4→36.47	[52]
22	Catalytic copyrolysis of DF and LDPE	Corn stover biochar	—	• Aliphatics: ≈82	[53]
23	Microwave catalytic pyrolysis of PS	Fe-loaded PS biochar	—	• Aromatics: 2.2→17.95	[54]
24	Catalytic pyrolysis of PW	Fe-loaded PW biochar	—	• Phenols: ≈17→ 0 • Toluene: 0→≈66	[55]
25	Microwave catalytic pyrolysis of bamboo	Zr-loaded bamboo biochar	• H_2: ≈29→ ≈47	• Aromatics: ≈0→ 42.54 • Phenols: 48.62→ ≈15	[56]
26	Microwave catalytic copyrolysis of *Chlorella* and waste cooking oil	P-doped soybean straw biochar	• H_2: ≈5→ ≈33 • CO_2: ≈35→≈10	• O-containing products: ≈25→ ≈3 • Aromatics: ≈13→≈57	[57]
27	Catalytic pyrolysis of olive pomace	NiO-loaded olive pomace biochar	—	• 47.1% conversion of oxygenated compounds	[58]
28	Catalytic pyrolysis of wastewater biosolids	Paper mill sludge biochar	• H_2: ≈32→ ≈43	—	[59]
29	Catalytic pyrolysis of PW	EN biochar	—	• Monophenols: 11.61→ 54.64	[60]
30	Microwave catalytic of CM	N and Fe coloaded bamboo biochar	• H_2: ≈22→ ≈25 • CO_2: ≈23→≈21	• Phenols: 68.78→ 80.28	[61]
31	Transesterification of lipids in SS	SS biochar	—	• Biodiesel: 33.5 wt%	[62]
32	Catalytic copyrolysis of CHR and PP	Co-loaded CHR biochar	—	• Alcohols: ≈50→ ≈18	[63]
33	Palm oil catalytic deoxygenation	Fe-P–loaded palm fiber biochar	—	• Biodiesel: 73.1	[64]
34	Catalytic pyrolysis of wood chip	Ni-loaded poplar biochar	• H_2: 3.01→ 27.15 (mmol/g)	—	[65]
35	Catalytic pyrolysis of wheat straw	Pb-loaded CM biochar	—	• Phenolics: 22.06→ 41.2 • Phenols: 19.06→ 37.5	[66]
36	Catalytic pyrolysis of SS	SS biochar	—	• Aromatics: ≈15→ ≈22 • Aliphatics: ≈20→ ≈32	[67]
37	Catalytic pyrolysis of PW	CO_2-activated PW biochar	—	• Phenols: 15.74→ 78.12 • Acids: ≈28→ ≈0	[15]
38	Catalytic HDO of bio-oil	Ni-loaded and pine nutshell biochar modified Hβ zeolite	—	• Benzene: 36.58	[68]
39	Microwave catalytic pyrolysis of corn cobs	Fe and P codoped *Choerospondias axillaris* biochar	—	• Phenols: 53.58→ ≈58	[69]

(Continues)

ijer, 2026, 1, Downloaded from https://onlinelibrary.wiley.com/doi/10.1155/er/4175129 by Hanyang University Library, Wiley Online Library on [24/11/2026]. See the Terms and Conditions (https://onlinelibrary.wiley.com/terms-and-conditions) on Wiley Online Library for rules of use; OA articles are governed by the applicable Creative Commons License

TABLE 4 | (Continued)

Entry	Biofuel upgrading process and feedstock	Biochar catalyst	Gas selectivity change	Bio-oil selectivity change (area%)	Ref.
40	Catalytic pyrolysis of EN	Cu-loaded EN biochar	—	• Esters: 2.22→ 35.77 • Acids: 32.54→ 0	[70]
41	Catalytic HTL of SP	Ni-loaded SP biochar	—	• Hydrocarbons: 15.05→ 21.06 • N-containing compounds: 42.09→ 32.65	[71]
42	Catalytic pyrolysis of algal biomass	Ni_2P-loaded chicken manure biochar	—	• Aromatics: ≈7→ ≈17 • Aliphatics: ≈20→ ≈37	[72]
43	Catalytic HTL of SP	CeO_2-loaded SP biochar	—	• Hydrocarbons: ≈16→ ≈24	[73]
44	Catalytic pyrolysis of DF	Nanocellulose biochar	• H_2: ≈55→ ≈85	• Phenolic monomers: ≈52→ ≈93	[74]
45	Catalytic pyrolysis of WPKC	Ni-loaded WPKC biochar	—	• Aromatics: ≈5→ 69.5	[75]
46	Microwave catalytic pyrolysis of *Sargassum*	Fe-loaded RH	• H_2: 39.3→ 46.4 • CO_2: 32.7→8.9	• Phenols: 19.3→ 28 • Esters: 29.7→ 42.7	[76]
47	Catalytic pyrolysis of bamboo	CH_3COOK-activated bamboo biochar	—	• Aromatics: 9→ 24 • O-containing compounds: 44→ 20	[77]
48	Catalytic copyrolysis of SS and RH	RH biochar	—	• Hydrocarbons: ≈15→ ≈62	[78]
49	Catalytic pyrolysis of CV	Fe-loaded CV biochar	—	• Hydrocarbons: ≈29→ ≈42 • Acids: ≈20→ ≈11	[79]
50	Catalytic esterification of bio-oil derived from reed	Sulfonated FRS biochar	—	• Phenols: ≈22→45.9	[80]
51	Catalytic pyrolysis of CG	Zn-loaded CG biochar	—	• Aromatics: 15.93→ 47.86 • Oxygenated compounds: 80.31→57.78	[81]
52	Catalytic esterification of lipids derived from cottonseed	Defatted cottonseed biochar	—	• Biodiesel: 97.4 wt%	[82]
53	Catalytic pyrolysis of waste cooking oil	Wheat straw biochar	—	• Aromatics: 81.5	[83]
54	Catalytic HTL of GC	Ga and NiFe-LDO–loaded GC biochar	—	• O/C molar ratio: 0.55→ 0.2 • H/C molar ratio: 1.45→1.28	[84]
55	Catalytic pyrolysis of EN	MB adsorbed EN-derived biochar	—	• Hydrocarbons: 15.52→ 29.09 • Nitrogen compounds: 34.46→17.04	[85]
56	Microwave catalytic pyrolysis of PW	FeCo-loaded PW biochar	• H_2 184% increase	• Phenols: 55→74	[86]
57	Catalytic pyrolysis of CS	N-doped CS and CD-derived biochar	—	• 8.32% increase in phenols	[87]
58	Catalytic pyrolysis of RH	P-doped PW sawdust biochar	—	• Acids: 20.77→ ≈ 2 • Phenols: 30.28→86.31	[88]

(Continues)

ijer, 2026, 1, Downloaded from https://onlinelibrary.wiley.com/doi/10.1155/er/4175129 by Hanyang University Library, Wiley Online Library on [24/11/2026]. See the Terms and Conditions (https://onlinelibrary.wiley.com/terms-and-conditions) on Wiley Online Library for rules of use; OA articles are governed by the applicable Creative Commons License

TABLE 4 | (Continued)

Entry	Biofuel upgrading process and feedstock	Biochar catalyst	Gas selectivity change	Bio-oil selectivity change (area%)	Ref.
59	Catalytic pyrolysis of DDGS	Fe–Co–loaded DDGS biochar	—	• Hydrocarbons: 36.42→ 44.53 • Aromatics: 0.73→ 25.37	[89]
60	Microwave catalytic pyrolysis of SP	Zn-loaded SP biochar	—	• N-containing compounds: 49.26→ 19.21 • Acids: 14.79→ 52.19	[90]
61	Microwave catalytic pyrolysis of PW	Co–Ni–loaded PW biochar	—	• Hydrocarbons: 47.2 • Styrene: 42.68	[91]
62	Catalytic pyrolysis of corncob	Corncob biochar	—	• Phenols: 55.96	[92]

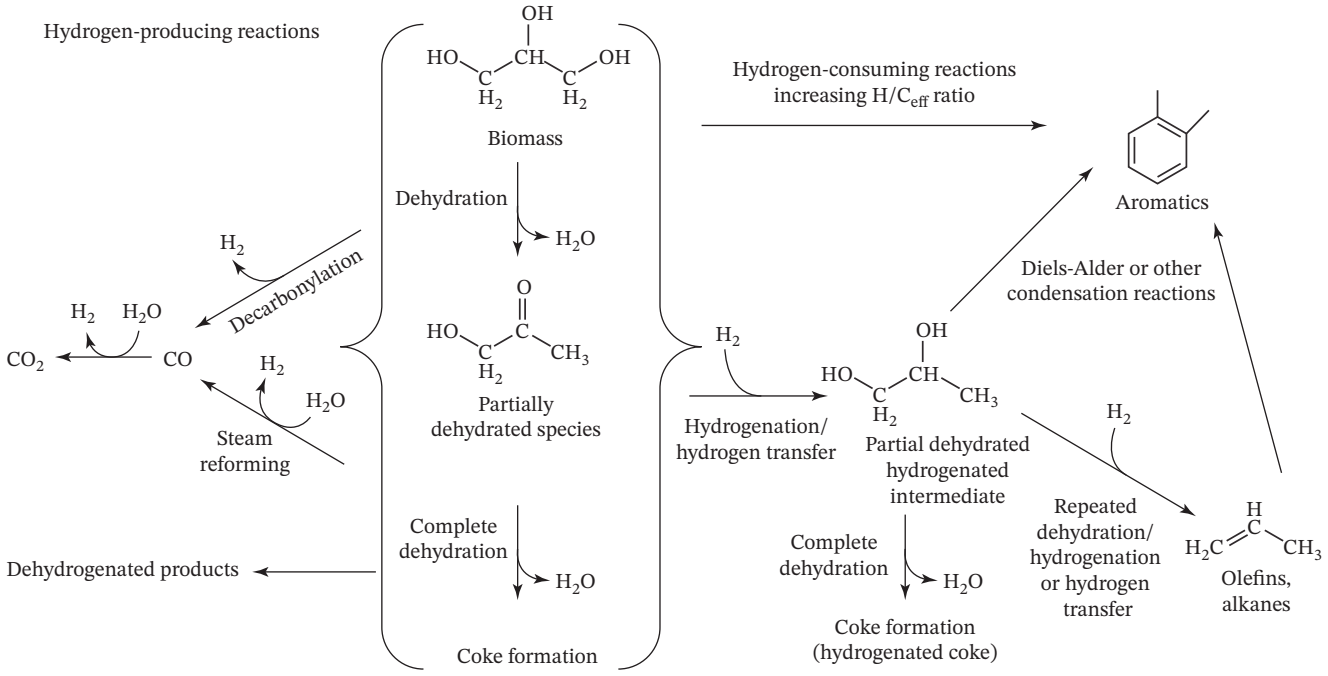


FIGURE 7 | Reaction pathways for pyrolysis for biofuel upgrading. Reproduced with permission from Huber and Corma [106], Copyright 2007, John Wiley and Sons.

chemistry, and coke gasification convert condensable organics into H_2-rich syngas and lighter noncondensables [120]. Compared with pyrolysis or HTL, steam reforming shifts the process objective from preserving condensable liquids to maximizing gas quality, suppressing tar carryover, and maintaining catalyst stability under strong deoxygenating and coke-forming conditions. Therefore, the most effective steam-reforming biochar catalysts combine metal sites for bond scission with supports that can activate steam and sustain oxygen-vacancy–assisted carbon removal.

Biochar-containing photocatalytic H_2 production is more distant from direct bio-oil upgrading but is relevant to integrated hydrogen–assisted biorefinery concepts. In this route, biochar is coupled with a semiconductor, such as TiO_2, and acts as a conductive and defect-rich scaffold that improves charge separation, interfacial electron transfer, and light-response behavior [121, 122]. Because the main product is H_2 rather than upgraded bio-oil, these systems should be evaluated as potential H_2-supply modules rather than as direct BCBU routes.

Esterification and transesterification are liquid-phase stabilization routes rather than deep-cracking or gasification routes. In esterification (Figure 12a), carboxylic acids in bio-oil react with an alcohol over Brønsted acid sites to form esters and water, thereby reducing acidity, corrosivity, and viscosity [125]. Because esters are less corrosive than carboxylic acids, esterification reduces the corrosivity of oil. During transesterification (Figure 12b), triglycerides react with short-chain alcohols to form fatty acid alkyl esters and glycerol, whereas fatty acids react with short-chain alcohols via esterification to form esters and water [126, 127]. These routes are used when the main objective is to stabilize or directly upgrade liquid fuels, rather than to maximize aromatics or syngas yields. Accordingly, the best catalyst for esterification/transesterification is usually not the one

ijer, 2026, 1, Downloaded from https://onlinelibrary.wiley.com/doi/10.1155/er/4175129 by Hanyang University Library, Wiley Online Library on [24/11/2026]. See the Terms and Conditions (https://onlinelibrary.wiley.com/terms-and-conditions) on Wiley Online Library for rules of use; OA articles are governed by the applicable Creative Commons License

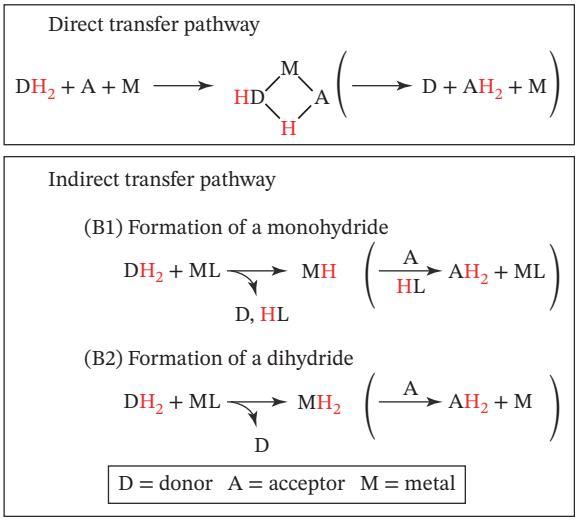


FIGURE 8 | CTH mechanisms. Reprinted from Baráth [108] and licensed under CC BY 4.0.

that drives the deepest cracking, but rather one whose acid–base character and pore accessibility match those of the dominant liquid-phase substrates.

4.2 | Primary Formation Mechanisms and Major Product Pools

In lignocellulosic feeds, cellulose and hemicellulose are first depolymerized to anhydrosugars, furans, aldehydes, ketones, and acids, whereas lignin follows radical depolymerization pathways that generate guaiacyls, syringols, catechols, phenols, methoxyphenolics, and monoaromatics through demethoxylation, dehydroxylation, and ring rearrangement [52, 128]. Therefore, the catalytic upgrading of lignocellulose-derived vapors usually involves competition between oxygen retention and oxygen removal, with phenols and aromatic hydrocarbons appearing during secondary catalytic reactions such as outrun condensation and char-forming routes.

These intermediate pools were strongly coupled rather than independent. Furans, ketones, acids, and phenolics compete through shared deoxygenation, hydrogen transfer, cyclization, oligomerization, and condensation pathways; therefore, the enrichment of one product family usually means that another family has been intercepted before condensation or before a different secondary route becomes dominant [52, 78, 128]. As a result, a catalyst should be interpreted as redirecting reaction traffic through a network rather than acting on a single isolated molecule class.

The precursor landscape substantially changed for algae, sludge, and other lipid- and protein-rich feeds. Lipids first undergo ester bond cleavage to form free fatty acids, which subsequently undergo cracking and deoxygenation via decarboxylation, decarbonylation, and β-scission to produce hydrocarbon fragments [129, 130]. Proteins first undergo peptide bond cleavage to form amino acids and short peptides, which subsequently react via deamination, decarboxylation, dehydration, and cyclization to form amides, amines, nitriles, pyrroles, and other nitrogen-containing intermediates [129]. In such systems, successful upgrading requires simultaneous control of oxygen and nitrogen removal and radical stabilization, which is why metal-assisted hydrogen transfer and denitrogenation are disproportionately important in HTL and in the catalytic processing of algal vapors.

For plastic-containing feeds, the reaction network was strongly polymer-dependent. Polyolefins (polyethylene [PE]/polypropylene [PP]) and polystyrene mainly provide hydrogen-rich radicals that promote hydrogen transfer, deoxygenation, and aromatization of biomass-derived oxygenates [131, 132]. Finally, because these products emerge from a coupled reaction network, catalyst properties are most meaningfully interpreted by asking which intermediate pool and rate-limiting elementary step they redirect, rather than by asking whether they simply increase the overall activity.

4.3 | Integrated Synthesis–Descriptor–Mechanism Framework for BCBU

The performance of BCBU is governed by the relationship between catalyst preparation, physicochemical descriptors, and

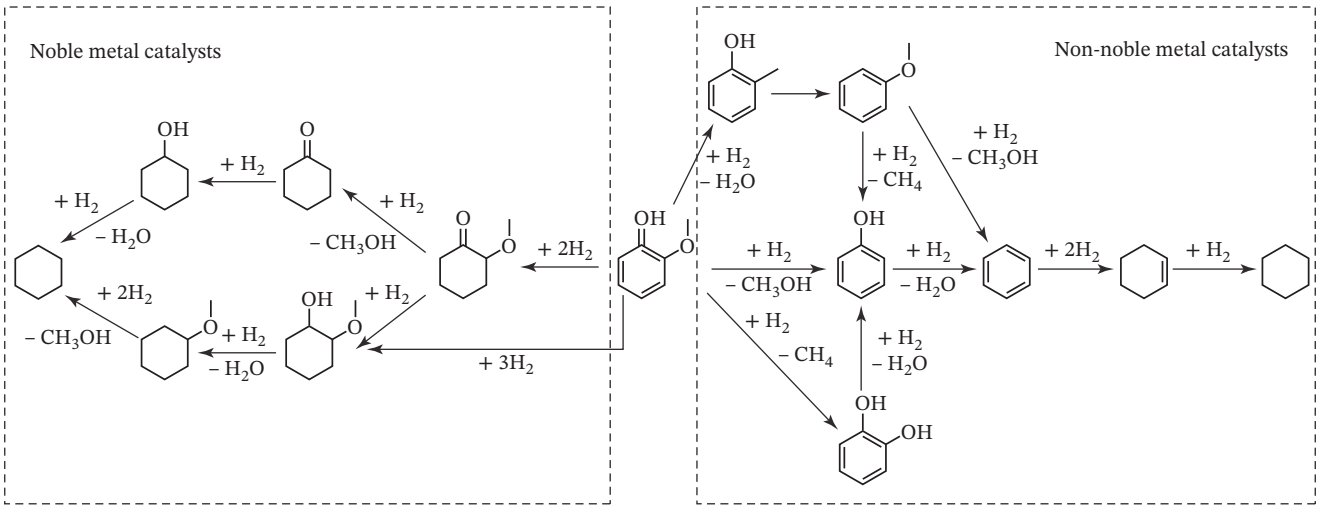


FIGURE 9 | Reaction pathways for HDO of a model bio-oil compound. Reprinted from Hellinger et al. [112], Copyright (2014), with permission from Elsevier.

ijer, 2026, 1, Downloaded from https://onlinelibrary.wiley.com/doi/10.1155/er/4175129 by Hanyang University Library, Wiley Online Library on [24/11/2026]. See the Terms and Conditions (https://onlinelibrary.wiley.com/terms-and-conditions) on Wiley Online Library for rules of use; OA articles are governed by the applicable Creative Commons License

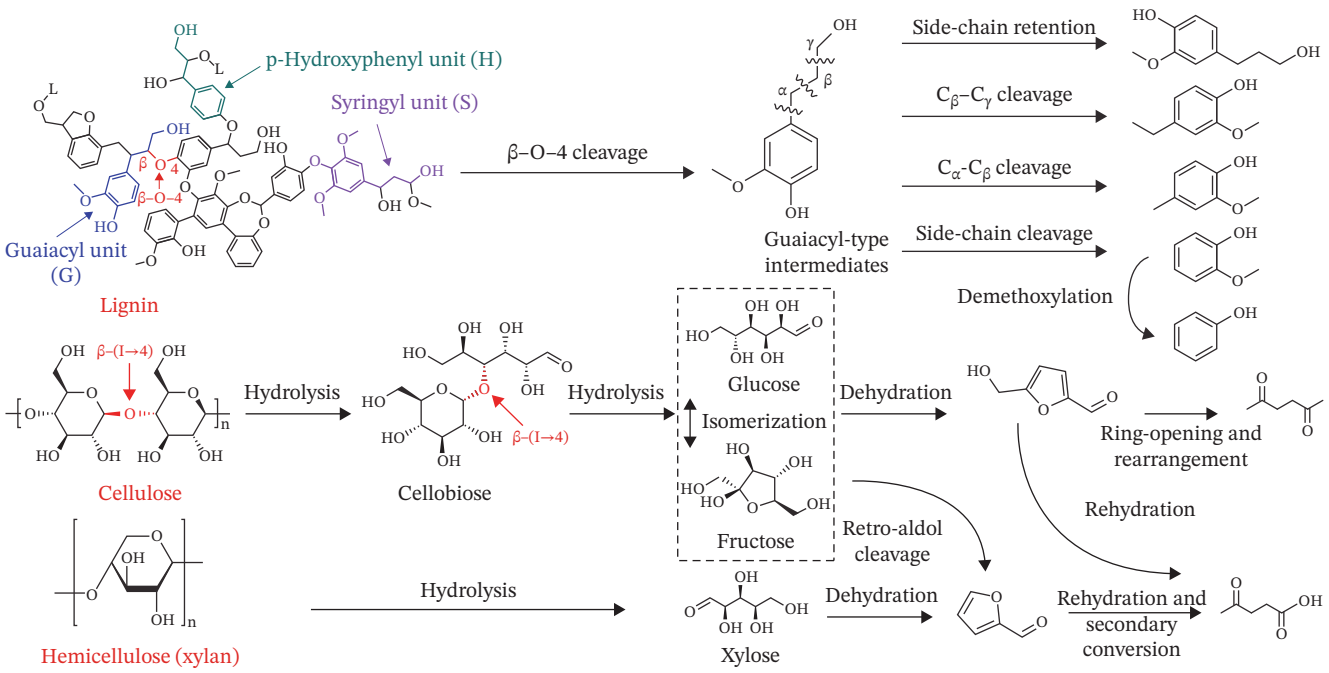


FIGURE 10 | Reaction pathways for HTL of biomass components. Reprinted from Gong et al. [116] and licensed under CC BY 4.0.

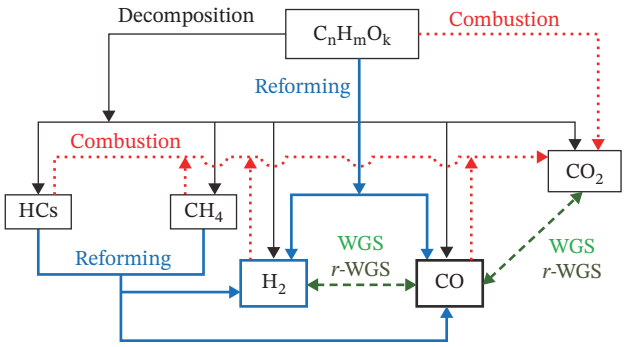


FIGURE 11 | Reaction pathways for steam reforming of bio-oil. Reprinted from Arandia et al. [119], Copyright (2017), with permission from Elsevier.

the mechanism of the selected upgrading route. Consequently, the performance of BCBU should be perceived as hierarchical rather than additive. Specifically, the selection of the upgrading route establishes the primary reaction constraint, while textural and structural properties regulate access to active sites. Additionally, surface chemistry influences adsorption and acid–base pathways, and heteroatom or metal functions dictate the extent and endpoint of deoxygenation. This comprehensive perspective shifts the focus of design from identifying a universally most active biochar catalyst to determining which synthesis-derived descriptor set aligns best with a specific upgrading route and target product. To connect the route definitions in Section 4.1 with catalyst-design logic, Table 5 summarizes the application mode, reaction environment, main catalytic role, and key design/evaluation criteria for each upgrading route. Thus, Table 5 should be read not as a performance ranking but as a framework for interpreting why the same biochar property, such as surface area, acidity, metal loading, heteroatom doping, pore accessibility, or microwave responsiveness, can have different catalytic meanings in different upgrading routes.

Catalyst preparation first defines a descriptor envelope. Conventional pyrolysis converts biomass into a carbon-rich matrix under oxygen-limited conditions, producing biochar with relatively high carbonization degree, thermal stability, retained mineral species, and tunable pore structure [93]. Microwave-assisted pyrolysis generates catalysts with additional energy-coupling descriptors because polar groups, defects, graphitized domains, and metal-containing phases can convert electromagnetic energy into localized heat through dipole polarization, interfacial polarization, conduction loss, or magnetic loss [61]. HTC-derived biochar or hydrochar is formed under aqueous and relatively low-temperature conditions and therefore often retains oxygen-rich surfaces that favor metal deposition, interfacial interaction, and contact with wet feedstocks or liquid-phase intermediates [101, 103]. These preparation-derived properties become catalytically meaningful only when they are translated into route-relevant functions.

In this context, the textural and structural characteristics determine the transport challenges that a catalyst can address. Surface area, by itself, does not serve as a universal indicator of activity. It gains significance only when the distribution of pore sizes, pore connectivity, and carbon ordering align with the size, phase, and residence-time specifications of the chosen upgrading pathway. Micropores can intensify adsorption and secondary conversion of small vapors; mesopores can improve access for bulky lignin fragments, lipid-derived species, and liquid-phase oxygenates; and interconnected pores can shorten diffusion paths [133]. The contrasting behavior of B- and P-doped sugarcane bagasse (SCB) biochars illustrates that surface area alone does not determine the performance of a catalyst [37]. B doping increased surface area, micropore volume, hydrocarbon content, and aromatic selectivity, whereas P doping decreased the surface area but still increased aromatic and diesel-range hydrocarbon selectivity, indicating that structural advantages and chemically induced selectivity can compensate for one another depending on the

ijer, 2026, 1, Downloaded from https://onlinelibrary.wiley.com/doi/10.1155/er/4175129 by Hanyang University Library, Wiley Online Library on [24/11/2026]. See the Terms and Conditions (https://onlinelibrary.wiley.com/terms-and-conditions) on Wiley Online Library for rules of use; OA articles are governed by the applicable Creative Commons License

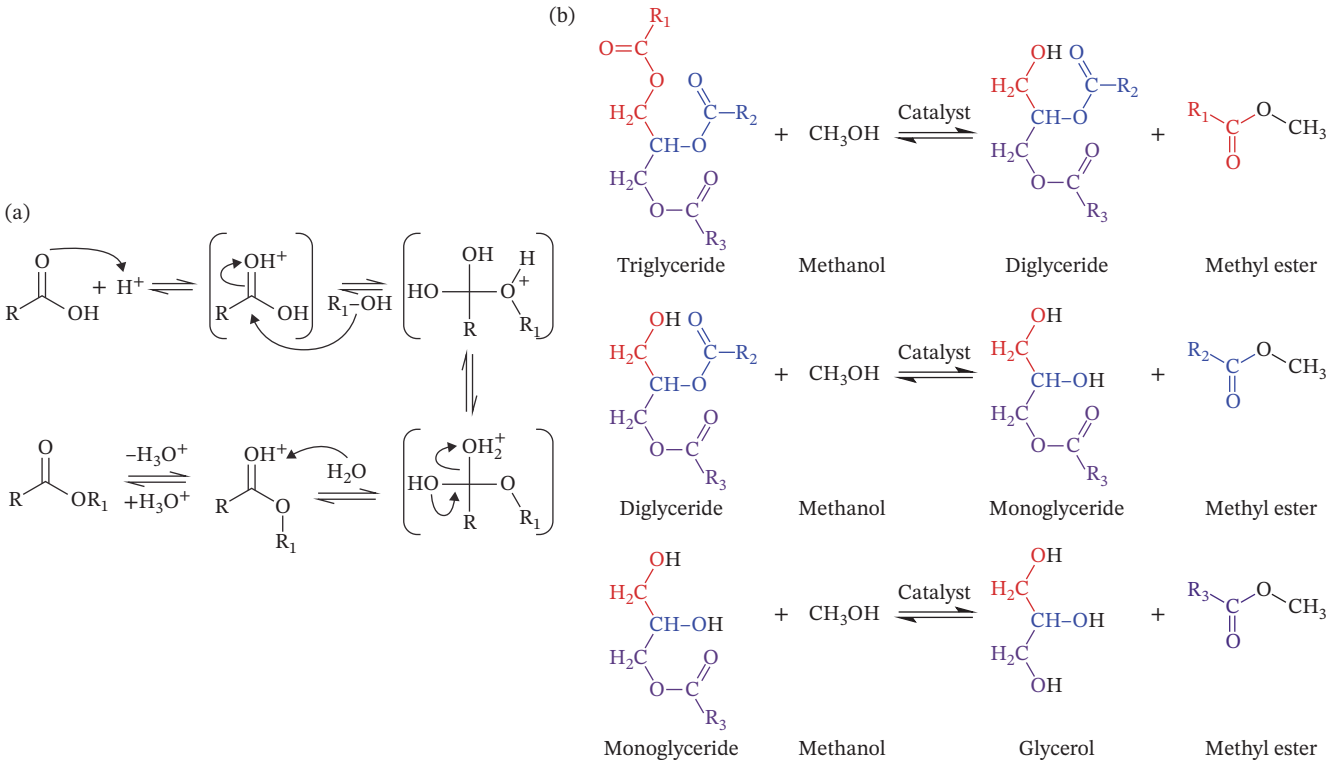


FIGURE 12 | Major reaction routes for (a) esterification and (b) transesterification. Part (a) reproduced with permission from Ciddor et al. [123], Copyright 2015, John Wiley and Sons; part (b) reproduced from Amador-Gómez et al. [124] and licensed under CC BY 4.0.

reaction pathway. Similarly, N–Fe biochar with moderate surface area enhanced phenol production under microwave irradiation because defect-assisted microwave coupling and local heat generation compensated for limited surface area [61].

Once intermediates reach the catalyst surface, the next control layer is surface chemistry. Surface oxygen functionalities, ash-derived alkali and alkaline earth metal (AAEM) species, grafted sulfonic groups, phosphate-derived Brønsted-acid sites, mineral/basic sites, and the hydrophilic/hydrophobic balance of the carbon surface regulate adsorption–desorption behavior and the local acid–base microenvironment. Mineral-rich or basic surfaces can promote decarboxylation/decarbonylation and transesterification, while acid–base surface environments can also direct ketonization pathways [134, 135]. In contrast, acidic surfaces are more closely associated with dehydration, esterification, and aromatization [80, 136–138]. This layer should be distinguished from heteroatom doping. Surface chemical properties mainly regulate adsorption, wettability, and local acid/base reactions, whereas heteroatom doping alters the electronic structure and defect chemistry of the carbon matrix [139]. CH_3COOK-activated bamboo biochar, which contains abundant C = O, C–O, and –OH groups, increased aromatics while reducing O-containing compounds, indicating that oxygenated/basic surface sites can promote secondary deoxygenation and ring formation [77]. Oxygen-containing surface groups often improve wettability and interfacial contact with polar liquid–phase intermediates and can enhance interactions with oxygenates/tars in pyrolysis vapors [140]. In liquid-phase acid-catalyzed upgrading, strong surface acidity and neighboring functional groups can outweigh large structural differences when mass-transfer limitations are weak, as suggested by sulfonated carbon catalysts and consistent with the sulfonated reed catalyst [80]. In other words, when mass-transfer limitations are weak during liquid-phase upgrading, the local acidic environment at the active sites can dominate over porosity.

Feedstock-derived AAEMs should be distinguished from intentionally introduced metals because their catalytic roles depend on their origin, chemical form, and location within the biochar. A direct comparison between intrinsic and externally introduced K revealed that the original wheat-straw biochar contained 6.22 wt % K, whereas an acid-washed biochar reloaded with KOH exhibited 7.96 wt% K [141]. Despite the similar K content, intrinsic K was more strongly integrated and distributed within the carbon matrix, exhibited lower volatility, and preferentially facilitated biochar self-reforming with H_2O and CO_2. In contrast, externally introduced K was concentrated on the biochar surface, exhibited greater volatility, and demonstrated enhanced activity in volatile cracking and the consumption of oxygen-containing functionalities. This comparison illustrates that the catalytic contribution of AAEMs cannot be predicted solely based on elemental concentration. Their speciation and spatial distribution also play a crucial role in determining whether they primarily modify the biochar matrix or directly convert pyrolysis vapors.

Heteroatom doping acts as a pathway-selection strategy rather than as a generic activity-enhancement method. B and P usually create polarized or electron-deficient environments that enhance acidity and favor dehydration, decarboxylation, and cyclization [37]. N introduces lone pair–containing defects that facilitate adsorption, electron transfer, and microwave polarization [142, 143]. S-containing or sulfonated functionalities are most relevant when strong Brønsted acidity is required, especially in acid-

ijer, 2026, 1, Downloaded from https://onlinelibrary.wiley.com/doi/10.1155/er/4175129 by Hanyang University Library, Wiley Online Library on [24/11/2026]. See the Terms and Conditions (https://onlinelibrary.wiley.com/terms-and-conditions) on Wiley Online Library for rules of use; OA articles are governed by the applicable Creative Commons License

TABLE 5 | Route-specific application modes and key design criteria of biochar-based catalysts for biofuel upgrading.

Upgrading route	Application mode/reaction environment	Main role of biochar-based catalyst	Key design and evaluation criteria
Catalytic pyrolysis	• Dry, oxygen-free vapor-phase route • Biochar used in situ with biomass or ex situ in a downstream bed • Targets rapid vapor upgrading before condensation	• Vapor-phase reaction-network regulator • Intercepts short-lived oxygenated vapors and radicals • Promotes cracking, deoxygenation, denitrogenation, and aromatization	• Hierarchical pores and efficient vapor contact • Accessible acid/base, mineral, heteroatom, or metal redox sites • Evaluate phenol, aromatic, hydrocarbon, acid, and O/N-containing product distributions
Microwave-assisted catalytic pyrolysis	• Microwave-driven pyrolysis or copyrolysis • Biochar used as both catalyst and microwave-responsive solid • Useful when rapid internal heating and controlled localized hotspots are beneficial	• Dual catalyst/susceptor • Converts electromagnetic energy into localized heat • Accelerates depolymerization, cracking, deoxygenation, and aromatization	• Dielectric loss, conductivity, graphitization degree, and defect density • N/P polar sites and Fe/Ni/Co or bimetallic hotspot formation • Evaluate heating efficiency, phenol/aromatic/hydrocarbon selectivity, H_2 generation, and microwave-response stability
CTH	• Liquid-phase upgrading with methanol, alcohols, formic acid, or formate • Applied to raw bio-oil, carbonyl-rich oxygenates, and C–O–rich intermediates • Operates under hydrogen-donor rather than vapor-cracking conditions	• Liquid-phase hydrogen-transfer platform • Activates hydrogen donors and stabilizes oxygenated intermediates • Promotes selective C = O hydrogenation and C–O hydrogenolysis	• High metal dispersion and controlled metal valence state • Moderate Lewis acid–base/redox balance plus mesopore accessibility and surface wettability • Evaluate donor use, carbonyl conversion, alcohol selectivity, and reusability
Catalytic HTL	• Wet upgrading of high-moisture biomass slurries in hot-compressed water • Biochar used as suspended catalyst or metal support • Suited to algae, sludge, food waste, and other wet feedstocks	• Hydrothermal liquid-phase upgrading catalyst • Stabilizes soluble intermediates during biocrude formation • Supports hydrogen transfer, decarboxylation, denitrogenation, and repolymerization suppression	• Hydrothermal stability under compressed-water conditions • Liquid-phase mass transfer and mesopore accessibility for soluble intermediates • Evaluate biocrude yield, HHV, O/C, and N reduction, hydrocarbon fraction, and boiling-range distribution
Steam reforming	• Downstream high-temperature conversion of bio-oil, tar, or oxygenated vapors with steam • Biochar-based catalyst placed in a reforming bed • Targets H_2-rich syngas rather than condensable liquid products	• Disperses reforming metals and assists steam activation • Promotes C–C C–H cleavage, water–gas shift chemistry, tar conversion, and coke removal	• Strong metal–support interaction and Ni/Fe/Ni–Ce dispersion • Steam-accessible porosity, oxygen-vacancy retention, antisintering properties, and coke resistance • Evaluate H_2 yield, H_2/CO ratio, tar conversion, time-on-stream stability, coke amount, support gasification resistance, carbon loss, and metal sintering
Esterification/ transesterification	• Liquid-phase stabilization of acid-rich bio-oils, free fatty acids, lipids, or triglycerides with alcohols • Used when the target is fuel stabilization or biodiesel formation • Not intended for deep vapor cracking or syngas production	• Solid acid/base catalyst for liquid-fuel stabilization • Converts acids or lipids into esters or fatty acid methyl ester (FAME) • Reduces acidity, viscosity, and corrosivity	• Accessible Brønsted acid/basic sites such as SO_3H, phosphate-derived, or mineral/basic sites • Pore accessibility to bulky lipid/free-fatty-acid substrates and alcohol/water tolerance • Evaluate ester or FAME yield, acid-value reduction, viscosity reduction, conversion, and reuse cycles

ijer, 2026, 1, Downloaded from https://onlinelibrary.wiley.com/doi/10.1155/er/4175129 by Hanyang University Library, Wiley Online Library on [24/11/2026]. See the Terms and Conditions (https://onlinelibrary.wiley.com/terms-and-conditions) on Wiley Online Library for rules of use; OA articles are governed by the applicable Creative Commons License

catalyzed esterification or liquid-fuel stabilization [144]. In microwave-assisted catalytic pyrolysis, N-containing defects contribute to dielectric loss and localized heating [61]. In CTH and platform molecule HDO, N-containing sites can stabilize metal nanoparticles or form M-Nx environments that assist oxygenate activation and liquid-phase hydrogen transfer [145]. Thus, the role of heteroatom doping varies according to the reaction environment. It can modulate acid-driven vapor upgrading, improve microwave coupling, stabilize metal sites, or alter hydrogen transfer pathways.

Metal loading fundamentally determines catalytic function by integrating specific capabilities such as redox processes, bond cleavage, hydrogen transfer, hydrogenolysis, and reforming into the carbon framework. Fe-based catalysts most often favor selective C–O cleavage, demethoxylation, and phenol enrichment [51]. Ni is generally more effective in hydrogen transfer and reforming reactions [146]. Co tends to push oxygenates toward hydrocarbons, particularly aromatic hydrocarbons [147]. Promoter metals, such as Ce, can further alter the oxygen vacancy density, coke resistance, and metal–support interactions [148]. Therefore, metal-loaded BCBU should be interpreted according to the target endpoint, such as phenol-rich vapor upgrading, liquid-phase CTH/HDO, denitrogenation, esterification, or H_2-rich reforming, rather than ranked on a single activity scale.

Co-doping and bimetallic modification are useful only when they provide complementary catalytic functions. In metal–metal systems, one component may provide dominant bond cleavage or hydrogen transfer chemistry, while the other stabilizes the oxidation state, improves dispersion, or adds oxygen-vacancy chemistry [33, 149]. Fe–Ni coloaded biochar further illustrates the complementary function principle because Fe-assisted aryl–O cleavage and Ni-assisted hydrogen transfer can jointly promote phenol formation from lignin-derived intermediates [44]. In metal-heteroatom systems, the heteroatom tunes the electronic environment, adsorption pattern, microwave response, or metal anchoring of the carbon matrix, while the metal performs the redox or bond-breaking step [150]. Co-doping should not be regarded as inherently superior to single-site modification. It becomes beneficial only when each dopant compensates for a clearly identified limitation, such as insufficient bond scission, weak hydrogen transfer, poor microwave absorption, low metal dispersion, or poor coke resistance. This explains why N–Fe systems are effective for microwave-assisted phenol enrichment, Ni–Ce systems for H_2-rich reforming with coke control, and Co–Ni/N-rich carbon systems for furan-type product formation in liquid-phase platform molecule upgrading [33, 61, 151].

The practical effects of metal loading are more clearly demonstrated by changes in the yield and properties of the resulting bio-oil. In the catalytic pyrolysis of lignin using pine-sawdust–derived biochar, the bio-oil yield decreased from 27.25 wt% without a catalyst to 24.85 wt% with unloaded biochar and further to ~22 wt % following the introduction of Fe. Although the liquid yield was reduced, the metal-loaded biochar catalysts enhanced the relative content of phenolic compounds to a range of 79.69%–90.46% [44]. This example illustrates that metal loading can enhance the concentration of target compounds while reducing the total yield of condensable liquids through further conversion of pyrolysis vapors. Similar yield–composition trade-offs have been observed in microwave-assisted biomass pyrolysis [86]. Compared to unmodified biochar, Fe loading increased the yield of combustible gas by ~50%, suggesting that a portion of the condensable vapors was redirected towards gas formation. Fe–Ni–loaded biochar further increased the combustible-gas yield to 574.84 mL/g while producing a bio-oil containing 33.9% hydrocarbons. In contrast, Fe–Co–loaded biochar increased the mono-phenol content of the oil to 74.0%. These findings indicate that metal-loaded biochars can significantly simplify bio-oil composition and enrich hydrocarbons or phenolic compounds, although these enhancements may be accompanied by a shift in the overall product distribution from liquid to gas.

Metal loading can enhance bulk fuel-quality indicators during the liquid-phase upgrading process. In the upgrading of rice-straw bio-oil using supercritical ethanol with CuO–Fe_3O_4 supported on activated rice-straw biochar, the higher heating value (HHV) increased from 21.3 to 32.1 MJ/kg, and the pH rose from 4.3 to 5.63 [152]. Additionally, over 90% of the carboxylic acids were converted into esters. The upgraded oil exhibited reduced oxygen content and increased carbon and hydrogen contents compared to the raw bio-oil. Consequently, metal-loaded biochar not only alters the product distribution but also enhances fuel quality by decreasing acidity and oxygen content while increasing energy density.

The impact of metal-loaded BCBU on the storage stability of bio-oil remains inadequately defined. For instance, a two-step esterification followed by HDO using Ni–Mo_2C supported on activated biochar resulted in 69% HDO and an overall carbon yield of 67%, suggesting significant chemical stabilization of oxygenated components [153]. Nevertheless, there was no documentation of long-term alterations in viscosity, phase separation, molecular weight, or insoluble content. In contrast, direct storage tests in a similar carbon-supported noble-metal HDO system indicated minimal changes in the properties of the upgraded heavy oil over a 12-week storage period [154]. This finding provides the type of evidence necessary to verify storage stability. However, it cannot be specifically attributed to the biochar support.

Metal-loaded biochars tend to enhance the composition and fuel quality of bio-oil more consistently than they increase the total liquid yield. These biochars typically enrich phenols, aromatics, hydrocarbons, alcohols, or esters while reducing acids, carbonyl compounds, and other oxygen- or nitrogen-containing species. However, intensified secondary cracking, reforming, and deoxygenation processes can reduce the yield of condensable liquids by redirecting carbon towards gas or coke. Consequently, it is essential to evaluate bio-oil yield independently from improvements in composition and fuel quality. Furthermore, as most studies deduce stability from reduced acidity or oxygen content rather than directly measuring aging behavior, the effects of metal-loaded biochar should generally be characterized as compositional upgrading or potential stabilization. This characterization should remain unless storage stability is confirmed through measurements of viscosity, phase separation, molecular weight, or insoluble content.

Descriptor layers can be applied differently to each upgrading route. In vapor-phase catalytic pyrolysis, accessible pore networks, vapor-contact efficiency, acid/base sites, retained AAEM species, heteroatom-derived acidity, and metal-assisted C–O cleavage are

ijer, 2026, 1, Downloaded from https://onlinelibrary.wiley.com/doi/10.1155/er/4175129 by Hanyang University Library, Wiley Online Library on [24/11/2026]. See the Terms and Conditions (https://onlinelibrary.wiley.com/terms-and-conditions) on Wiley Online Library for rules of use; OA articles are governed by the applicable Creative Commons License

central to phenol, aromatic, or hydrocarbon formation. Fe-loaded biochar for phenol-rich oil formation illustrates this relationship. Fe sites promote C–O cleavage and demethoxylation of lignin-derived methoxyphenols, whereas the pyrolysis-derived carbon matrix provides vapor-phase contact and secondary-conversion sites [51]. However, the product endpoint depends on how transport, surface chemistry, and metal identity interact. Fe can be advantageous for selective phenol production, whereas Ni or bimetallic systems may become more appropriate when denitrogenation, hydrocarbon formation, or reforming is targeted [33].

In microwave-assisted catalytic pyrolysis, the catalyst must serve as both a chemically active phase and an energy-coupling material. Therefore, dielectric loss, defect density, graphitization degree, conductivity, and metal-assisted hotspot formation become route-defining descriptors in addition to conventional acidity, porosity, and redox properties [61, 86]. In N–Fe coloaded biochar, N-containing defects enhance microwave absorption and local heat generation, whereas Fe sites provide C–O cleavage and redox chemistry for phenol-enriched bio-oil formation [61]. In Fe–Co- or Co–Ni–modified microwave-derived biochars, metal sites can simultaneously assist microwave absorption and bond cleavage, linking these catalysts to hydrocarbon product formation under microwave-assisted upgrading conditions [91].

In HTL and other wet-feedstock routes, the catalyst operates in hot compressed water rather than in a dry vapor stream. Consequently, hydrothermal stability, liquid-phase accessibility, mesopore accessibility, and wettability become more important than dry surface area alone. In such liquid-phase environments, oxygen-containing groups can improve interfacial contact with polar intermediates, while mesopores and metal dispersion become more important than vapor-contact efficiency [117, 118, 140].

CTH and platform-molecule HDO represent liquid-phase hydrogen-transfer or hydrogenolysis routes rather than vapor-cracking routes. In CTH, the catalyst must activate both a hydrogen donor and a liquid-phase oxygenated compound. Therefore, mesoporosity, wettability, metal dispersion, and balanced acid/redox sites are critical [107, 109]. CuO-loaded rape-straw biochar increased alcohol formation during bio-oil CTH with methanol, indicating that the biochar support can provide liquid-phase oxygenate accessibility, while CuO sites provide hydrogen-transfer functionality [50]. In platform molecule upgrading, biochar acts as a carbon scaffold that influences product endpoints rather than as an inert support. Ni supported on sulfuric-acid–modified biochar has been used for furfural conversion to 2-methylfuran, while Cu–Ni–encapsulated biochar and Co–Ni/N–rich biochar-based carbon catalysts have been applied to HMF conversion to 2,5-dimethylfuran [110, 151, 155]. These cases reinforce that metal loading must be matched to the desired reaction endpoint. Cu-containing systems are appropriate for partial hydrogenation, while those containing Ni are suitable for hydrogenation, hydrogenolysis, and HDO. In contrast, Co–Ni/N–rich systems have advantages to the formation of more complex furan-type products.

In steam reforming and pyrolysis-steam reforming, the target shifts from preserving condensable liquid products to producing H_2-rich syngas. Thus, steam-accessible porosity, thermal stability, metal dispersion, redox-metal stability, oxygen-vacancy retention, coke resistance, and time-on-stream stability become decisive [33, 65, 156]. Ni-loaded biochar can promote C–C/C–H cleavage, tar cracking, and reforming reactions, whereas Ni–Ce biochar can use Ce^{4+}/Ce^{3+} cycling to generate oxygen vacancies that assist carbon-deposit removal and reforming stability [33]. This reforming-oriented role differs fundamentally from phenol enrichment or alcohol formation because the catalyst is evaluated by H_2 yield, tar conversion, coke suppression, and long-term stability rather than by liquid product selectivity.

Esterification and transesterification require a different descriptor set because these routes are used for liquid-fuel stabilization or biodiesel formation rather than deep cracking, aromatization, or syngas production. Accessible Brønsted acid sites, pore accessibility to carboxylic acids, free fatty acids, or triglycerides, alcohol tolerance, water tolerance, and reusability are more important than strong vapor-cracking ability [125–127]. The case of sulfonated reed biochar illustrates that a low surface area does not inherently limit high performance, particularly when acid-catalyzed esterification serves as the primary mechanism and the active sulfonic environment remains accessible to liquid-phase substrates [80]. As a result, esterification/transesterification should be treated as a targeted stabilization route rather than grouped with deoxygenation routes that seek extensive C–O bond cleavage or aromatic hydrocarbon formation.

In summary, the design of BCBU should be approached by first considering the target route and product endpoint, then working backward to determine the necessary descriptor set, and finally selecting the appropriate synthesis route and posttreatment strategy. In this sense, biochar catalysts should be conceptualized as route-specific catalytic platforms whose synthesis and posttreatment must be selected according to the dominant mechanism, reaction phase, feedstock-derived intermediate pool, and desired product endpoint.

4.4 | Catalyst Stability

Catalyst stability is one of the most critical factors affecting its application prospects [33]. The BCBUs can undergo deactivation by coke formation, structural collapse, and active site leaching, which may limit its reuse rate in industry. Reusability is an important variable affecting the economic and environmental benefits of industrial processes and must therefore be accurately determined. Several studies have evaluated the reusability of BCBUs. For example, Guo et al. [33] found that a biochar-supported Ni–Ce (Ni/Ce = 2) catalyst lost its Brunauer–Emmett–Teller (BET) surface area from 350.6 to 120.8 m^2/g, total pore volume from 0.40 to 0.13 cm^3/g, and average pore size from 23.05 to 18.23 nm, while its average Ni particle size increased from 8.0 to 22.7 nm after five cycles of steam reforming of residual wood/leave mixture. The decrease in the surface area and pore volume was mainly ascribed to carbon accumulation on the catalyst. The growth of metal crystals expedited metal particle aggregation and promoted carbon accumulation, deteriorating the catalytic performance. Also, more use of the catalyst in the biomass steam reforming led to less oxygen vacancies and C–O groups [33]. The loss of oxygen vacancies and C–O groups could decrease the catalytic activity [157]. The biochar support was also oxidized by H_2O and CO_2 and/or replaced with more stable coke with increasing the reaction cycle, affecting the catalyst stability [158].

ijer, 2026, 1, Downloaded from https://onlinelibrary.wiley.com/doi/10.1155/er/4175129 by Hanyang University Library, Wiley Online Library on [24/11/2026]. See the Terms and Conditions (https://onlinelibrary.wiley.com/terms-and-conditions) on Wiley Online Library for rules of use; OA articles are governed by the applicable Creative Commons License

Luo et al. [61] repeated microwave pyrolysis of cow manure (CM) over a N–Fe–doped bamboo-derived biochar catalyst. The use of the catalyst for five cycles decreased the bio-oil yield and phenolic selectivity. After five pyrolysis cycles, the bio-oil yield decreased from 47.97 to 41.73 wt%, and the phenolic selectivity decreased from 80.28% to 70.94%. In addition, during the pyrolysis process, Fe^0 and Fe^{2+} were oxidized to Fe^{3+}, and the reduction of N and Fe and the conversion of N- and Fe-containing species reduced the intensity and number of weak acid sites and medium acid sites on the catalyst. Carbon deposition and a partial pore structure collapse decreased the catalyst's surface area from 265.21 to 52.27 m^2/g and average pore volume from 0.14 to 0.09 cm^3/g [61]. It was also observed that thermal stability of the catalyst collected after the five-cycle pyrolysis is lower than the fresh one, mainly attributed to the carbon deposition and the loss of components with higher mechanical strengths (e.g., graphitic carbon and Fe_3C species).

Zou et al. [53] tried to reuse 10 times a corn stover–derived biochar catalyst in copyrolysis of *Douglas fir* (DF) and low-density PE (LDPE). An increase in reuse cycle decreased the selectivity of monoaromatic hydrocarbons (MAHs) and H_2, most likely due to carbon deposition and loss of active sites on the biochar catalyst [159, 160]. The deactivation of biochar catalyst is because of the loss of active sites caused by coke deposition, structural collapse, and escape of unstable active sites [161–163]. When a biochar feedstock contains AAEMs (e.g., K and Ca), the biochar's ability for coke formation can be reduced [75].

5 | Comparative Analysis of BCBU Performance

5.1 | Comparative Analysis of BCBU Performance in Similar Processes

Various BCBUs have been used for biofuel upgrading. The performance of BCBUs can be evaluated based on the support materials (e.g., metals and heteroatoms) or the biofuel upgrading methods employed (e.g., catalytic pyrolysis and steam reforming). Given that catalytic performance as reported in the literature is significantly influenced by variables such as feedstock type, reactor configuration, reaction temperature, catalyst-to-feedstock ratio, and product-reporting format, direct comparisons across all studies may yield misleading conclusions. Therefore, this review employed a constrained benchmarking approach. For comparisons within the same process, studies were categorized by upgrading route, and only those cases sharing the most frequently overlapping reaction window were included. In catalytic pyrolysis and microwave-assisted catalytic pyrolysis, where sufficient comparable datasets were available, the comparison was limited to reactions conducted at 500–600°C and catalyst-to-feedstock ratios between 2:1 and 1:2. Phenol and hydrocarbon contents were selected as common quantitative indicators because they were the most consistently reported upgraded bio-oil fractions in these studies. Figure 13 summarizes the phenol and hydrocarbon concentrations obtained under the reaction conditions.

A comparative analysis of numerous studies has shown that the catalytic pyrolysis of coconut pericarp (CP) using BCBU derived from CP biochar affords the highest phenol content of 67.08% [49]; this was attributed to the elevated lignin content of CP and the efficacious catalytic action of the CP biochar–containing AAEM species. The catalytic pyrolysis of pine wood (PW) using PW-derived BCBU loaded with Ni and activated with $ZnCl_2$ yielded the highest quantity of hydrocarbons, accounting for 44.79% [52]. This study also reported a phenol content of 33.9%, resulting in a combined phenol and hydrocarbon content of 78.69%, the highest among studies conducted under similar reaction conditions. This phenomenon was attributed to the provision of additional catalytically active sites on the catalyst surface by ZnO particles via $ZnCl_2$ activation, as well as to the extensive surface area and microporous framework of BCBU.

The use of an Fe-loaded furfural residue (FR) biochar catalyst in microwave-assisted catalytic pyrolysis afforded the highest phenol selectivity of 67% [43]; this was attributed to the large pore volume and specific surface area of the FR biochar and the

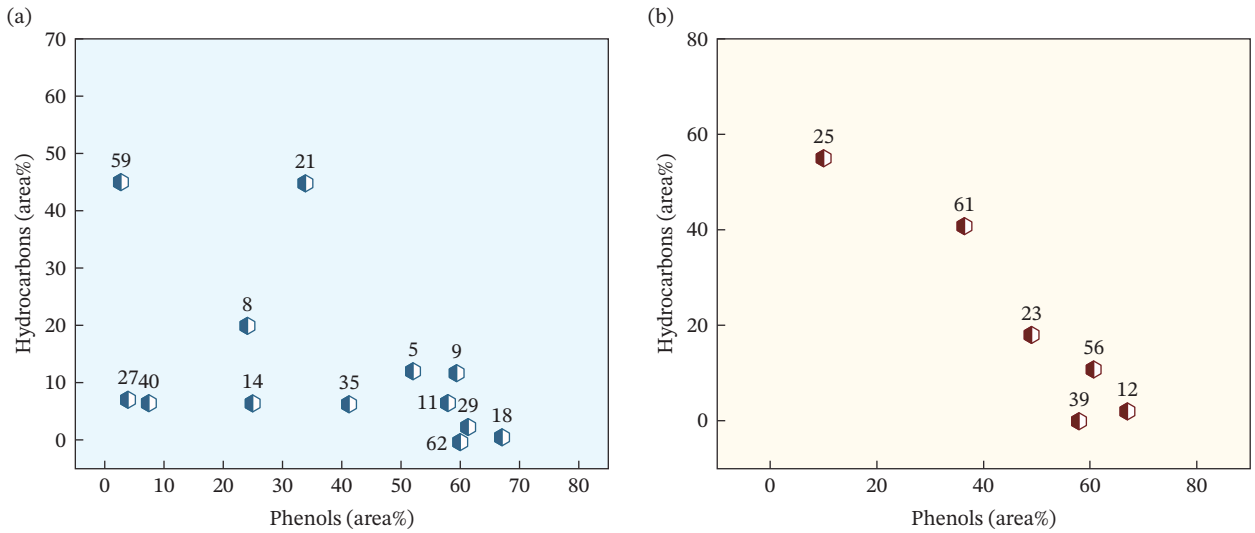


FIGURE 13 | Comparison of BCBU performance in biofuel upgrading process (a) catalytic pyrolysis and (b) microwave-assisted catalytic pyrolysis. The contents of hydrocarbons and phenols used to draw this figure are brought from the several references listed in Table 4 (entries 5, 8, 9, 11, 12, 14, 18, 21, 23, 25, 27, 29, 35, 39, 40, 56, 59, 61, and 62) without normalization.

ijer, 2026, 1, Downloaded from https://onlinelibrary.wiley.com/doi/10.1155/er/4175129 by Hanyang University Library, Wiley Online Library on [24/11/2026]. See the Terms and Conditions (https://onlinelibrary.wiley.com/terms-and-conditions) on Wiley Online Library for rules of use; OA articles are governed by the applicable Creative Commons License

excellent deoxygenation and phenol-promoting effects of Fe. A maximum hydrocarbon recovery rate of 40.7% was achieved using PW-derived BCBU loaded with Fe–Co, with a corresponding phenol recovery rate of 36.5%, yielding the highest combined phenol and hydrocarbon content under the specified conditions [91]. This high productivity was attributed to the superior thermal conductivity of the bimetallic alloy catalyst, which resulted from its higher microwave absorption rate than that of single-metal catalysts. Furthermore, the Fe–Co catalyst facilitates the cleavage of β-O-4 bonds, thereby generating substrates for the synthesis of aromatic hydrocarbons and phenols.

5.2 | Comparison of BCBU Utilization in Various Processes

In accordance with the route-specific catalyst roles and design criteria outlined in Section 4.3 and Table 5, the evaluation of BCBU's practical value should focus on identifying specific process advantages offered by biochar-derived catalysts, rather than presuming their universal catalytic superiority. Current research indicates that biochar-derived catalysts are particularly applicable to pyrolysis-centered routes. Conversely, their roles in HTL, CTH, steam reforming, and esterification/transesterification are more specific to each process and should be assessed using performance metrics appropriate to each route.

From a technological-readiness perspective, fast/catalytic pyrolysis currently appears to be the most mature route among those discussed here, because pilot-scale circulating fluidized-bed systems have already reported maximum bio-oil yields of 60 wt%, and a continuous 15 kg/h sawdust pyrolysis system produced 41.05 wt% bio-oil [164, 165]. HTL is also progressing toward practical deployment, as shown by a pilot-scale continuous plug-flow reactor capable of processing 60 L/h of wet feedstock and producing 6 L/h of biocrude, with biocrude yields of 52.19 and 47.06 wt% for two food-waste streams [166]. In contrast, the representative biochar–assisted microwave–assisted catalytic pyrolysis, steam reforming, CTH, and esterification studies discussed above remain predominantly at the bench scale or in proof-of-concept, despite strong performance gains.

For industrial implementation, however, actual pilot/continuous demonstrations of biochar catalysts are essential. Process scale-up validates biomass throughput, thermal integration, and fluid dynamics, whereas catalyst scale-up proves the mechanical, chemical, and operational durability of biochar catalyst under continuous operating conditions. Therefore, decoupling process scale-up from catalyst scale-up is important. For biochar catalyst scale-up, various parameters need to be considered as follows: (1) Biomass precursors vary naturally in mineral (ash), lignin, and moisture content. For synthesis reproducibility, scaling up biochar synthesis (via pyrolysis or HTC) requires controlling heating rates and residence times to ensure consistent surface area, pore size distribution (e.g., meso- and macroporosity), and functional group density across large batches [167]; (2) powdered biochar causes severe reactor pressure drops, so particle size control is required. Scale-up demands shaping biochar into pellets, extrudates, or beads using binders (e.g., lignin, lignosulfonate, and calcium hydroxide) without occluding porous networks [168]; (3) attrition resistance and mechanical integrity are also important issues. Biochar is inherently brittle; hence, hydrodynamic shear and particle–particle collisions generate fine particulates, particularly in fluidized bed or stirred-tank reactors [169]. Mechanical degradation of biochar catalyst causes bed height reduction, channeling, filter clogging, and pressure drop spikes, so demonstrating attrition resistance and dynamic stress testing in continuous flow loops might be needed [170, 171]; (4) micron-scale biochar fines tend to carry over into liquid or gaseous product streams, contaminating bio-oil, syngas, or chemical isolates [172]. Therefore, high-efficiency continuous catalyst recovery methods (e.g., controlled oxidative regeneration and in situ steam/CO_2 regeneration [173, 174]) must be demonstrated; (5) BCBUs often incorporate metals. In liquid-phase reactions (e.g., HTL, CTH, and esterification/transesterification), leaching of active metals into the reaction stream deactivates the catalyst and poisons downstream units [175]. Continuous operation needs to prove low active–metal leaching and resistance to coke deposition; and (6) in fixed-bed reactors, uneven biochar packing creates flow channeling and local hot spots. Also, carbonaceous materials and residual ash (e.g., AAEMs) can accelerate erosion on reactor walls and/or pipes under high fluid velocities. Therefore, reactor compatibility should be carefully proved with BCBUs.

Biochar catalysts are inherently more variable than conventional inorganic catalysts because their ash content, AAEM composition, pore structure, oxygenated functional groups, and metal-anchoring environments depend strongly on the biomass source, pretreatment, carbonization temperature, activation chemistry, and metal-loading procedure [21, 28, 80]. Therefore, scale-up studies should verify whether the catalyst properties that are effective at the bench scale can be reproduced across different batches and feedstock sources. These issues are particularly important for biochar catalysts because the same mineral species and surface groups that promote deoxygenation, microwave absorption, or esterification may also contribute to variability, fouling, or catalyst loss during continuous operation [176].

The required scale-up descriptors also differ by upgrading route. In catalytic pyrolysis, BCBU should be evaluated for vapor-contact efficiency, resistance to pore blockage, coke deposition, and regeneration under repeated vapor exposure. In microwave-assisted catalytic pyrolysis, the stability of dielectric loss, graphitization degree, defect density, and metal-assisted hotspot formation must be tested under larger reactor volumes, where microwave penetration, heat distribution, and catalyst-bed uniformity can become limiting. In CTH, the scale-up descriptors should include hydrogen-donor utilization efficiency, donor-derived byproduct separation, liquid-phase mass transfer, metal leaching, catalyst recovery from polar bio-oil fractions, and stability during repeated hydrogen-transfer cycles. In HTL, hydrothermal stability, metal leaching, and retention of mesopore accessibility in hot compressed water are more important than dry surface area alone. In steam reforming, the critical indicators are time-on-stream stability, tar conversion, H_2 productivity, coke resistance, oxygen-vacancy retention, and metal sintering resistance. In esterification and transesterification, the main scale-up concerns are acid/base-site stability, alcohol tolerance, water tolerance, catalyst recovery from liquid products, and reuse cycles. Moreover, future industrially relevant studies should report not only product selectivity but also catalyst productivity,

ijer, 2026, 1, Downloaded from https://onlinelibrary.wiley.com/doi/10.1155/er/4175129 by Hanyang University Library, Wiley Online Library on [24/11/2026]. See the Terms and Conditions (https://onlinelibrary.wiley.com/terms-and-conditions) on Wiley Online Library for rules of use; OA articles are governed by the applicable Creative Commons License

catalyst-to-feed ratio, kg feed converted per kg catalyst, time-on-stream, number of regeneration cycles, activity recovery after regeneration, catalyst make-up rate, metal leaching, coke amount, and wastewater generated during catalyst preparation or regeneration.

5.3 | BCBU Design Strategy

Designing BCBUs requires matching the intrinsic composition of the biomass feedstock (e.g., woody biomass, agricultural residues, SS, and algae) with the desired catalytic function, whether as a standalone catalyst, a heteroatom-doped carbon catalyst, or a catalyst support. Variations in the contents of AAEMs, lipids, proteins, moisture, nitrogen, and minerals (ash) dictate the required thermochemical conversion pathway, pore engineering strategy, and active site development.

Woody biomass (e.g., pine sawdust and eucalyptus) is dominated by lignocellulose with marginal inorganic ash, providing a dense, carbon-rich precursor [93]. Maximizing the specific surface area to create high-performance solid acid catalysts or metal supports would be crucial to prepare biochar catalysts from wood biomass. Because intrinsic ash is marginal, pore blockage is low. High-temperature pyrolysis (600–900°C) followed by physical (e.g., CO_2 and steam) or chemical (e.g., KOH and H_3PO_4) activation yields hierarchical micro/mesoporous networks exceeding 1000 m^2/g [177–179]. The clean carbon lattice allows chemical functionalization (e.g., sulfonation via concentrated H_2SO_4) for esterification, hydrolysis, and dehydration reactions.

Agricultural residues (e.g., rice husk (RH) and rice straw (RS)) contain high levels of AAEMs (e.g., K and Ca) alongside substantial biogenic SiO_2 [180]. Inherent AAEMs can be leveraged for base catalysis, or SiO_2 can be used as an in situ sacrificial template for mesopore engineering. During pyrolysis, organic-matter loss relatively enriches retained K-, Ca-, and Mg-containing inorganic components in the biochar, providing basic catalytic functionality [82]. These function directly as heterogeneous base catalysts for biodiesel transesterification and biomass gasification/tar cracking without requiring external metal impregnation. In SiO_2-rich feedstocks (e.g., RH and wheat straw), SiO_2 nanoparticles remain dispersed throughout the carbon matrix during pyrolysis [181]. Etching the resulting biochar with alkaline solutions (e.g., NaOH) selectively dissolves the SiO_2 domains [182], leaving behind interconnected mesopores and macrochannels that reduce mass transfer limitations for bulky reactants.

SS is characterized by high moisture, high nitrogen, and an inorganic fraction dominated by iron, aluminum, phosphorus, and trace heavy metals [183]. High ash content is transformed from a waste liability into active mineral sites, while heavy metals are anchored within a stable matrix. Predrying or copyrolysis is necessary due to high moisture. Pyrolysis at 500–800°C converts inherent iron salts into magnetic iron oxides (e.g., Fe_3O_4 and γ-Fe_2O_3) or zero-valent iron (Fe^0) embedded within the biochar frame [184–186]. Inherent magnetic iron phases allow easy catalyst recovery using external magnetic fields. When higher surface area is required, pre- or postacid washing can leach out inert calcium/phosphate salts, though this removes part of the catalytic mineral phase [187].

Algal biomass (e.g., micro- and macroalgae) features high contents of protein (i.e., high N contents) and lipid, extreme moisture, and elevated alkali/halide salts (especially in marine macroalgae) [188, 189]. Wet algal slurry is ideal for HTC at 180–250°C under autogenous pressure, bypassing energy-intensive drying [190]. The resulting biochar rich in oxygen/nitrogen groups can be further activated via secondary high-temperature pyrolysis (600–800°C) to induce graphitization [191]. Thermal breakdown of algal proteins during carbonization incorporates nitrogen into the graphitic lattice as pyridinic N, pyrrolic N, and quaternary N [192]. Pyridinic N and quaternary N alter the charge distribution of adjacent carbon atoms, creating active Lewis-acidic sites for selective dehydration and deoxygenation reactions [193, 194]. Marine algae contain high halides (e.g., Cl^-) and soluble salts (e.g., Na^+ and K^+) that can cause low surface area through ash sintering [195]. Therefore, desalting via cold-water washing prior to carbonization prevents pore collapse and equipment corrosion.

Recent research has demonstrated that the physicochemical properties of waste-derived biochar can be customized through the functionalization with various methods, such as layered double hydroxides (LDHs) [196–198], metal–organic framework–assisted metal–oxide dispersion [199], and task-specific ionic-liquid interfacial engineering [200], beyond utilizing intrinsic feedstock characteristics. However, biochar catalysts prepared using such methods have not yet been tested for biofuel upgrading, although the material-design strategies can provide useful guidance for BCBU. Specifically, controlling the metal composition and dispersion, pore accessibility, surface functionality, and biochar–metal interfacial interactions may help tailor oxygenate adsorption and activation, acid–base/redox site availability, mass transfer, and catalyst stability during biofuel upgrading.

6 | Economic and Environmental Impacts

The use of biofuels as sustainable alternative fuels necessitates the implementation of industrial-scale upgrading processes. The application of sustainable biochar catalysts in these upgrading processes can provide environmental and economic benefits. Therefore, several studies have evaluated the environmental and economic aspects of the biofuel upgrading process using biochar catalysts. Guo et al. [34] performed a life cycle assessment (LCA) of the synthesis of nickel-loaded Santa Barbara Amorphous (SBA)-15 and biochar catalysts. An assessment of the catalyst synthesis process, including transportation, pretreatment/synthesis, impregnation, pyrolysis/calcination, and pyrolysis reforming, revealed that the biochar catalyst reduced gas emissions by ~14% compared with the SBA-15 catalyst. This initiative not only yields environmental advantages but also confers economic benefits by potentially reducing carbon taxes on greenhouse gas emissions. In addition to the economic benefits of these environmental advantages, upgrading biofuel products or byproducts can yield further economic gains. Jung et al. [62] identified the potential of SS as a feedstock for biodiesel production via esterification with an SS-derived catalyst, which could yield economic benefits exceeding $3 billion annually.

Furthermore, the gas produced by upgrading biofuels using $ZnCl_2$-modified Chinese herb residue (CHR) can be utilized for chemical vapor deposition [63, 83]. This approach ensures

ijer, 2026, 1, Downloaded from https://onlinelibrary.wiley.com/doi/10.1155/er/4175129 by Hanyang University Library, Wiley Online Library on [24/11/2026]. See the Terms and Conditions (https://onlinelibrary.wiley.com/terms-and-conditions) on Wiley Online Library for rules of use; OA articles are governed by the applicable Creative Commons License

economic viability by using biofuel production by-products to synthesize high-value-added materials. Zhu et al. [83] demonstrated that using carbon nanotubes (CNTs) produced during biofuel upgrading via BCBU can yield additional economic advantages. According to this study, 10 tons of waste cooking oil yielded 5.5 tons of high-quality biofuel, along with 213 kg of CNT and gas. At the same process scale, technoeconomic calculations indicated a daily economic benefit of $33,772 for biofuel production alone. They increased to $38,643 when CNT and other coproducts were also valued. Conversely, studies have identified negative environmental and economic impacts associated with the introduction of activators into the biofuel upgrading process using BCBU [52, 60]. The introduction of activators, including acidification, adversely affects the economy, ecotoxicity, and environmental parameters. Chemical activation introduces activator-specific environmental trade-offs rather than a uniform environmental penalty. In a same-study comparison using *Quercus alba*, H_3PO_4, KOH, and $ZnCl_2$ gave global warming/terrestrial-acidification values of 2.90/0.03, 2.63/0.02, and 3.12/0.03, respectively (units: kg CO_2-eq and kg SO_2-eq). KOH showed the largest overall ecological footprint across most impact categories, and $ZnCl_2$ showed the highest global warming burden and ecotoxicity [201]. In a separate direct comparison, NaOH was slightly less burdensome than KOH, with climate-change impacts of 3.70 versus 3.88 kg CO_2-eq and terrestrial acidification values of 2.07×10^{-3} versus 2.11×10^{-3} kg SO_2-eq [202]. H_3PO_4 is often regarded as more favorable than $ZnCl_2$ because of easier recovery and generally lower environmental concerns, although H_3PO_4-based routes can still impose substantial burdens depending on the feedstock and process design; for example, one olive tree route reported 5.210 kg CO_2-eq [203]. $ZnCl_2$-based activation also imposes an additional waste-management burden because posttreatment commonly involves HCl leaching, which generates Zn-containing liquid waste unless the activating agent is recovered and recycled [204]. Therefore, the environmental implications of activation are better described as activator-specific tradeoffs. $ZnCl_2$ is often associated with high global warming and waste treatment burdens and frequently shows the largest footprint across multiple categories; NaOH is slightly less burdensome than KOH when directly compared, and H_3PO_4 is often relatively favorable but not universally low.

Similar environmental trade-offs are observed in metal loading. While metals such as Fe, Ni, Co, Cu, and Zn enhance deoxygenation, hydrogen transfer, and reforming processes, their increased loading also elevates metal-precursor consumption and the environmental impact associated with metal extraction and catalyst production. In a related LCA, NiO production was responsible for over 80% of several environmental impact categories linked to metal-catalyst production [205]. Increasing the NiO content from 5 to 20 wt% resulted in a rise of ~61%–92% in most impact categories. These findings suggest that the environmental benefits of using renewable biochar support can be partially negated when high metal loading is necessary. Consequently, the optimal design target should focus on the minimum metal loading that achieves the desired catalytic performance and lifetime, rather than the maximum possible loading.

Metal release is particularly significant during liquid-phase upgrading, as alcohols, water, organic acids, hydrogen-donor solvents, and regeneration solutions can mobilize weakly anchored metals [206]. For instance, a $CuO–Fe_3O_4$ catalyst supported on activated rice-straw biochar initially achieved an ester yield of 48.57% during bio-oil upgrading in supercritical ethanol [152]. After four reuse cycles, the ester yield declined by ~16%, while the residual acid fraction increased from 4.11% to 10.08%. This reduction was partly attributed to the leaching of supported metal oxides. However, the concentrations of Fe and Cu in the liquid products were not directly reported, complicating the differentiation between leaching and other factors such as coke deposition, pore blockage, or structural deterioration. A carbon-based K_xFe_yOz catalyst provides a more quantitative example [207]. Waste-oil conversion decreased only from 98.3% to 93.4% after five cycles, with K leaching into the biodiesel measured directly at 3.5 μg/L. Although this catalyst was not derived from conventional biomass biochar, it illustrates that catalytic reusability and active-species loss should be evaluated concurrently.

Environmental assessment of metal-loaded BCBU should therefore include metal-resource consumption, catalyst recovery, cumulative metal loss, regeneration energy and chemical demand, wastewater generation, and spent-catalyst management. Spent metal-loaded biochar should not be treated as conventional biochar or directly applied to soil without appropriate leachability and toxicity assessments, as metal-containing wastewater, catalyst fines, and improperly disposed spent catalysts may become sources of secondary pollution.

To situate the BCBU-specific case studies within a wider sustainability framework, it is beneficial to employ related LCA/technoeconomic analysis (TEA) studies at the catalyst, support, and process levels. These analyses can provide insights into how the environmental and economic outcomes are influenced by factors such as catalyst production, the choice of support, activation methods, and the scale of the process. At the catalyst level, Frazier et al. [205] compared biochar and metal catalysts for syngas cleaning and reported that biochar catalyst production reduced greenhouse gas emissions by 93% and required 95.7% less energy than metal catalyst production. At the carbon-support level, Alhashimi and Aktas [208] compared biochar with activated carbon (AC) and reported average energy demands of 6.1 MJ/kg for biochar and 97 MJ/kg for AC, with average greenhouse gas emissions of 0.9 kg CO_2-eq/kg and 6.6 kg CO_2-eq/kg. Gu et al. [209] also developed cradle-to-gate life-cycle inventory data for AC produced from woody-biomass–derived biochar and showed that greenhouse gas emissions from biochar-derived AC were less than half those from coal-derived AC, with values of 8.60 kg CO_2-eq/kg AC and 18.28 kg CO_2-eq/kg AC. These quantitative LCA examples indicate that biochar-derived catalysts and supports can offer environmental advantages over conventional metal catalysts or fossil-derived AC, but these advantages depend on the selected functional unit, biomass source, activation energy, land-use assumptions, catalyst productivity, and catalyst lifetime.

Broader technoeconomic datasets also show that the economic feasibility of BCBU depends on process scale, feedstock cost, catalyst reuse, and product selling price. Lee et al. performed a preliminary TEA of biodiesel production over solid biochar at a production capacity of 30,000 t/year and reported that, when the biodiesel selling price was $1.70/kg, the payback period ranged from 1.91 years (without discounting) to 2.06 years (at a 10%

ijer, 2026, 1, Downloaded from https://onlinelibrary.wiley.com/doi/10.1155/er/4175129 by Hanyang University Library, Wiley Online Library on [24/11/2026]. See the Terms and Conditions (https://onlinelibrary.wiley.com/terms-and-conditions) on Wiley Online Library for rules of use; OA articles are governed by the applicable Creative Commons License

discount rate). In addition, the break-even biodiesel price was calculated as \$1.55/kg at a 10% discount rate [210]. In a more recent simulated industrial–scale biodiesel process using a sulfonated Zn–doped recyclable biochar catalyst derived from coconut husk, Pravin and Baskar obtained a maximum biodiesel conversion of 94.8% under optimized conditions of a 10:1 methanol-to-oil molar ratio, 4.8% catalyst loading, 54.5°C, and 87.4 min reaction time. The TEA reported a minimum selling price of \$0.81/kg biodiesel, a return on investment of 21.59%, and a reimbursement period of 4.63 years, while the carbon-footprint analysis estimated 752.07 t CO_2/year, corresponding to 0.088 kg CO_2/kg biodiesel [211]. Together with the environmental LCA examples above, these TEA results suggest that future BCBU assessments should report not only product selectivity and catalyst surface area but also catalyst productivity, catalyst lifetime, reuse cycles, activator recovery, wastewater characteristics, metal leaching, coproduct credits, minimum selling price, payback period, and LCA/TEA system boundaries.

7 | Current Limitations and Future Research Recommendations

To advance BCBU-enabled biofuel upgrading, future research should address several clearly defined knowledge gaps. First, feedstock heterogeneity remains a major barrier to predictive catalyst design because aquatic and algal biomasses show high compositional variability, agricultural residues are strongly influenced by AAEM-rich ash, and woody biomass generally provides a more stable basis for catalyst preparation. Therefore, future studies should classify feedstocks into low-ash woody, high-AAEM agricultural, and high-variability aquatic/algal groups and report ash content, AAEM profile, and major biopolymer composition along with catalyst performance. Pretreatments such as water washing, hot-water deashing, and mild acid washing should also be systematically compared to reduce feedstock heterogeneity before biochar synthesis and upgrading experiments. Second, the sustainability of catalyst synthesis remains insufficiently resolved because activator selection is often treated only as a porosity-control strategy rather than as an environmental variable. $ZnCl_2$ can impose a high environmental burden unless the process filtrates are recovered and recycled, whereas KOH is effective but complicates closed-loop recovery and produces caustic wastewater [204, 212]. H_3PO_4 appears more suitable for circular activation because waste phosphoric acid can be valorized and reused with minimal performance loss [213]. Therefore, future studies should report activator mass balance, recovery yield, wastewater characteristics, and catalyst performance together. Third, deactivation mechanisms remain insufficiently distinguished because coke deposition, pore blockage, mineral poisoning, metal sintering, and loss of active surface functionalities can all reduce activity through different pathways [214]. Future work should therefore pair catalytic tests with coke analysis, metal-leaching data, regeneration cycles, and time-on-stream stability. Finally, BCBU-based upgrading should be linked with continuous or pilot-scale reactor studies, including hydrogen-assisted or electrified systems, to evaluate catalyst productivity, catalyst make-up rate, regeneration efficiency, and process scalability. Overall, the field should move toward four practical priorities: feedstock-resolved catalyst design, closed-loop activator recovery, mechanism-based regeneration, and standardized continuous or pilot-scale testing. These priorities could help shift BCBU research from empirical catalyst screening toward a more predictive and industrially relevant platform for sustainable biofuel upgrading.

8 | Conclusions

This review examines the use of biochar-derived catalysts for biofuel upgrading by linking catalyst preparation strategies to their catalytic functions in pyrolysis, microwave-assisted pyrolysis, HTL, steam reforming, and esterification/transesterification. By organizing the literature according to synthesis route (pyrolysis, microwave pyrolysis, and HTC) and modification strategy (activation, heteroatom doping, and metal loading), this review shows that upgrading behavior is governed by the combined effects of pore architecture, surface functional groups, acid–base/redox properties, and metal/heteroatom interactions rather than by any single catalyst parameter. Across lignocellulosic, algal, sludge, and other waste-derived feedstocks, biochar catalysts have been used to promote route-specific outcomes, including deoxygenation, denitrogenation, hydrogen transfer, reforming, and liquid fuel stabilization. The comparative and technoenvironmental discussions further indicate that the value of these catalysts should be assessed not only in terms of product selectivity and upgrading efficiency but also with respect to reusability, regeneration, and process-dependent economic and environmental trade-offs. Overall, the reviewed studies have identified biochar as a versatile and tunable catalytic platform, the effectiveness of which depends on matching the catalyst structure and chemistry to the selected upgrading route and feedstock characteristics.

Nomenclature

AAEM:	Alkali and alkaline earth metal
AC:	Activated carbon
BCBU:	Biochar-based catalyst used for biofuel upgrading
BET:	Brunauer–Emmett–Teller
CD:	Cow dung
CG:	*Cladophora glomerata*
CHR:	Chinese herb residue
CM:	Cow manure
CNCs:	Cellulose nanocrystals
CNT:	Carbon nanotube
CP:	Coconut pericarp
CS:	Corn straw
CTH:	Catalytic transfer hydrogenation
CV:	*Chlorella vulgaris*
DDGSs:	Distillers dried grains with solubles
DF:	Douglas fir
EN:	*Enteromorpha clathrate*
EUC:	*Eucalyptus nicholii*
FAME:	Fatty acid methyl ester
FR:	Furfural residue

ijer, 2026, 1, Downloaded from https://onlinelibrary.wiley.com/doi/10.1155/er/4175129 by Hanyang University Library, Wiley Online Library on [24/11/2026]. See the Terms and Conditions (https://onlinelibrary.wiley.com/terms-and-conditions) on Wiley Online Library for rules of use; OA articles are governed by the applicable Creative Commons License

FRS:	Freshwater reed straw
GC:	*Gracilaria corticata*
HDO:	Hydrodeoxygenation
HHV:	Higher heating value
HTC:	Hydrothermal carbonization
HTL:	Hydrothermal liquefaction
HW:	Horticultural waste
LCA:	Life cycle assessment
LDO:	Layered double oxide
LDPE:	Low-density polyethylene
MAH:	Monoaromatic hydrocarbon
MB:	Methylene blue
PE:	Polyethylene
PP:	Polypropylene
PS:	Peanut shell
PW:	Pine wood
RH:	Rice husk
RS:	Rice straw
SBA:	Santa Barbara Amorphous
SCB:	Sugarcane bagasse
SP:	*Spirulina platensis*
SS:	Sewage sludge
TEA:	Technoeconomic analysis
HMF:	Hydroxymethylfurfural
WPKC:	Waste palm kernel cake
LDHs:	Layered double hydroxides.

Author Contributions

Seung Won Kim: investigation, visualization, writing – original draft. **Eilhann E. Kwon**: supervision, validation, writing – review and editing. **Jechan Lee**: conceptualization, writing – original draft, writing – review and editing.

Acknowledgments

The authors have nothing to report.

Funding

This study was carried out with the support of the Cooperative Research Program for Agriculture Science and Technology Development (Project Number RS-2026-25509944), Rural Development Administration, Republic of Korea.

Conflicts of Interest

The authors declare no conflicts of interest.

Data Availability Statement

No primary research results, software, or code have been included, and no new data were generated or analyzed as part of this review.

References

1. C. W. Forsberg, B. E. Dale, D. S. Jones, T. Hossain, A. R. C. Morais, and L. M. Wendt, "Replacing Liquid Fossil Fuels and Hydrocarbon Chemical Feedstocks With Liquid Biofuels From Large-Scale Nuclear Biorefineries," *Applied Energy* 298 (2021): 117225.

2. L. Cherwoo, I. Gupta, G. Flora, et al., "Biofuels an Alternative to Traditional Fossil Fuels: A Comprehensive Review," *Sustainable Energy Technologies and Assessments* 60 (2023): 103503.

3. Priya, P. S. Deora, Y. Verma, R. A. Muhal, C. Goswami, and T. Singh, "Biofuels: An Alternative to Conventional Fuel and Energy Source," *Materials Today: Proceedings* 48 (2022): 1178–1184.

4. Y. Liu and Y. Huang, "Assessing the Interrelationship Between Fossil Fuels Resources and the Biomass Energy Market for Achieving a Sustainable and Green Economy," *Resources Policy* 88 (2024): 104397.

5. A. Eisentraut, "The Biofuel and Bioenergy Roadmaps of the International Energy Agency," *Bioenergy and Water* 3 (2013).

6. V. Pelagalli, M. Langone, S. Matassa, et al., "Pyrolysis of Municipal Sewage Sludge: Challenges, Opportunities and New Valorization Routes for Biochar, Bio-Oil, and Pyrolysis Gas," *Environmental Science: Water Research & Technology* 10, no. 10 (2024): 2282–2312.

7. I. J. T. Junior, J. L. F. Alves, C. Z. Brusamarello, and M. Di Domenico, "Impact of Operational Parameters on the Yield of Biochar, Bio-Oil, and Pyrolytic Gas in Lignocellulosic Biomass Pyrolysis: A Systematic Review," *Bioresource Technology Reports* 30 (2025): 102155.

8. F. Wei, S. Sang, S. Liu, J.-P. Zhao, X.-Y. Zhao, and J.-P. Cao, "BECCS Carbon-Negative Technologies Based on Biomass Thermochemical Conversion: A Review of Critical Pathways and Research Advances," *Fuel* 390 (2025): 134743.

9. F.-G. Bodur, T. Güngören-Madenoğlu, G. Özdemir, L. Ballice, and N. Kabay, "Biochemical and Biohythane Production From Anaerobically Digested Water Plant by Hydrothermal Liquefaction/Gasification," *International Journal of Hydrogen Energy* 52 (2024): 183–201.

10. H. Fatehi, W. Weng, Z. Li, X.-S. Bai, and M. Aldén, "Recent Development in Numerical Simulations and Experimental Studies of Biomass Thermochemical Conversion," *Energy & Fuels* 35, no. 9 (2021): 6940–6963.

11. H. Song, G. Yang, P. Xue, et al., "Recent Development of Biomass Gasification for H2 Rich Gas Production," *Applications in Energy and Combustion Science* 10 (2022): 100059.

12. Y. Zhang, Y. Liang, S. Li, et al., "A Review of Biomass Pyrolysis Gas: Forming Mechanisms, Influencing Parameters, and Product Application Upgrades," *Fuel* 347 (2023): 128461.

13. I. Mohan, A. K. Panda, V. Volli, and S. Kumar, "An Insight on Upgrading of Biomass Pyrolysis Products and Utilization: Current Status and Future Prospect of Biomass in India," *Biomass Conversion and Biorefinery* 14, no. 5 (2024): 6185–6203.

14. G. Chen, L. Liang, N. Li, X. Lu, B. Yan, and Z. Cheng, "Upgrading of Bio-Oil Model Compounds and Bio-Crude Into Biofuel by Electrocatalysis: A Review," *ChemSusChem* 14, no. 4 (2021): 1037–1052.

15. S. Liu, G. Wu, Y. Gao, et al., "Understanding the Catalytic Upgrading of Bio-Oil From Pine Pyrolysis Over CO_2-Activated Biochar," *Renewable Energy* 174 (2021): 538–546.

16. T. A. Silva, E. A. do Couto, P. P. Assemany, et al., "Biofuel From Wastewater-Grown Microalgae: A Biorefinery Approach Using Hydrothermal Liquefaction and Catalyst Upgrading," *Journal of Environmental Management* 368 (2024): 122091.

17. X. Yuan, Y. Cao, J. Li, et al., "Recent Advancements and Challenges in Emerging Applications of Biochar-Based Catalysts," *Biotechnology Advances* 67 (2023): 108181.

18. S. Yadav, S. Ponnada, I. Kumari, and R. K. Sharma, "Biochar as Catalyst," in *Biochar-Based Catalysts: Preparation, Characterization and Applications*, eds. S. A. Bhawani, K. Umar, M. N. Mohamad Ibrahim, and K. M. Alotaibi, (Springer Nature Singapore, 2024): 17–28.

19. N. Adamu, K. Umar, W. D. Oh, T. Parveen, and A. Lawal, "Application of Biochar-Based Metal Catalyst and Their Uses," in *Biochar-Based Catalysts: Preparation, Characterization and Applications*,

ijer, 2026, 1, Downloaded from https://onlinelibrary.wiley.com/doi/10.1155/er/4175129 by Hanyang University Library, Wiley Online Library on [24/11/2026]. See the Terms and Conditions (https://onlinelibrary.wiley.com/terms-and-conditions) on Wiley Online Library for rules of use; OA articles are governed by the applicable Creative Commons License

eds. S. A. Bhawani, K. Umar, M. N. Mohamad Ibrahim, and K. M. Alotaibi, (Springer Nature Singapore, 2024): 75–107.

20. F. Li, N. Wang, X. He, et al., "Biochar-Based Catalytic Upgrading of Plastic Waste Into Liquid Fuels Towards Sustainability," *Communications Earth & Environment* 6, no. 1 (2025): 329.

21. K. Velusamy, J. B. Isabel, S. Periyasamy, et al., "Role of Biochar as a Greener Catalyst in Biofuel Production: Production, Activation, and Potential Utilization – A Review," *Journal of the Taiwan Institute of Chemical Engineers* 177 (2025): 105732.

22. S. Gea, Y. A. Hutapea, A. F. R. Piliang, et al., "A Comprehensive Review of Experimental Parameters in Bio-Oil Upgrading From Pyrolysis of Biomass to Biofuel Through Catalytic Hydrodeoxygenation," *BioEnergy Research* 16, no. 1 (2023): 325–347.

23. M. Bilal and M. Al-Naji, "Recent Developments of the Biorefinery of γ-Valerolactone," *Discover Catalysis* 2, no. 1 (2025): 10.

24. M. F. M. Ahmad Zamri, S. H. A. Hassan, S. K. Tiong, et al., "Progress and Challenges of Mesoporous Catalysts in Upgraded Pyrolysis of Biomass for Biofuel Production," *Journal of Analytical and Applied Pyrolysis* 182 (2024): 106651.

25. J. Chopra, V. Rangarajan, S. Rathnasamy, and P. Dey, "Life Cycle Assessment as a Key Decision Tool for Emerging Pretreatment Technologies of Biomass-to-Biofuel: Unveiling Challenges, Advances, and Future Potential," *BioEnergy Research* 17, no. 2 (2024): 857–876.

26. S. Ameen, Z. Hussain, R. Khalid, and M. I. Din, "A Critical Review on Pyrolysis of Maize Biomass for Bio-Oil and Biochar Production With Its Potential Outcomes," *International Journal of Chemical Reactor Engineering* 23, no. 5 (2025): 541–554.

27. J. Zhao, Y. Jiang, X. Chen, C. Wang, and H. Nan, "Unlocking the Potential of Element-Doped Biochar: From Tailored Synthesis to Multifunctional Applications in Environment and Energy," *Biochar* 7, no. 1 (2025): 77.

28. J. Lee, K.-H. Kim, and E. E. Kwon, "Biochar as a Catalyst," *Renewable and Sustainable Energy Reviews* 77 (2017): 70–79.

29. N. T. L. Chi, S. Anto, T. S. Ahamed, et al., "A Review on Biochar Production Techniques and Biochar Based Catalyst for Biofuel Production From Algae," *Fuel* 287 (2021): 119411.

30. M. Jagadale, P. K. Sarangi, N. Jose, et al., "A Comprehensive Review on Biochar Catalyst for Advancement of Pyrolytic Conversion of Biomass Into Valuable Biofuels," *Journal of the Taiwan Institute of Chemical Engineers* 177 (2025): 106232.

31. L. Zhong, J. Zhu, S. Liu, et al., "Biochar-Driven Green Separation and Catalytic Upgrading of Bio-Oil: Mechanisms, Applications, and Future Perspectives," *Energy & Fuels* 39, no. 42 (2025): 19977–19997.

32. K. Ramandeep, B. B. Krishna, N. Rathnayake, T. Bhaskar, and K. Shah, "Role of Carbo-Catalyst on Upgrading the Pyrolysis Vapors of Spent *Eucalyptus nicholii* Biomass: Towards Sustainable Phenolics Production," *Renewable Energy* 242 (2025): 122468.

33. J. Guo, J. L. C. Foo, L. Ge, et al., "Steam-Assisted One-Step Fabrication of Ni-Ce Biochar Catalysts for Enhanced Biomass Pyrolysis-Steam Reforming," *Chemical Engineering Journal* 509 (2025): 161302.

34. Y. Guo, K. Sun, L. Kong, et al., "Pyro-Reforming of Cigarette Butts for Co-Productions of Hydrogen and Organics Over Nickel Catalyst Supporting on Biochar From Cigarette," *International Journal of Hydrogen Energy* 109 (2025): 150–163.

35. H. Xu, S. Lv, W. Wu, et al., "Catalytic Conversion of the Heavy Fraction of Bio-Oil Into Phenol-Rich Oils Using an Fe-Carbon Catalyst During Straw Pyrolysis," *Journal of Analytical and Applied Pyrolysis* 186 (2025): 106902.

36. Y. Zhang, J. Wang, H. Zhang, et al., "In-Situ Reaction Strengthening Mechanism of the Pyrolysis Water and Bio-Oil During the Biomass Pyrolysis Over CaO and Ni-Char Dual Catalytic System," *Energy* 319 (2025): 134913.

37. P. Premchand, D. Fino, F. Demichelis, et al., "Synthesis of Metal-Free Heteroatom (N, P, O, and B) Doped Biochar Catalysts for Enhanced Catalytic Co-Pyrolysis of Walnut Shells and Palm Oil Fatty Acid Distillate to Produce High-Quality Bio-Oil," *Journal of Environmental Chemical Engineering* 12, no. 5 (2024): 113630.

38. B. Wang, Y. Chen, W. Chen, et al., "Enhancement of Aromatics and Syngas Production by Co-Pyrolysis of Biomass and Plastic Waste Using Biochar-Based Catalysts in Microwave Field," *Energy* 293 (2024): 130711.

39. X. Chen, S. Li, Y. Lin, et al., "Pyrolysis and Catalytic Upgrading of Pine Wood Sawdust Over Modified Biochar Catalyst in a Tandem Microreactor," *Journal of Analytical and Applied Pyrolysis* 181 (2024): 106607.

40. B. Cao, Y. Zheng, S. Esakkimuthu, et al., "Catalytic Pyrolysis of Wood Dust for Monophenol Over Macroalgal Biochar-Based Catalyst: Effects of Activation Agents and Atmospheres During Catalyst Synthesis on Its Performance," *Algal Research* 80 (2024): 103544.

41. J. Eimontas, N. Striūgas, K. Zakarauskas, I. Kiminaitė, and I. Pitak, "Metallised Seaweed-Derived Bio-Char Catalyst Preparation and Its Application in the Pyrolysis Process for the Waste Fishing Nets and Marine Biomass Utilisation," *Fuel* 357 (2024): 129922.

42. X. Tang, X. Y. Li, Q. F. He, et al., "In-Situ and Ex-Situ Selective Catalysis of Biochar-Based Catalysts for the Production of High-Quality Bio-Oil and H2-Rich Gas From Tobacco Stem," *Journal of Environmental Chemical Engineering* 12, no. 6 (2024): 114268.

43. P. Li, Q. Hu, B. Wang, et al., "Investigation of Products Characteristics From Microwave Catalytic Pyrolysis of Furfural Residue Based on the Effects of Fe/Mn Modified Biochar," *Industrial Crops and Products* 218 (2024): 119030.

44. S. Liu, G. Wu, L. Zhang, et al., "Promoted Production of Phenol From Lignin Pyrolysis Over Biochar-Based Catalysts by Fe and Ni Co-Loading," *Journal of Analytical and Applied Pyrolysis* 182 (2024): 106708.

45. S. Zhang, Y. Wu, Y. Wang, et al., "Facile Demineralization of Biochar and Its Catalytic Upgrading of Bio-Oil From Fast Pyrolysis of Bagasse," *Fuel* 349 (2023): 128714.

46. L. Liu, W. Zhou, Y. Wang, et al., "Cascaded Catalytic Copyrolysis of Microalgae and LDPE With Ni/Biochar and HZSM-5 for Improving High-Grade Bio-Oil Production," *ACS Sustainable Chemistry & Engineering* 11, no. 44 (2023): 15964–15974.

47. S. Qiu, C. Chen, S. Wan, et al., "Microwave Catalytic Co-Pyrolysis of Sugarcane Bagasse and *Chlorella vulgaris* Over Metal Modified Bio-Chars: Characteristics and Bio-Oil Analysis," *Journal of Environmental Chemical Engineering* 11, no. 5 (2023): 110917.

48. R. Zou, C. Wang, M. Qian, et al., "Catalytic Fast Co-Pyrolysis of Douglas Fir and Low-Density Polyethylene With Nanocellulose-Derived Carbon Catalyst for Enhancing Selectivity of Hydrogen in Syngas and Mono-Aromatic Hydrocarbon in Bio-Oil Products," *Chemical Engineering Journal* 474 (2023): 145640.

49. H. T. L. Arantes, M. A. Machado, M. C. Santoro, et al., "Effect of Activated Biochar as a Low-Cost Catalyst on the Quality of Catalytic Intermediate Co-Pyrolysis Oil From Waste Polystyrene and Green Coconut Pericarp," *Fuel Processing Technology* 240 (2023): 107539.

50. X. Yang, S. Shao, X. Li, and D. Tang, "Catalytic Transfer Hydrogenation of Bio-Oil Over Biochar-Based CuO Catalyst Using Methanol as Hydrogen Donor," *Renewable Energy* 211 (2023): 21–30.

51. S. Liu, G. Wu, L. Zhang, Y. Huang, J. Zhou, and S. Zhang, "Catalytic Pyrolysis of Pine Sawdust Over Activated Carbon-Supported Fe for Phenol-Rich Bio-Oil," *Journal of Analytical and Applied Pyrolysis* 171 (2023): 105959.

52. S. Gupta, P. Patel, and P. Mondal, "Catalytic Pyrolysis Using a Nickel-Functionalized Chemically Activated Biochar Catalyst: Insight Into

ijer, 2026, 1, Downloaded from https://onlinelibrary.wiley.com/doi/10.1155/er/4175129 by Hanyang University Library, Wiley Online Library on [24/11/2026]. See the Terms and Conditions (https://onlinelibrary.wiley.com/terms-and-conditions) on Wiley Online Library for rules of use; OA articles are governed by the applicable Creative Commons License

Process Kinetics, Products, and Mechanism," *ACS Sustainable Chemistry & Engineering* 10, no. 18 (2022): 5770–5780.

53. R. Zou, C. Wang, M. Qian, et al., "Catalytic Co-Pyrolysis of Solid Wastes (Low-Density Polyethylene and Lignocellulosic Biomass) Over Microwave Assisted Biochar for Bio-Oil Upgrading and Hydrogen Production," *Journal of Cleaner Production* 374 (2022): 133971.

54. Q. Bu, M. Cao, M. Wang, S. V. Vasudevan, and H. Mao, "Enhancement of Bio-Oil Quality Over Self-Derived Bio-Char Catalyst via Microwave Catalytic Pyrolysis of Peanut Shell," *Journal of Analytical and Applied Pyrolysis* 164 (2022): 105534.

55. S. Liu, G. Wu, S. S. A. Syed-Hassan, et al., "Catalytic Pyrolysis of Pine Wood Over Char-Supported Fe: Bio-Oil Upgrading and Catalyst Regeneration by CO2/H2O," *Fuel* 307 (2022): 121778.

56. X. Shi, P. Li, X. Wang, et al., "Enhancement of the Production of Aromatics and Bio-Syngas From Microwave Ex-Situ Pyrolysis Based on Zn/Zr Modified Biochar and Multi-Catalysts," *Energy* 261 (2022): 125307.

57. Z. Su, K. Jin, J. Wu, et al., "Phosphorus Doped Biochar as a Deoxygenation and Denitrogenation Catalyst for Ex-Situ Upgrading of Vapors From Microwave-Assisted Co-Pyrolysis of Microalgae and Waste Cooking Oil," *Journal of Analytical and Applied Pyrolysis* 164 (2022): 105538.

58. E. Balaghi Inaloo, M. Saidi, and A. Taheri Najafabadi, "Valuable Biofuel Production via Pyrolysis Process of Olive Pomace Over Alkali and Transition Metal Oxides Catalysts Supported on Activated Biochar," *ChemistrySelect* 7, no. 36 (2022): e202200789.

59. Z. Liu, M. Hughes, Y. Tong, et al., "Paper Mill Sludge Biochar to Enhance Energy Recovery From Pyrolysis: A Comprehensive Evaluation and Comparison," *Energy* 239 (2022): 121925.

60. B. Cao, D. Jiang, Y. Zheng, et al., "Evaluation of Biochar-Derived Carbocatalysts for Pyrolytic Conversion of Sawdust: Life Cycle Assessment Towards Monophenol Production," *Fuel* 330 (2022): 125476.

61. J. Luo, G. Gong, C. Cui, et al., "Microwave-Induced One-Pot Preparation of Bifunctional N-Fe/BC Catalysts and Oriented Production of Phenol-Enriched Bio-Oil From Biomass Pyrolysis: Catalyst Synthesis, Performance Evaluation, and Mechanism Insight via Theoretical Calculations," *ACS Catalysis* 12, no. 18 (2022): 11318–11339.

62. S. Jung, M. Kim, Y.-H. Kim, et al., "Use of Sewage Sludge Biochar as a Catalyst in Production of Biodiesel Through Thermally Induced Transesterification," *Biochar* 4, no. 1 (2022): 67.

63. W. Luo, S. Zhang, D. Zhang, et al., "Co-Pyrolysis of Chinese Herb Residue and Reused Polypropylene: Comparison of Pyrolysis Product Diversification and Upgrading Over Metal/ZSM-5 and Metal/Biochar Catalysts," *Fuel Processing Technology* 235 (2022): 107368.

64. N. Kaewtrakulchai, M. Fuji, and A. Eiad-Ua, "Catalytic Deoxygenation of Palm Oil Over Metal Phosphides Supported on Palm Fiber Waste Derived Activated Biochar for Producing Green Diesel Fuel," *RSC Advances* 12, no. 40 (2022): 26051–26069.

65. Y. Wang, L. Huang, T. Zhang, and Q. Wang, "Hydrogen-Rich Syngas Production From Biomass Pyrolysis and Catalytic Reforming Using Biochar-Based Catalysts," *Fuel* 313 (2022): 123006.

66. C. Zeng, Y. Jiang, R. Xu, L. Han, and X. Zhang, "Phenols-Enriched Biofuel and H2-Rich Gas From Catalytic Fast Pyrolysis/Gasification of Agricultural Biomass Over a Novel Heavy Metals-Containing Livestock Manure Biochar Catalyst," *Journal of Analytical and Applied Pyrolysis* 167 (2022): 105680.

67. J. Bai, Q. Lv, X. Fu, et al., "Catalytic Reforming of Sewage Sludge Pyrolysis Products Over the Self-Derived Char," *Journal of Analytical and Applied Pyrolysis* 168 (2022): 105759.

68. Y. Wu, Y. Sun, K. Liang, et al., "Enhancing Hydrodeoxygenation of Bio-Oil via Bimetallic Ni-V Catalysts Modified by Cross-Surface Migrated-Carbon From Biochar," *ACS Applied Materials & Interfaces* 13, no. 18 (2021): 21482–21498.

69. Z. Zeng, X. Tian, Y. Wang, et al., "Microwave-Assisted Catalytic Pyrolysis of Corn Cobs With Fe-Modified *Choerospondias axillaris* Seed-Based Biochar Catalyst for Phenol-Rich Bio-Oil," *Journal of Analytical and Applied Pyrolysis* 159 (2021): 105306.

70. B. Cao, J. Yuan, D. Jiang, et al., "Seaweed-Derived Biochar With Multiple Active Sites as a Heterogeneous Catalyst for Converting Macroalgae Into Acid-Free Biooil Containing Abundant Ester and Sugar Substances," *Fuel* 285 (2021): 119164.

71. B. Wang, Z. He, B. Zhang, and Y. Duan, "Study on Hydrothermal Liquefaction of Spirulina Platensis Using Biochar Based Catalysts to Produce Bio-Oil," *Energy* 230 (2021): 120733.

72. F. Li, D. J. Sweeney, Y. Dai, and C.-H. Wang, "Effect of Novel Ni2P-Loaded Catalysts on Algal Pyrolysis Bio-Oil," *Renewable and Sustainable Energy Reviews* 151 (2021): 111575.

73. S. Kandasamy, K. Devarayan, N. Bhuvanendran, et al., "Accelerating the Production of Bio-Oil From Hydrothermal Liquefaction of Microalgae via Recycled Biochar-Supported Catalysts," *Journal of Environmental Chemical Engineering* 9, no. 4 (2021): 105321.

74. C. Wang, H. Lei, Y. Zhao, et al., "Integrated Harvest of Phenolic Monomers and Hydrogen Through Catalytic Pyrolysis of Biomass Over Nanocellulose Derived Biochar Catalyst," *Bioresource Technology* 320 (2021): 124352.

75. P. Maneechakr and S. Karnjanakom, "Improving the Bio-Oil Quality via Effective Pyrolysis/Deoxygenation of Palm Kernel Cake Over a Metal (Cu, Ni, or Fe)-Doped Carbon Catalyst," *ACS Omega* 6, no. 30 (2021): 20006–20014.

76. Y. Dong, B. Tian, F. Guo, et al., "Application of Low-Cost Fe-Based Catalysts in the Microwave-Assisted Pyrolysis of Macroalgae and Lignocellulosic Biomass for the Upgradation of Bio-Oil," *Fuel* 300 (2021): 120944.

77. H. Yang, Z. Chen, W. Chen, Y. Chen, X. Wang, and H. Chen, "Role of Porous Structure and Active O-Containing Groups of Activated Biochar Catalyst During Biomass Catalytic Pyrolysis," *Energy* 210 (2020): 118646.

78. Z. Qiu, Y. Zhai, S. Li, et al., "Catalytic Co-Pyrolysis of Sewage Sludge and Rice Husk Over Biochar Catalyst: Bio-Oil Upgrading and Catalytic Mechanism," *Waste Management* 114 (2020): 225–233.

79. B. Nejati, P. Adami, A. Bozorg, A. Tavasoli, and A. H. Mirzahosseini, "Catalytic Pyrolysis and Bio-Products Upgrading Derived From *Chlorella vulgaris* Over Its Biochar and Activated Biochar-Supported Fe Catalysts," *Journal of Analytical and Applied Pyrolysis* 152 (2020): 104799.

80. X. Yue, D. Chen, J. Luo, Q. Xin, and Z. Huang, "Upgrading of Reed Pyrolysis Oil by Using Its Biochar-Based Catalytic Esterification and the Influence of Reed Sources," *Applied Energy* 268 (2020): 114970.

81. H. Nikkhah, A. Tavasoli, and S. Jafarian, "Investigating the Influence of Acid Washing Pretreatment and Zn/Activated Biochar Catalyst on Thermal Conversion of *Cladophora glomerata* to Value-Added Bio-Products," *Energy Conversion and Management* 225 (2020): 113392.

82. G. Park, J. Park, J. Y. Kim, D. Lee, and E. E. Kwon, "Use of Defatted Cottonseed-Derived Biochar for Biodiesel Production: A Closed-Loop Approach," *Biochar* 7, no. 1 (2025): 4.

83. G. Zhu, M. Zhu, E. Wang, et al., "Natural Biochar Catalyst: Realizing the Co-Valorization of Waste Cooking Oil Into High-Quality Biofuel and Carbon Nanotube Precursor via Catalytic Pyrolysis Process," *Chemical Engineering Journal* 486 (2024): 150195.

84. Y. Li, C. Zhu, J. Jiang, et al., "Catalytic Hydrothermal Liquefaction of *Gracilaria corticata* Macroalgae: Effects of Process Parameter on Bio-Oil Up-Gradation," *Bioresource Technology* 319 (2021): 124163.

85. J. Yang, X. Gong, B. Cao, et al., "Integrated "Adsorption-Catalysis-Adsorption" Green Strategy for Efficient Adsorption for the Removal of Methylene Blue and Catalytic Preparation of Hydrocarbon-Rich, Low N/O Bio-Oil," *Fuel* 354 (2023): 129286.

ijer, 2026, 1, Downloaded from https://onlinelibrary.wiley.com/doi/10.1155/er/4175129 by Hanyang University Library, Wiley Online Library on [24/11/2026]. See the Terms and Conditions (https://onlinelibrary.wiley.com/terms-and-conditions) on Wiley Online Library for rules of use; OA articles are governed by the applicable Creative Commons License

86. F. Guo, Y. Dong, K. Dong, et al., "Role of Biochar-Based Catalysts in Microwave-Induced Biomass Pyrolysis: Structural Properties and Modification With Fe-Series Metals," *Fuel* 341 (2023): 127769.

87. Y. Yang, J. Wang, Y. Zhang, et al., "In-Situ Bio-Oil Directional Conversion Mechanism of Catalytic Biomass Pyrolysis Over Nitrogen-Doped Carbon Preparation by Grading of Nitrogen-Rich Cow Dung," *Journal of Analytical and Applied Pyrolysis* 178 (2024): 106392.

88. Y. Su, Y. Zhang, S. Zhang, and Y. Xiong, "Exploring the Selectivity of Renewable Phenol From Catalytic Pyrolysis of Biomass via Activated Carbon Catalyst," *Journal of Analytical and Applied Pyrolysis* 190 (2025): 107166.

89. L. Tian, S. Liu, N. Tahir, et al., "Preparation of Metal-Modified Carbon-Based Catalyst and Experimental Study on Catalytic Pyrolysis of Distillers Dried Grains With Solubles," *Journal of Analytical and Applied Pyrolysis* 183 (2024): 106771.

90. A. Nawaz, G. A. N. Rohman, A. G. A. Jameel, A. C. Ummer, and S. A. Razzak, "Engineered Biochar-Based Catalytic Pyrolysis of Spirulina Plantensis Microalgae for the Production of High Value Compounds in Microwave Reactor," *Algal Research* 81 (2024): 103583.

91. Z. Sun, H. Wei, F. Guo, et al., "Study on the Characteristics of Microwave Pyrolysis of Pine Wood Catalyzed by Bimetallic Catalysts Prepared With Microwave-Assisted Hydrothermal Char," *Journal of Analytical and Applied Pyrolysis* 181 (2024): 106597.

92. S. Wang, K. Wu, J. Yu, B. Luo, C. Chu, and H. Zhang, "Kinetic and Thermodynamic Analysis of Biomass Catalytic Pyrolysis With Nascent Biochar in a Two-Stage Reactor," *Combustion and Flame* 251 (2023): 112671.

93. Y. Jiang, X. Gao, K. Sun, et al., "Similarity and Difference of Biochar and Hydrochar From Leaves, Bark, and Wood of the Same Sycamore Tree," *Bioresource Technology* 434 (2025): 132778.

94. H. Yang, R. Yan, H. Chen, D. H. Lee, and C. Zheng, "Characteristics of Hemicellulose, Cellulose and Lignin Pyrolysis," *Fuel* 86, no. 12-13 (2007): 1781–1788.

95. K. Umar, T. Parveen, N. H. M. Kaus, and H. A. A. Jamjoum, "Functionalization of Biochar for Catalysis," in *Biochar-Based Catalysts: Preparation, Characterization and Applications*, eds. S. A. Bhawani, K. Umar, M. N. Mohamad Ibrahim, and K. M. Alotaibi, (Springer Nature Singapore, 2024): 29–50.

96. J. Serafin, B. Dziejarski, X. Vendrell, K. Kiełbasa, and B. Michalkiewicz, "Biomass Waste Fern Leaves as a Material for a Sustainable Method of Activated Carbon Production for CO2 Capture," *Biomass and Bioenergy* 175 (2023): 106880.

97. C. Wu, V. L. Budarin, M. J. Gronnow, et al., "Conventional and Microwave-Assisted Pyrolysis of Biomass Under Different Heating Rates," *Journal of Analytical and Applied Pyrolysis* 107 (2014): 276–283.

98. G. Ischia and L. Fiori, "Hydrothermal Carbonization of Organic Waste and Biomass: A Review on Process, Reactor, and Plant Modeling," *Waste and Biomass Valorization* 12, no. 6 (2021): 2797–2824.

99. M. Sevilla and A. B. Fuertes, "Chemical and Structural Properties of Carbonaceous Products Obtained by Hydrothermal Carbonization of Saccharides," *Chemistry – A European Journal* 15, no. 16 (2009): 4195–4203.

100. S. K. Hoekman, A. Broch, and C. Robbins, "Hydrothermal Carbonization (HTC) of Lignocellulosic Biomass," *Energy & Fuels* 25, no. 4 (2011): 1802–1810.

101. J. Wang, Y. Wang, J. Wang, et al., "Comparison of Cadmium Adsorption by Hydrochar and Pyrochar Derived From Napier Grass," *Chemosphere* 308 (2022): 136389.

102. A. Wagner and M. Kaupenjohann, "Suitability of Biochars (Pyro- and Hydrochars) for Metal Immobilization on Former Sewage-Field Soils," *European Journal of Soil Science* 65, no. 1 (2014): 139–148.

103. C. Gai, F. Zhang, T. Yang, et al., "Hydrochar Supported Bimetallic Ni–Fe Nanocatalysts With Tailored Composition, Size and Shape for Improved Biomass Steam Reforming Performance," *Green Chemistry* 20, no. 12 (2018): 2788–2800.

104. T. Dickerson and J. Soria, "Catalytic Fast Pyrolysis: A Review," *Energies* 6, no. 1 (2013): 514–538.

105. K. Iisa, C. Mukarakate, R. J. French, et al., "From Biomass to Fuel Blendstocks via Catalytic Fast Pyrolysis and Hydrotreating: An Evaluation of Carbon Efficiency and Fuel Properties for Three Pathways," *Energy & Fuels* 37, no. 24 (2023): 19653–19663.

106. G. W. Huber and A. Corma, "Synergies Between Bio- and Oil Refineries for the Production of Fuels From Biomass," *Angewandte Chemie International Edition* 46, no. 38 (2007): 7184–7201.

107. M. J. Gilkey and B. Xu, "Heterogeneous Catalytic Transfer Hydrogenation as an Effective Pathway in Biomass Upgrading," *ACS Catalysis* 6, no. 3 (2016): 1420–1436.

108. E. Baráth, "Hydrogen Transfer Reactions of Carbonyls, Alkynes, and Alkenes With Noble Metals in the Presence of Alcohols/Ethers and Amines as Hydrogen Donors," *Catalysts* 8, no. 12 (2018): 671.

109. S. Shao, W. Wang, X. Yang, Z. Ye, J. Sun, and X. Li, "Efficient Catalytic Transfer Hydrogenation of Raw Bio-Oil Over Various CuO Catalysts," *Fuel* 353 (2023): 129028.

110. I. Mudi, A. Hart, A. Ingram, and J. Wood, "A Kinetic Model of Furfural Hydrogenation to 2-Methylfuran on Nanoparticles of Nickel Supported on Sulfuric Acid-Modified Biochar Catalyst," *Catalysts* 14, no. 1 (2024): 54.

111. I. Mudi, A. Hart, A. Ingram, and J. Wood, "Catalytic Hydrodeoxygenation of Vanillin, a Bio-Oil Model Compound Over Renewable Ni/Biochar Catalyst," *Catalysts* 13, no. 1 (2023): 171.

112. M. Hellinger, H. W. P. Carvalho, S. Baier, D. Wang, W. Kleist, and J.-D. Grunwaldt, "Grunwaldt, Catalytic Hydrodeoxygenation of Guaiacol Over Platinum Supported on Metal Oxides and Zeolites," *Applied Catalysis A: General* 490 (2015): 181–192.

113. Y. Han, S. K. Hoekman, Z. Cui, U. Jena, and P. Das, "Hydrothermal Liquefaction of Marine Microalgae Biomass Using Co-Solvents," *Algal Research* 38 (2019): 101421.

114. A. Amadei, M. P. Bracciale, M. Damizia, et al., "Hydrothermal Liquefaction of Organic Waste Model Compounds: The Effect of the Heating Rate on Biocrude Yield and Quality From Mixtures of Cellulose–Albumin–Sunflower Oil," *ACS Omega* 9, no. 40 (2024): 41194–41207.

115. P. Duan and P. E. Savage, "Catalytic Hydrothermal Hydrodenitrogenation of Pyridine," *Applied Catalysis B: Environmental* 108–109 (2011): 54–60.

116. T. Gong, M.-H. Ni, B. Liu, et al., "Product Characteristics and Evidence-Supported Mechanistic Interpretation of Subcritical Hydrothermal Liquefaction of Lignocellulosic Biomass," *Processes* 14, no. 11 (2026): 1820.

117. J. Yang, C. Hong, Y. Xing, et al., "Study on the Hydrothermal Liquefaction of Antibiotic Residues With Molecular Sieve Catalysts in the Ethanol–water System: Focus on Product Distribution and Characterization," *RSC Advances* 11, no. 43 (2021): 26763–26772.

118. Y. Liu, H. Du, Y. Meng, S. Lu, J. Zhang, and H. Wang, "Catalytic Hydrothermal Liquefaction of Microalgae Over Reduced Graphene Oxide Support Ni Catalyst," *Fuel Processing Technology* 242 (2023): 107653.

119. A. Arandia, A. Remiro, L. Oar-Arteta, J. Bilbao, and A. G. Gayubo, "Reaction Conditions Effect and Pathways in the Oxidative Steam Reforming of Raw Bio-Oil on a Rh/CeO_2-ZrO_2 Catalyst in a Fluidized Bed Reactor," *International Journal of Hydrogen Energy* 42, no. 49 (2017): 29175–29185.

120. R. Trane, S. Dahl, M. S. Skjøth-Rasmussen, and A. D. Jensen, "Catalytic Steam Reforming of Bio-Oil," *International Journal of Hydrogen Energy* 37, no. 8 (2012): 6447–6472.

ijer, 2026, 1, Downloaded from https://onlinelibrary.wiley.com/doi/10.1155/er/4175129 by Hanyang University Library, Wiley Online Library on [24/11/2026]. See the Terms and Conditions (https://onlinelibrary.wiley.com/terms-and-conditions) on Wiley Online Library for rules of use; OA articles are governed by the applicable Creative Commons License

121. G. Qin, C. Tang, Y. Yang, G. Ding, M. Li, and S. Chen, "S-Scheme TiO2/Biochar Heterojunction Derived From Waste Rice Noodles: A Low-Cost Waste-to-Catalyst Strategy for Enhanced Photocatalytic Hydrogen Production," *Chemical Engineering Journal* 522 (2025): 167763.

122. A. Y. Zerga, M. Tahir, H. Alias, and A. R. Mohamed, "Sludge-Derived Biochar Nanotexture to Construct BC/TiO2 Composite With Metallic Elements Influential Effect for Efficient Photocatalytic Hydrogen Evolution," *Fuel* 369 (2024): 131678.

123. L. Ciddor, J. A. Bennett, J. A. Hunns, K. Wilson, and A. F. Lee, "Catalytic Upgrading of Bio-Oils by Esterification," *Journal of Chemical Technology & Biotechnology* 90, no. 5 (2015): 780–795.

124. L. P. Amador-Gómez, D. Hernández-Romero, J. M. Rivera-Villanueva, et al., "Transesterification/Esterification Reaction Catalysed by Functional Hybrid MOFs for Efficient Biodiesel Production," *Reactions* 6, no. 4 (2025): 58.

125. A. Osatiashtiani, B. Puértolas, C. C. S. Oliveira, et al., "On the Influence of Si: Al Ratio and Hierarchical Porosity of FAU Zeolites in Solid Acid Catalysed Esterification Pretreatment of Bio-Oil," *Biomass Conversion and Biorefinery* 7, no. 3 (2017): 331–342.

126. N. Sanjel, J. Gu, and S. Oh, "Transesterification Kinetics of Waste Vegetable Oil in Supercritical Alcohols," *Energies* 7, no. 4 (2014): 2095–2106.

127. M. Berrios, J. Siles, M. A. Martín, and A. Martín, "A Kinetic Study of the Esterification of Free Fatty Acids (FFA) in Sunflower Oil," *Fuel* 86, no. 15 (2007): 2383–2388.

128. P. Zong, Y. Jiang, Y. Tian, et al., "Pyrolysis Behavior and Product Distributions of Biomass Six Group Components: Starch, Cellulose, Hemicellulose, Lignin, Protein and Oil," *Energy Conversion and Management* 216 (2020): 112777.

129. X. Wang, L. Sheng, and X. Yang, "Pyrolysis Characteristics and Pathways of Protein, Lipid and Carbohydrate Isolated From Microalgae Nannochloropsis Sp," *Bioresource Technology* 229 (2017): 119–125.

130. J.-G. Na, Y.-K. Park, D. I. Kim, et al., "Rapid Pyrolysis Behavior of Oleaginous Microalga, Chlorella Sp. KR-1 With Different Triglyceride Contents," *Renewable Energy* 81 (2015): 779–784.

131. T. Xie, L. Huo, Z. Yao, et al., "Co-Pyrolysis of Biomass and Polyethylene: Mechanistic Insights Into Functional Group Transformations on Solid Matrix," *Chemical Engineering Journal* 482 (2024): 149166.

132. K. Anshu, H. I. Kenttämaa, and S. K. Thengane, "A Comprehensive Review on Co-Pyrolysis of Lignocellulosic Biomass and Polystyrene," *Renewable and Sustainable Energy Reviews* 205 (2024): 114832.

133. J. Li, X. Li, G. Zhou, et al., "Catalytic Fast Pyrolysis of Biomass With Mesoporous ZSM-5 Zeolites Prepared by Desilication With NaOH Solutions," *Applied Catalysis A: General* 470 (2014): 115–122.

134. A. Gumidyala, T. Sooknoi, and S. Crossley, "Selective Ketonization of Acetic Acid Over HZSM-5: The Importance of Acyl Species and the Influence of Water," *Journal of Catalysis* 340 (2016): 76–84.

135. E. K. L. Mares, M. A. Gonçalves, P. T. S. da Luz, G. N. da Rocha Filho, J. R. Zamian, and L. R. V. da Conceição, "Acai Seed Ash as a Novel Basic Heterogeneous Catalyst for Biodiesel Synthesis: Optimization of the Biodiesel Production Process," *Fuel* 299 (2021): 120887.

136. Y. Jiang, C. Li, L. Zhang, et al., "Impacts of Acidic or Basic Sites on Poplar Sawdust on Pyrolytic Products and Pyrolysis Kinetics," *Journal of Analytical and Applied Pyrolysis* 174 (2023): 106151.

137. Y. Shen, C. Liu, C. Cui, et al., "Effect of Cu-Modified HZSM-5 Zeolites on Catalytic Pyrolysis of Lignin to Producing Aromatic Hydrocarbons," *Fuel* 361 (2024): 130719.

138. J. Dong, Y. Tang, Y. Hu, et al., "Effect of CaO Addition on Fast Pyrolysis Behavior of Solid Waste Components Using Py GC/MS," *Journal of Analytical and Applied Pyrolysis* 188 (2025): 107055.

139. S. Campisi, C. E. Chan-Thaw, and A. Villa, "Understanding Heteroatom-Mediated Metal–Support Interactions in Functionalized Carbons: A Perspective Review," *Applied Sciences* 8, no. 7 (2018): 1159.

140. Z. Zhu, H. Tan, J. Wang, S. Yu, and K. Zhou, "Hydrodeoxygenation of Vanillin as a Bio-Oil Model Over Carbonaceous Microspheres-Supported Pd Catalysts in the Aqueous Phase and Pickering Emulsions," *Green Chemistry* 16, no. 5 (2014): 2636–2643.

141. Z. Tan, T. Lu, W. Jerzak, et al., "Effects of Intrinsic and External Potassium on Biochar Structure Evolution in Volatile-Char Interactions During Biomass Pyrolysis," *Journal of Analytical and Applied Pyrolysis* 193 (2026): 107472.

142. X. Chen, F. Zhang, D. Lan, et al., "State-of-the-Art Synthesis Strategy for Nitrogen-Doped Carbon-Based Electromagnetic Wave Absorbers: From the Perspective of Nitrogen Source," *Advanced Composites and Hybrid Materials* 6, no. 6 (2023): 220.

143. N. Kasera, P. Kolar, and S. G. Hall, "Nitrogen-Doped Biochars as Adsorbents for Mitigation of Heavy Metals and Organics From Water: A Review," *Biochar* 4, no. 1 (2022): 17.

144. L. J. Konwar, P. Mäki-Arvela, and J.-P. Mikkola, "SO_3H-Containing Functional Carbon Materials: Synthesis, Structure, and Acid Catalysis," *Chemical Reviews* 119, no. 22 (2019): 11576–11630.

145. I. S. Marques, B. Jarrais, R. Ramos, et al., "Nitrogen-Doped Biochar-Supported Metal Catalysts: High Efficiency in Both Catalytic Transfer Hydrogenation of Furfural and Electrocatalytic Oxygen Reactions," *Catalysis Today* 418 (2023): 114080.

146. Y.-L. Ding, H.-Q. Wang, M. Xiang, P. Yu, R.-Q. Li, and Q.-P. Ke, "The Effect of Ni-ZSM-5 Catalysts on Catalytic Pyrolysis and Hydro-Pyrolysis of Biomass," *Frontiers in Chemistry* 8 (2020): 790.

147. T. Jin, D. Zhang, J. Peng, et al., "Pretreatment of HZSM-5 With Organic Alkali and Cobalt: Application in Catalytic Pyrolysis of Lignin to Produce Monocyclic Aromatic Hydrocarbons," *Fuel Processing Technology* 233 (2022): 107308.

148. L. Fu, Z. Liu, X. Li, Y. Li, H. Yang, and Y. Liu, "Boosting Bio-Lipids Deoxygenation via Tunable Metal-Support Interaction in Nickel/Ceria-Based Catalysts," *Fuel* 322 (2022): 124027.

149. C. W. Park, J. W. Kim, H. U. Kim, et al., "Bimetallic Ni-Re Catalysts for the Efficient Hydrodeoxygenation of Biomass-Derived Phenols," *International Journal of Energy Research* 45, no. 11 (2021): 16349–16361.

150. J. Wu, L. Liu, X. Yan, et al., "Highly Dispersed Pd Nanoparticles Immobilized on N-Doped Hollow Carbon Spheres for Efficient Catalytic Hydrodeoxygenation of Biomass-Derived Vanillin Under Atmospheric Conditions," *ACS Sustainable Chemistry & Engineering* 13, no. 1 (2025): 276–288.

151. X. Liao, H. Cui, H. Luo, Y. Lv, and P. Liu, "Highly Efficient Selective Hydrodeoxygenation of 5-Hydroxymethylfurfural to 2,5-Dimethylfuran Over Co-Ni In-Situ Encapsulated in Biochar-Based Carbon Catalysts: The Crucial Role of CoNi Alloys and Co-Nx Species," *Chemical Engineering Journal* 503 (2025): 158336.

152. A. Ibrahim, I. Elsayed, and E. B. Hassan, "Catalytic Upgrading of Rice Straw Bio-Oil via Esterification in Supercritical Ethanol Over Bimetallic Catalyst Supported on Rice Straw Biochar," *Energies* 17, no. 2 (2024): 407.

153. H. Wang, S. Liu, Y. Dai, C. S. Kim, and K. J. Smith, "Two-Step Bio-Oil Upgrading Using Carbon-Supported Mo_2C Catalysts," *Energy & Fuels* 38, no. 1 (2024): 647–658.

154. S. Oh, H. S. Choi, U.-J. Kim, I.-G. Choi, and J. W. Choi, "Storage Performance of Bio-Oil After Hydrodeoxygenative Upgrading With Noble Metal Catalysts," *Fuel* 182 (2016): 154–160.

155. C. Zhu, H. Wang, H. Li, et al., "Selective Hydrodeoxygenation of 5-Hydroxymethylfurfural to 2,5-Dimethylfuran Over Alloyed Cu–Ni Encapsulated in Biochar Catalysts," *ACS Sustainable Chemistry & Engineering* 7, no. 24 (2019): 19556–19569.

ijer, 2026, 1, Downloaded from https://onlinelibrary.wiley.com/doi/10.1155/er/4175129 by Hanyang University Library, Wiley Online Library on [24/11/2026]. See the Terms and Conditions (https://onlinelibrary.wiley.com/terms-and-conditions) on Wiley Online Library for rules of use; OA articles are governed by the applicable Creative Commons License

156. P. Cabrera-Reyes, J. Palomo, F. J. García-Mateos, et al., "Sustainable Carbon-Based Nickel Catalysts for the Steam Reforming of Model Compounds of Pyrolysis Liquids," *Fuel Processing Technology* 253 (2024): 108028.

157. Y. Liu, M. Paskevicius, H. Wang, et al., "Role of O-Containing Functional Groups in Biochar During the Catalytic Steam Reforming of Tar Using the Biochar as a Catalyst," *Fuel* 253 (2019): 441–448.

158. C. W. Low, A. Veksha, R. Aryal, W. P. Chan, and G. Lisak, "Catalytic Reforming of Biomass Pyrolysis Gas Over Ni Catalysts: Alumina, Spent Fluid Catalytic Cracking Catalyst and Char as Supports," *Applied Catalysis A: General* 691 (2025): 120074.

159. K. Sun, Q. Huang, M. Ali, Y. Chi, and J. Yan, "Producing Aromatic-Enriched Oil From Mixed Plastics Using Activated Biochar as Catalyst," *Energy & Fuels* 32, no. 4 (2018): 5471–5479.

160. K. Sun, Q. Huang, Y. Chi, and J. Yan, "Effect of ZnCl2-Activated Biochar on Catalytic Pyrolysis of Mixed Waste Plastics for Producing Aromatic-Enriched Oil," *Waste Management* 81 (2018): 128–137.

161. C. Wang, R. Zou, H. Lei, et al., "Biochar-Advanced Thermocatalytic Salvaging of the Waste Disposable Mask With the Production of Hydrogen and Mono-Aromatic Hydrocarbons," *Journal of Hazardous Materials* 426 (2022): 128080.

162. Y. Zhang, H. Lei, Z. Yang, K. Qian, and E. Villota, "Renewable High-Purity Mono-Phenol Production From Catalytic Microwave-Induced Pyrolysis of Cellulose Over Biomass-Derived Activated Carbon Catalyst," *ACS Sustainable Chemistry & Engineering* 6, no. 4 (2018): 5349–5357.

163. L. Dai, Z. Zeng, X. Tian, et al., "Microwave-Assisted Catalytic Pyrolysis of Torrefied Corn Cob for Phenol-Rich Bio-Oil Production Over Fe Modified Bio-Char Catalyst," *Journal of Analytical and Applied Pyrolysis* 143 (2019): 104691.

164. J. Y. Park, J.-K. Kim, C.-H. Oh, J.-W. Park, and E. E. Kwon, "Production of Bio-Oil From Fast Pyrolysis of Biomass Using a Pilot-Scale Circulating Fluidized Bed Reactor and Its Characterization," *Journal of Environmental Management* 234 (2019): 138–144.

165. B. Soni and S. K. Karmee, "Towards a Continuous Pilot Scale Pyrolysis Based Biorefinery for Production of Biooil and Biochar From Sawdust," *Fuel* 271 (2020): 117570.

166. S. Summers, A. Valentine, Z. Wang, and Y. Zhang, "Pilot-Scale Continuous Plug-Flow Hydrothermal Liquefaction of Food Waste for Biocrude Production," *Industrial & Engineering Chemistry Research* 62, no. 31 (2023): 12174–12182.

167. O. Mašek, W. Buss, A. Roy-Poirier, et al., "Consistency of Biochar Properties Over Time and Production Scales: A Characterisation of Standard Materials," *Journal of Analytical and Applied Pyrolysis* 132 (2018): 200–210.

168. J. Peng, L. Zhang, E. Surgot Meulien, X. T. Bi, J. C. Lim, and W.-H. Chen, "Waste Plastics as an Effective Binder for Biochar Pelletization," *Energy & Fuels* 35, no. 17 (2021): 13840–13846.

169. E. Arango-Durango, A. Coppola, F. Massa, F. Scala, and K. Umeki, "Attrition-Driven Carbon and Mineral Matter Distribution During Biochar Production From Pine Bark in Fluidized Beds," *Energy & Fuels* 40, no. 26 (2026): 14048–14060.

170. Z. Wang and M. Sedighi, "Disintegration of Biochar Adsorbent Under the Hydraulic Conditions of Fixed Bed Water Treatment," *Chemosphere* 336 (2023): 139294.

171. D. Wu, L. Song, B. Zhang, and Y. Li, "Effect of the Mechanical Failure of Catalyst Pellets on the Pressure Drop of a Reactor," *Chemical Engineering Science* 58, no. 17 (2003): 3995–4004.

172. C. Lindfors, M. Nieminen, T. Alhalabi, E. Pienihäkkinen, J. Lahtinen, and A. Oasmaa, "Novel Hot Vapor Filter Design for Biomass Pyrolysis," *Energy & Fuels* 37, no. 6 (2023): 4460–4469.

173. H. Sun, D. Feng, Y. Zhang, S. Sun, Y. Zhao, and F. Zhang, "Regeneration of Deactivated Biochar for Catalytic Tar Reforming by Partial Oxidation: Effect of Oxygen Concentration and Regeneration Time," *Fuel* 330 (2022): 125572.

174. H. Liu, C. Ye, Z. Ye, et al., "Catalytic Cracking and Catalyst Deactivation/Regeneration Characteristics of Fe-Loaded Biochar Catalysts for Tar Model Compound," *Fuel* 334 (2023): 126810.

175. Y. Wang, P. Prinsen, K. S. Triantafyllidis, et al., "Comparative Study of Supported Monometallic Catalysts in the Liquid-Phase Hydrogenation of Furfural: Batch Versus Continuous Flow," *ACS Sustainable Chemistry & Engineering* 6, no. 8 (2018): 9831–9844.

176. L. Puri, Y. Hu, and G. Naterer, "Critical Review of the Role of Ash Content and Composition in Biomass Pyrolysis," *Frontiers in Fuels* 2 (2024): 1378361.

177. N. Anderson, H. Gu, and R. Bergman, "Comparison of Novel Biochars and Steam Activated Carbon From Mixed Conifer Mill Residues," *Energies* 14, no. 24 (2021): 8472.

178. S. Yorgun and D. Yıldız, "Preparation and Characterization of Activated Carbons From Paulownia Wood by Chemical Activation With H3PO4," *Journal of the Taiwan Institute of Chemical Engineers* 53 (2015): 122–131.

179. I. I. Salame and T. J. Bandosz, "Comparison of the Surface Features of Two Wood-Based Activated Carbons," *Industrial & Engineering Chemistry Research* 39, no. 2 (2000): 301–306.

180. I. M. Nwajiaku, J. S. Olanrewaju, K. Sato, T. Tokunari, S. Kitano, and T. Masunaga, "Change in Nutrient Composition of Biochar From Rice Husk and Sugarcane Bagasse at Varying Pyrolytic Temperatures," *International Journal of Recycling of Organic Waste in Agriculture* 7, no. 4 (2018): 269–276.

181. X. Xiao, B. Chen, and L. Zhu, "Transformation, Morphology, and Dissolution of Silicon and Carbon in Rice Straw-Derived Biochars Under Different Pyrolytic Temperatures," *Environmental Science & Technology* 48, no. 6 (2014): 3411–3419.

182. Y. Sun, G. Su, Z. He, et al., "Porous Carbons Derived From Desiliconized Rice Husk Char and Their Applications as an Adsorbent in Multivalent Ions Recycling for Spent Battery," *Journal of Chemistry* 2022, no. 1 (2022): 8225088.

183. Z. Khanmohammadi, M. Afyuni, and M. R. Mosaddeghi, "Effect of Pyrolysis Temperature on Chemical and Physical Properties of Sewage Sludge Biochar," *Waste Management & Research: The Journal for a Sustainable Circular Economy* 33, no. 3 (2015): 275–283.

184. J. Yu, X. Li, M. Wu, et al., "Synergistic Role of Inherent Calcium and Iron Minerals in Paper Mill Sludge Biochar for Phosphate Adsorption," *Science of the Total Environment* 834 (2022): 155193.

185. K. Yoon, G. Kwon, E. Kim, J. Rinklebe, and H. Song, "Production of Fe-Biochar From Paper-Mill Sludge and Its Application to Se(VI) and Se(IV) Removal," *Chemical Engineering Journal* 484 (2024): 149470.

186. C. Yu, D. Zhang, X. Dong, and Q. Lin, "Pyrolytic Behavior of a Zero-Valent Iron Biochar Composite and Its Cu(ii) Removal Mechanism," *RSC Advances* 8, no. 59 (2018): 34151–34160.

187. J. Alvarez, G. Lopez, M. Amutio, J. Bilbao, and M. Olazar, "Preparation of Adsorbents From Sewage Sludge Pyrolytic Char by Carbon Dioxide Activation," *Process Safety and Environmental Protection* 103 (2016): 76–86.

188. K. Kebelmann, A. Hornung, U. Karsten, and G. Griffiths, "Intermediate Pyrolysis and Product Identification by TGA and Py-GC/MS of Green Microalgae and Their Extracted Protein and Lipid Components," *Biomass and Bioenergy* 49 (2013): 38–48.

189. T. Pak, K. E. Gomari, S. Bose, et al., "Biochar From Brown Algae: Production, Activation, and Characterisation," *Bioresource Technology Reports* 24 (2023): 101688.

ijer, 2026, 1, Downloaded from https://onlinelibrary.wiley.com/doi/10.1155/er/4175129 by Hanyang University Library, Wiley Online Library on [24/11/2026]. See the Terms and Conditions (https://onlinelibrary.wiley.com/terms-and-conditions) on Wiley Online Library for rules of use; OA articles are governed by the applicable Creative Commons License

190. N. Patel, B. Acharya, and P. Basu, "Hydrothermal Carbonization (HTC) of Seaweed (Macroalgae) for Producing Hydrochar," *Energies* 14, no. 7 (2021): 1805.

191. M. Ren, Z. Jia, Z. Tian, et al., "High Performance N-Doped Carbon Electrodes Obtained via Hydrothermal Carbonization of Macroalgae for Supercapacitor Applications," *ChemElectroChem* 5, no. 18 (2018): 2686–2693.

192. W. Chen, H. Yang, Y. Chen, M. Xia, X. Chen, and H. Chen, "Transformation of Nitrogen and Evolution of N-Containing Species During Algae Pyrolysis," *Environmental Science & Technology* 51, no. 11 (2017): 6570–6579.

193. X. Wang, J. Zhou, D. Jiang, et al., "Elucidating Nitrogen Functional Site Effects in the Catalytic Pyrolysis of Algae: Combined Experimental and DFT," *Journal of Analytical and Applied Pyrolysis* 195 (2026): 107646.

194. A. Li, X. Tang, Y. Wen, et al., "Enhancing Pyrolysis Oil Quality Through In-Situ Catalytic Pyrolysis of Biochar With Temperature-Driven Nitrogen Configuration Modulation: Mechanistic Insights Into the Catalytic Process," *Journal of Analytical and Applied Pyrolysis* 192 (2025): 107323.

195. M. I. Bird, C. M. Wurster, P. H. de Paula Silva, A. M. Bass, and R. de Nys, "Algal Biochar – Production and Properties," *Bioresource Technology* 102, no. 2 (2011): 1886–1891.

196. N. Jaswal, Sahil, A. K. Sharma, V. Bahadur, and P. Kumar, "Valorizing *Saccharum officinarum* and Plastic Waste Biochar With Zn-Al LDH for Congo Red Dye Removal: Kinetics and Isotherms Insights," *Inorganic Chemistry Communications* 178 (2025): 114654.

197. N. Jaswal, N. Sarma, P. Justa, A. K. Sharma, P. Kumar, and P. Kumar, "Functionalising *Pinus roxburghii* Biochar With Mg–Fe-LDH for Effective Organic Pollutant Mitigation in Wastewater," *Catalysis Letters* 155, no. 1 (2025): 20.

198. N. Jaswal, Priyanka, H. Kumar, A. Raza, and P. Kumar, "Waste-Derived Co–Fe LDH@biochar for Sustainable Wastewater Remediation and Antimicrobial Applications," *Next Materials* 13 (2026): 102831.

199. V.-A. Thai, T.-B. Nguyen, W.-H. Chen, C.-W. Chen, R.-A. Doong, and C.-D. Dong, "Fe-MOFs-Derived Fe_3O_4-Doped Biochar From Waste Chopsticks: A Novel Catalyst for Tetrabromobisphenol a Degradation via Peroxymonosulfate Activation," *Environmental Research* 278 (2025): 121620.

200. Y. Zou, Z. Zou, B. Wan, et al., "Interface-Engineered Biochar Catalysts Functionalized With Hydroxylamine-Imidazolium Ionic Liquids for Efficient CO2 Fixation Under Ambient Conditions," *Chemical Engineering Journal* 524 (2025): 169221.

201. M. Amin, E. Chung, and H. H. Shah, "Effect of Different Activation Agents for Activated Carbon Preparation Through Characterization and Life Cycle Assessment," *International Journal of Environmental Science and Technology* 20, no. 7 (2023): 7645–7656.

202. J. Saleem, Z. K. B. Moghal, F. Tahir, and G. McKay, "Environmental Performance of Olive Stone–Plastic Waste Activated Carbon Composites," *RSC Advances* 16, no. 11 (2026): 10297–10309.

203. M. Amin, H. H. Shah, A. Iqbal, Z. U. R. Farooqi, M. Krawczuk, and A. Zia, "Conversion of Waste Biomass Into Activated Carbon and Evaluation of Environmental Consequences Using Life Cycle Assessment," *Applied Sciences* 12, no. 11 (2022): 5741.

204. M. Fan, Y. Shao, Y. Wang, et al., "Preparation of Activated Carbon With Recycled $ZnCl_2$ for Maximizing Utilization Efficiency of the Activating Agent and Minimizing Generation of Liquid Waste," *Chemical Engineering Journal* 500 (2024): 157278.

205. R. Frazier, E. Jin, and A. Kumar, "Life Cycle Assessment of Biochar Versus Metal Catalysts Used in Syngas Cleaning," *Energies* 8, no. 1 (2015): 621–644.

206. I. Sádaba, M. López Granados, A. Riisager, and E. Taarning, "Deactivation of Solid Catalysts in Liquid Media: The Case of Leaching of Active Sites in Biomass Conversion Reactions," *Green Chemistry* 17, no. 8 (2015): 4133–4145.

207. O. Y. Thayee Al-Janabi, B. M. Ali, H. A. Abdulkareem, A. H. Hussein, E. T. B. Al-Tikrity, and P. J. S. Foot, "Porous Carbon Nanospheres In Situ Doped KxFeyOz as Novel Magnetic Nanocatalyst for Biodiesel Production," *Fuel* 398 (2025): 135456.

208. H. A. Alhashimi and C. B. Aktas, "Life Cycle Environmental and Economic Performance of Biochar Compared With Activated Carbon: A Meta-Analysis," *Resources, Conservation and Recycling* 118 (2017): 13–26.

209. H. Gu, R. Bergman, N. Anderson, and S. Alanya-Rosenbaum, "Life Cycle Assessment of Activated Carbon From Woody Biomass," *Wood and Fiber Science* 50, no. 3 (2018): 229–243.

210. J.-C. Lee, B. Lee, Y. S. Ok, and H. Lim, "Preliminary Techno-Economic Analysis of Biodiesel Production Over Solid-Biochar," *Bioresource Technology* 306 (2020): 123086.

211. R. Pravin and G. Baskar, "Technoeconomic and Carbon Footprint Analysis of Simulated Industrial Scale Biodiesel Production Process From Mixed Macroalgal and Non-Edible Seed Oil Using Sulphonated Zinc Doped Recyclable Biochar Catalyst," *Bioresource Technology* 395 (2024): 130351.

212. S. Kim and S.-E. Lee, "Recovery of Reactive Potassium Compounds as Chemical Agents in Wastewaters From KOH-Activated Carbon Production," *Carbon Letters* 35, no. 5 (2025): 2147–2156.

213. H. Niu, H. Jin, Q. Sun, Y. Shi, X. Zhang, and Y. Cai, "Activation of Biochars by Waste Phosphoric Acids: An Integrated Disposal Route of Waste Acids and Solid Waste," *ACS Sustainable Chemistry & Engineering* 9, no. 48 (2021): 16403–16414.

214. J. Li, T. Wang, T. Hao, X. Yao, K. Xu, and J. Liu, "Application of Biochar Catalysts in Tar Catalytic Reforming: A Review on Preparation, Modification, Deactivation, and Regeneration," *Energy* 317 (2025): 134734.

ijer, 2026, 1, Downloaded from https://onlinelibrary.wiley.com/doi/10.1155/er/4175129 by Hanyang University Library, Wiley Online Library on [24/11/2026]. See the Terms and Conditions (https://onlinelibrary.wiley.com/terms-and-conditions) on Wiley Online Library for rules of use; OA articles are governed by the applicable Creative Commons License